Available online at www.sciencedirect.com
SCIENCE DIRECT®
Physics Reports 377 (2003) 1–80
PHYSICS REPORTS
www.elsevier.com/locate/physrep

Thermal conduction in classical low-dimensional lattices

Stefano Lepri[a,b,*], Roberto Livi[b,c], Antonio Politi[b,d]

[a] *Dipartimento di Energetica "S. Stecco", via S. Marta 3 I-50139 Florence, Italy*
[b] *Istituto Nazionale di Fisica della Materia-Unità di Firenze, Via G. Sansone 1 I-50019 Sesto Fiorentino, Italy*
[c] *Dipartimento di Fisica, Via G. Sansone 1 I-50019 Sesto Fiorentino, Italy*
[d] *Istituto Nazionale di Ottica Applicata, largo E. Fermi 6 I-50125 Florence, Italy*

Accepted 31 October 2002

editor: D.K. Campbell

Abstract

Deriving macroscopic phenomenological laws of irreversible thermodynamics from simple microscopic models is one of the tasks of non-equilibrium statistical mechanics. We consider stationary energy transport in crystals with reference to simple mathematical models consisting of coupled oscillators on a lattice. The role of lattice dimensionality on the breakdown of the Fourier's law is discussed and some universal quantitative aspects are emphasized: the divergence of the finite-size thermal conductivity is characterized by universal laws in one and two dimensions. Equilibrium and non-equilibrium molecular dynamics methods are presented along with a critical survey of previous numerical results. Analytical results for the non-equilibrium dynamics can be obtained in the harmonic chain where the role of disorder and localization can be also understood. The traditional kinetic approach, based on the Boltzmann–Peierls equation is also briefly sketched with reference to one-dimensional chains. Simple toy models can be defined in which the conductivity is finite. Anomalous transport in integrable non-linear systems is briefly discussed. Finally, possible future research themes are outlined.

PACS: 63.10.+a; 05.60.−k; 44.10.+i

Keywords: Thermal conductivity; Classical lattices

Contents

* Corresponding author. Dipartimento di Energetica "S. Stecco", via S. Marta 3 I-50139 Florence, Italy.
E-mail address: stefano.lepri@unifi.it (S. Lepri).

0370-1573/03/$ - see front matter
doi:10.1016/S0370-1573(02)00558-6

1. Introduction

The customary macroscopic approach to non-equilibrium phenomena relies crucially on the definition of transport coefficients through phenomenological constitutive equations. Under the hypothesis of being close enough to global equilibrium, this is usually accomplished by postulating the proportionality among fluxes and thermodynamic forces [1]. For instance when dealing with energy transport in a solid one defines the thermal conductivity κ through the *Fourier's law* [1]

$$\mathbf{J}_Q = -\kappa \nabla T \ , \tag{1}$$

[1] The thermal conductivity should be represented in general as a tensor. Here we assume to consider a simple cubic crystal, in the absence of any external force field. Accordingly, κ has a diagonal representation with equal diagonal elements.

where the heat flux $\mathbf{J}_Q$ is the amount of heat transported through the unit surface per unit time and $T(\mathbf{x},t)$ is the local temperature. Such a phenomenological relation was first proposed in 1808 by Fourier as an attempt to explain the thermal gradient present inside the Earth—a problem that had raised a long and controversial debate inside the scientific community at that time. Eq. (1) is assumed to be valid close to equilibrium. Actually, the very definition of local energy flux $\mathbf{J}_Q(\mathbf{x},t)$ and of temperature field $T(\mathbf{x},t)$ relies on the *local equilibrium hypothesis* i.e. on the possibility of defining a local temperature for a macroscopically small but microscopically large volume at each location $\mathbf{x}$ for each time t.

The ultimate goal of a complete theory would be to derive an equation like (1) from some statistical-mechanics calculation, a task which may be formidably difficult. For insulating crystals where heat is transported by lattice vibrations, the first and most elementary attempt to give a microscopic foundation to Fourier's law dates back to Debye. By rephrasing the results of the kinetic theory for the (diluted) phonon gas, he found that the thermal conductivity should be proportional to $Cv\ell$ where C is the heat capacity and v, ℓ are the phonon mean velocity and free path, respectively. In 1929, Peierls further extended this idea and formulated a Boltzmann equation [2] that shows how anharmonicity is necessary to obtain genuine diffusion of the energy through the so-called *Umklapp* processes. Since then, the Boltzmann–Peierls approach became one the cornerstones in the theory of lattice thermal conductivity. Standard methods, like the relaxation-time approximation, allow to compute, say, the temperature dependence of κ.

From a more fundamental point of view, there are however basic questions that go beyond the actual calculation of the transport coefficient. For example, under what condition is local equilibrium realized? Can we ensure that a unique non-equilibrium stationary state is attained on physically accessible time scales? In this respect, simple mathematical models are an invaluable theoretical playground to provide a more firm foundation to heat conductivity and to understand more deeply the hypotheses underlying Eq. (1). Admittedly, this program is still nowadays far from being accomplished, at least from a mathematically rigorous point of view [3]. On the other hand, even in the absence of solvable examples, one can rely on numerical simulations as a tool to investigate many of those items.

As usual in theoretical physics, the guiding criterion of mathematical simplicity leads naturally to consider 1d or 2d periodic lattices (i.e. chains or planes) of point-like atoms interacting with their neighbors through non-linear forces. The hope is to reproduce realistic thermodynamic properties of their three-dimensional counterparts without having to refer to specific structures. This brings to the fore the following question: what are the minimal requirements for a dynamical model to satisfy or not Eq. (1)? Although it may appear surprising, this issue has been addressed in the literature already in the late 60s without yet receiving a definite answer. To a large extent, the present review aims at settling this question by reconciling the very many (and sometimes contrasting) numerical results that appeared since then. In fact, several times in the past wrong interpretations have been given to the outcome of numerical simulations. In the absence of a general theoretical framework, it has been overemphasized the role of deterministic chaos in ensuring a normal heat transport. Indeed, while ergodicity (implied to some extent by a chaotic dynamics) is certainly a necessary condition to establish energy diffusion, it has become clear that it is not at all sufficient, as too-rapidly claimed more than a decade ago [4].

As it is known in the context of fluids [5], much of the difficulties arise from the fact that transport coefficients in low spatial dimensions may *not exist at all*, thus implying a breakdown of

usual hydrodynamics. In the present context, this usually manifests itself as: (i) a slow decay of equilibrium correlations of the heat current; (ii) a divergence of the *finite-size conductivity* $\kappa(N,T)$ in the thermodynamic limit $N \to \infty$ (where N is the number of atoms in the sample). One of our concerns will thus be to clarify, through the analysis of several examples, under what conditions this should occur. Particular emphasis has been put on the universality of quantitative data like the decay law of equilibrium correlation of the flux.

A by-no-means side issue that is also considered in the present review is the coupling with thermal baths. It is only after having properly set the interaction between the system of interest and thermal reservoirs that one can be sure that a physically meaningful non-equilibrium regime is established. Ideally, a thermal bath is a set of (infinitely) many degrees of freedom, so that it can either absorb or release energy, without appreciably changing its own state. Unfortunately, such a type of reservoir is very difficult to treat analytically and too much time demanding in numerical simulations. Accordingly, various shortcuts have been proposed and are here recalled, ranging from stochastic to non-linear deterministic rules.

Up to now we have mainly emphasized the theoretical issues that motivate the study of transport in low-dimensional lattices. Of course, a further relevant motivation is the existence of a variety of real systems that could be, at least in principle, effectively described by 1d or 2d models. For instance, reduced dimensionality has been indeed invoked to explain experiments on heat transport in anisotropic crystals [6,7] or magnetic systems [8]. Remarkably, a dependence of thermal conductivity on the chain length of solid polymers has also been experimentally observed [9]. More generally, modern experimental techniques [10] allow to directly probe the transport properties of semiconductor films [11,12] and single-walled nanotubes [13,14] that markedly display two-dimensional features at low temperatures. Some theoretical investigations of thermal conductance for a quantum wire in ballistic [15] and anharmonic [16] regimes have been also recently undertaken. Another important example is the problem of heat conductivity in quantum spin chains [17].

The present work is not simply a review paper in the customary sense: many results were not previously published and older results are critically reconsidered. This is of course particularly crucial when dealing with numerical data. The plan of the article is the following. In Section 2 we present the simple lattice models that will be considered throughout the review. To be as self-contained as possible, we derive the microscopic expression of the heat flux with reference to the specific case of one-dimensional systems with nearest-neighbor interactions. The advantage of this presentation is twofold: it provides the expression to be referred to in the following and allows to understand the hypotheses behind its derivation without having to dwell into more involved notations. As already mentioned, an important point for non-equilibrium molecular dynamics is the way thermal reservoirs are modeled. Section 3 contains a brief survey of some simple schemes that have been used in the literature on the topic. The relevant differences among the most widely used methods are also discussed. Most of our understanding of energy transport in lattices relies on the harmonic approximation for the microscopic dynamics. One major advantage of treating the simple harmonic chain is that non-equilibrium properties can be derived in a non-perturbative way. This is reviewed in Section 4. Harmonic chains are also presumably the only class of systems in which the consequences of the presence of quenched disorder can be effectively studied. A discussion of chains with isotopic disorder and of the role of localization on the heat conduction is given.

A very sketchy discussion of the two "traditional" approaches, the Boltzmann–Peierls kinetic theory for phonons and the Green–Kubo method, is presented in Section 5. Since detailed accounts

exist in many textbooks, we limited ourselves to recall those issues that are relevant in the present context. In Section 6 we present a detailed account of the many numerical studies performed with models where total momentum is conserved. Both equilibrium and non-equilibrium simulations are discussed and compared. Section 7 is, instead, devoted to the "complementary" class of systems where the interaction with an external substrate breaks total momentum conservation. This turns out to be a crucial difference in ensuring normal heat transport.

The peculiar behavior of integrable systems is briefly summarized in Section 8, while the role of dimensionality of the physical space can be appreciated in Section 9, where we illustrate the behavior of some 2d models. The last chapter is finally devoted to summarizing the key points that have been so far understood and, more importantly, to the still open questions. The more technical discussions have been confined to the Appendices in order not to downgrade the readability of the main body of the text.

2. Definitions

2.1. Models

The present Report deals mainly with classical arrays of coupled oscillators. To be more specific, we introduce the models for the one-dimensional case. The generalization to two dimension is rather straightforward and will be recalled later when needed.

A schematic setup of the systems that will be mostly studied in the following is drawn in Fig. 1, where we have depicted a chain of N coupled atoms, the first and the last of which interact also with a thermal bath. Let m_l and x_l be, respectively, the mass and the position of the lth particle. Only nearest-neighbor interactions will be considered for simplicity. The first class of models we wish to consider are defined by an Hamiltonian of the form ($p_l = m_l \dot{x}_l$)

$$\mathscr{H} = \sum_{l=1}^{N} \left[\frac{p_l^2}{2m_l} + V(x_{l+1} - x_l) \right] . \tag{2}$$

Boundary conditions need also to be specified by defining x_0 and x_{N+1}. Typical choices are periodic, fixed or free boundaries. As only internal forces, that depend on relative positions, are present, the total momentum is conserved and thus a zero (Goldstone) mode exist. In the harmonic limit, model (2) admits at least a phonon branch whose frequency vanishes for vanishing wavenumber. Long-wavelength waves move at the sound velocity and for this reason one sometimes refer to (2) as *acoustic* models.

An important example is the well-known Lennard–Jones potential

$$V(z) = \varepsilon \left[\left(\frac{a}{z} \right)^{12} - 2 \left(\frac{a}{z} \right)^{6} \right] . \tag{3}$$

In this formulation a is the equilibrium distance and ε the well depth. The other example we will often consider is the celebrated Fermi–Pasta–Ulam (FPU) potential [18]

$$V(z) = \frac{g_2}{2} (z-a)^2 + \frac{g_3}{3} (z-a)^3 + \frac{g_4}{4} (z-a)^4 , \tag{4}$$

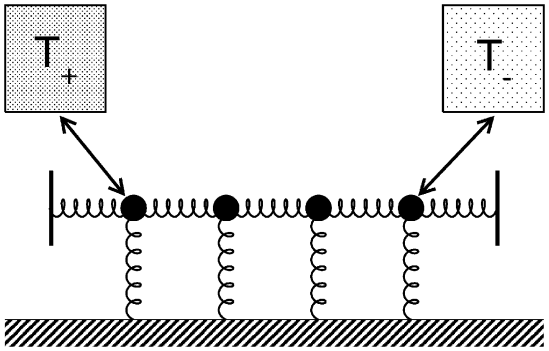

Fig. 1. A pictorial representation of a chain of $N=4$ mutually coupled oscillators in interaction with an external substrate and coupled with two thermal reservoirs working at different temperatures.

that can be regarded as resulting from an expansion of V close to its equilibrium position $z=a$. Due to its simple algebraic form, the model is computationally very convenient. Two important particular cases are worth mentioning: the quadratic plus cubic ($g_4=0$) and quadratic plus quartic ($g_3=0$) potentials that, for historical reasons, are referred to as the FPU-α and FPU-β models, respectively. In the former one, sufficiently small coupling constant g_3 and/or energies must be considered to avoid runaway instability of trajectories.

Models like (2) are a very drastic idealization of a real crystal. Natural low-dimensional lattice structures are usually embedded in three-dimensional matrices that couple them to the environment. Furthermore, artificial arrays of atoms can be constructed by growing them on a substrate exerting a pinning force on the atoms in such a way to stabilize the lattice (in general, this is not necessary in the three-dimensional case). At the simplest level of modelization, this can be described by adding an external, on-site, potential. For instance, neglecting the transverse motion leads to one-dimensional models of the form

$$\mathscr{H}=\sum_{l=1}^{N}\left[\frac{p_l^2}{2m_l}+U(x_l)+V(x_{l+1}-x_l)\right]\ . \tag{5}$$

The substrate potential U breaks the invariance $x_l\to x_l+const.$ of (2) and the total momentum is no longer a constant of the motion. Accordingly, all branches of the dispersion relation have a gap at zero wavenumber. We therefore refer to (5) as *optical* models.

Dimensionless variables will be used throughout whenever possible, especially when reporting simulation data. The choice of the most natural units is usually dictated by the particular model at hand. For example, for the FPU model with $m_l=m$, it is convenient to set a, m and the angular frequency $\omega_0=\sqrt{g_2/m}$ to unity. This implies, for instance, that the sound velocity $a\omega_0$ is also unity and that the energy is measured in units of $m\omega_0^2a^2$.

2.2. Temperature

The first problem that has to be solved in order to interpret molecular-dynamics simulations in a thermodynamic perspective is the definition of temperature in terms of dynamical variables.

In Appendix A, we show that the problem can be tackled rigorously, although at the expense of introducing some technicalities (see also [19,20]). Here below, we follow the traditional approach based on the virial theorem,

$$T = \langle \mathbf{u} \cdot \nabla \mathscr{H} \rangle_\mu \ , \tag{6}$$

where $\mathbf{u}$ is any vector fulfilling the condition $\nabla \cdot \mathbf{u} = 1$, the symbol $\langle \cdot \rangle_\mu$ indicates the μ-canonical ensemble average, and units are chosen in such a way that the Boltzmann constant is $k_B = 1$.

μ-canonical averages are the most appropriate ones whenever an isolated system is numerically investigated, but as soon as the system is put in contact with one or more heat baths, canonical averages should be considered instead. Fortunately, it is well known, though only partially proved, that averages are independent of the chosen ensemble in the thermodynamic limit. Nevertheless, when working with finite systems one has to be aware of the existence of finite-size corrections as discussed in the celebrated paper by Lebowitz et al. [21].

Moreover, in molecular-dynamics simulations, averages are more conveniently computed by following single trajectories over time. This is not a problem whenever ergodicity can be invoked, so as to ensure that ensemble and time averages are equivalent to one another. However, time averages of quantities corresponding to thermodynamic observables have been found to converge to the expected ensemble averages even in systems that are known not to be ergodic in a strictly mathematical sense (as e.g. the FPU-β model at sufficiently small energy values) and even when fluctuations around the mean value are not consistent with equilibrium predictions. This suggests that a weaker condition than ergodicity might suffice to ensure the equivalence of time and ensemble averages of the physically relevant observables. [2]

According to Eq. (6), many formally different, but physically equivalent, definitions of temperature are possible. For instance, the choice $\mathbf{u}=(0,\ldots,0,\, p_1/N,\ldots,\, p_N/N)$ yields the usual definition adopted in the canonical ensemble.

$$T = \left\langle \frac{\sum_{i=1}^{N} p_i^2}{Nm} \right\rangle_\mu \ , \tag{7}$$

while the choice $\mathbf{u} = (0,\ldots,0,\, p_i, 0,\ldots,0)$ leads to a local definition of temperature,

$$T = \left\langle \frac{p_i^2}{m} \right\rangle_\mu \ . \tag{8}$$

The identification of an optimal definition of temperature to be adopted in numerical studies is strictly related to the convergence properties of time-averages. In this sense, it has been observed that definitions like the above ones involving only momenta converge always quite rapidly, also when the dynamics is weakly chaotic, while definitions involving an explicit dependence on space coordinates may converge over much longer time scales [20].

[2] A possible candidate might be the weak ergodicity criterion, proposed by Khinchin [22], that is equivalent to assume a sufficiently fast decay of the time-correlation functions at least for thermodynamically relevant observables, like temperature internal energy, specific heat, etc.

2.3. Flux

The goal of this section is to give a meaningful definition of heat flux [23,24]. This requires some care since it involves the transformation of an implicit "mesoscopic" definition into a workable microscopic definition. For the sake of simplicity, we discuss the problem with reference to one-dimensional systems with nearest-neighbor interactions, the extension to the more general case being more technically involved but conceptually equivalent. The heat flux $j(x,t)$ at time t in the spatial position x is nothing but the energy current, implicitly defined by the continuity equation

$$\frac{\mathrm{d}h(x,t)}{\mathrm{d}t} + \frac{\partial j(x,t)}{\partial x} = 0 \ , \tag{9}$$

where $h(x,t)$ is the energy density. It is important to realize that the energy flux defined as above *does not*, in general, coincide with heat flux, as the former arises also from macroscopic motion [1]. Nonetheless, in solids and one-dimensional fluids no steady motion can occur, so that the two fluxes do coincide and we can interchangeably use both names.

With reference to an ensemble of interacting particles, we can write the microscopic energy density as the sum of the isolated contributions located in the instantaneous position of each particle

$$h(x,t) = \sum_n h_n \delta(x - x_n) \ , \tag{10}$$

where $\delta(x)$ is the Dirac distribution and

$$h_n = \frac{p_n^2}{2m_n} + U(x_n) + \frac{1}{2}[V(x_{n+1} - x_n) + V(x_n - x_{n-1})] \tag{11}$$

is the energy contribution of the nth particle. The first two terms on the r.h.s. correspond to the kinetic energy and, respectively, to the potential energy $U(x_n)$ associated with the (possible) interaction with an external field. The last term amounts to half of the potential energy of the pairwise interactions with the neighboring particles. In a similar way, we can write the heat flux as the sum of localized contributions,

$$j(x,t) = \sum_n j_n \delta(x - x_n) \ . \tag{12}$$

The problem amounts therefore to give a definition of the local heat flux j_n. One should keep in mind that the latter quantity has not the same physical dimensions of $j(x,t)$.

In the limit of small oscillations around the equilibrium position, density fluctuations can be neglected and h_n is equal to the energy density times the lattice spacing a. The time derivative of h_n

$$\frac{\mathrm{d}h_n}{\mathrm{d}t} = m_n \dot{x}_n \ddot{x}_n + \dot{x}_n U'(x_n) - \frac{1}{2}[(\dot{x}_{n+1} - \dot{x}_n)F(x_{n+1} - x_n) + (\dot{x}_n - \dot{x}_{n-1})F(x_n - x_{n-1})] \ , \tag{13}$$

where the prime denotes derivative with respect to the argument and $F(x) = -V'(x)$ can be rewritten, with the help of the equations of motion derived from (5)

$$m_n \ddot{x}_n = -U'(x_n) - F(x_{n+1} - x_n) + F(x_n - x_{n-1}) \ , \tag{14}$$

as

$$\frac{\mathrm{d}h_n}{\mathrm{d}t} = -\frac{1}{2}[(\dot{x}_{n+1} + \dot{x}_n)F(x_{n+1} - x_n) - (\dot{x}_n + \dot{x}_{n-1})F(x_n - x_{n-1})] \ . \tag{15}$$

This equation can, in turn, be rewritten as

$$\frac{\mathrm{d}h_n}{\mathrm{d}t} + \frac{j_n - j_{n-1}}{a} = 0 \ , \tag{16}$$

where

$$j_n = a\phi_n := \tfrac{1}{2}\, a(\dot{x}_{n+1} + \dot{x}_n)\, F(x_{n+1} - x_n) \tag{17}$$

which can thus be interpreted as the local heat flux.

More in general, if density fluctuations cannot be neglected, a different approach has to be followed in order to determine a workable expression for j_n. The key idea consists in Fourier transforming Eq. (9),

$$\frac{\mathrm{d}\tilde{h}(k,t)}{\mathrm{d}t} = -\mathrm{i}k\tilde{j}(k,t) \ , \tag{18}$$

where

$$\tilde{h}(k,t) = \int \mathrm{d}x\, h(x,t)\mathrm{e}^{-\mathrm{i}kx} \quad \tilde{j}(k,t) = \int \mathrm{d}x j(x,t)\mathrm{e}^{-\mathrm{i}kx} \ . \tag{19}$$

In fact, according to the idea that the heat flux is a macroscopic observable, one can define it as the component of $\tilde{h}(k,t)$ that is proportional to the wave-vector k, i.e. the leading contribution over sufficiently large scales. From Eq. (10),

$$\frac{\mathrm{d}\tilde{h}(k,t)}{\mathrm{d}t} = \sum_n \left(\frac{\mathrm{d}h_n}{\mathrm{d}t} - \mathrm{i}k\dot{x}_n h_n\right)\mathrm{e}^{-\mathrm{i}kx_n} \ . \tag{20}$$

From Eq. (15), the first sum in the r.h.s. can be written by a suitable shift of indexes as

$$\sum_n \frac{\mathrm{d}h_n}{\mathrm{d}t}\,\mathrm{e}^{-\mathrm{i}kx_n} = \frac{1}{2}\sum_n (\phi_n - \phi_{n-1})\mathrm{e}^{-\mathrm{i}kx_n} = \frac{1}{2}\sum_n \phi_n \mathrm{e}^{-\mathrm{i}kx_n}(1 - \mathrm{e}^{-\mathrm{i}k(x_{n+1}-x_n)}) \ . \tag{21}$$

In the low-k limit, the above expression reduces to

$$\sum_n \frac{\mathrm{d}h_n}{\mathrm{d}t}\,\mathrm{e}^{-\mathrm{i}kx_n} \approx -\frac{\mathrm{i}k}{2}\sum_n (x_{n+1} - x_n)\phi_n \mathrm{e}^{-\mathrm{i}kx_n} \ . \tag{22}$$

By replacing this expression back into Eq. (21) and with the help of Eq. (18), we find that

$$j_n = \tfrac{1}{2}\,(x_{n+1} - x_n)(\dot{x}_{n+1} + \dot{x}_n)F(x_{n+1} - x_n) + \dot{x}_n h_n \ . \tag{23}$$

In the limit of small oscillations (compared to the lattice spacing), the second term in the above formula can be neglected and $x_n - x_{n-1} \simeq a$, so that Eq. (23) reduces to definition (17). Another class of systems for which energy fluctuations can be neglected is that for which the canonical variable "x_n" does not describe the longitudinal motion along the chain, but corresponds to different degrees of freedom (e.g., transversal oscillations or the rotation of a classical spin). In all such cases,

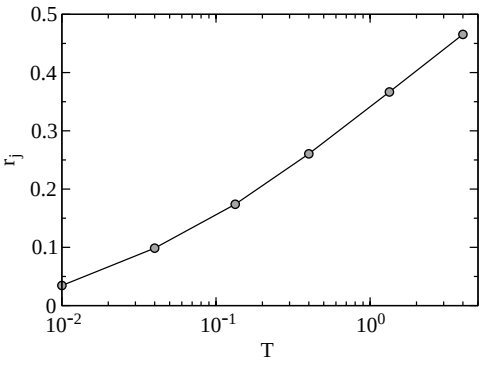

Fig. 2. The ratio r_j between the two contributions to the heat flux versus temperature in a chain of 32 particles with nearest-neighbor Lennard–Jones interactions. T is the average temperature of the two reservoirs while the temperature difference ΔT is set equal to $T/2$.

the position where the energy h_n is localized along the chain is fixed in time and, accordingly, no term proportional to h_n can arise.

In order to give a flavor of the relative weight of the two contributions to the heat flux, we have studied a chain of equal-mass particles interacting through the Lennard–Jones potential (3). In the low-temperature limit, the chain behaves indeed as a solid, and we expect that the ratio

$$r_j = \frac{\langle 2\dot{x}_n h_n \rangle}{\langle (x_{n+1} - x_n)(\dot{x}_{n+1} + \dot{x}_n) F(x_{n+1} - x_n) \rangle} \tag{24}$$

goes to 0. In the opposite limit $T \to \infty$, the only relevant interaction is the repulsive part of the potential that is responsible for elastic collisions, i.e. the system becomes equivalent to a hard-point gas. In this limit, the only relevant contribution to the heat flux arises from the kinetic term of h_n, i.e.

$$j_n \approx \tfrac{1}{2} m_n \dot{x}_n^3 \ . \tag{25}$$

This can be understood by looking at the integral of the flux over the average time between consecutive collisions of the same two particles. The first term in the r.h.s. of Eq. (23) is not negligible only during the infinitesimal collision time when, however, the distance $x_{n+1} - x_n$ vanishes. Therefore, in spite of the Dirac δ behaviour of the force, its integral contribution remains negligible. Analogously, the term $\dot{x}_n V(x_{n+1} - x_n)$, arising from the potential energy, does not contribute, since V remains finite during the collision. Such a conclusion is confirmed by numerical simulations which show that the average value of j_n as defined in Eq. (25) coincides with the energy flux through the boundaries.

Altogether, r_j is expected to diverge for increasing temperature. This is illustrated in Fig. 2, where we report the data resulting from the simulation of a chain put in contact with two heat reservoirs with a temperature difference $\Delta T = T/2$ and average temperature T.[3]

[3] The numerical results have been obtained by implementing a Nosé-Hoover thermostat with $\Theta = 1$—see the next chapter for further details about the thermostat scheme.

Most non-linear models, aiming at a characterization of solid-like structures have been written with reference to the deviation $q_n = x_n - na$ from the equilibrium position na. This is, for instance, the case of the FPU models (4) that can be seen as the result of truncating the expansion of the potential energy in powers of $(q_n - q_{n+1})$. The result of introducing the displacement q_n and getting rid of the actual position x_n, is that physical distances disappear from the model and the lattice spacing becomes an arbitrary value. As a consequence, if a is chosen too small, one can have unphysical pictures of particles crossing each other and yet keeping the same nearest neighbors. A meaningful interpretation of such models is obtained only by associating them with a sufficiently large spacing a and thus by computing the heat flux from the definition (17).

Finally, we want to introduce a less symmetric but more compact expression for j_n that can be obtained by exploiting the equality $\langle \dot{V}(q_{n+1} - q_n)\rangle = 0$ that holds in the stationary regime. By determining the derivatives from the equations of motion, we find that

$$\langle \dot{q}_{n+1} F(q_{n+1} - q_n)\rangle = \langle \dot{q}_n F(q_{n+1} - q_n)\rangle \tag{26}$$

which allows expressing the average local heat flow as

$$\langle j_n\rangle = a\langle \dot{q}_{n+1} F(q_{n+1} - q_n)\rangle \ . \tag{27}$$

In the stationary regime, it is easily seen that the equality $\langle \mathrm{d}/\mathrm{d}t(\dot{q}_n)^2\rangle = 0$ implies that

$$\langle \dot{q}_n F(q_{n+1} - q_n)\rangle = \langle \dot{q}_n F(q_n - q_{n-1})\rangle \ . \tag{28}$$

The combined use of Eqs. (26) and (28) for suitable values of n shows that in the bulk

$$\langle j_n\rangle = \langle j_{n-1}\rangle := j \ . \tag{29}$$

Accordingly, the average local heat flux is constant along the chain as it should. At the boundaries, one finds that, for whatever choice of the heat bath, the heat flux equals the energy flow towards the corresponding reservoir. This can be seen by just writing the balance equation for the kinetic energy of the first (last) particle of the chain.

The quantity that will be mostly used in the following is the total heat flux

$$J = \sum_n j_n \ . \tag{30}$$

Notice that, from definition (29), $\langle J\rangle = Nj$ in the stationary regime. From definition (23), J is readily recognized to be the one-dimensional version of the general expression (see e.g. [25])

$$\mathbf{J} = V\mathbf{j} = \sum_i \left[\dot{\mathbf{x}}_i h_i + \frac{1}{2} \sum_{j\neq i} (\mathbf{x}_i - \mathbf{x}_j)(\dot{\mathbf{x}}_i + \dot{\mathbf{x}}_j)\mathbf{F}_{ij} \right] \tag{31}$$

which is valid for every state of the matter.

To understand better the physical meaning of the definition given above and for later reference, it is useful to consider the case of the simple harmonic chain, i.e. (4) with $g_3 = g_4 = 0$ and $m_n = m$. If periodic boundary conditions are assumed, the Hamiltonian is diagonalized by passing to the normal

coordinates

$$Q_k = \frac{1}{\sqrt{N}} \sum_{l=1}^{N} q_l \, \mathrm{e}^{\mathrm{i}(2\pi k/N)l}, \quad Q_{-k} = Q_k^*, \quad k = -\frac{N}{2} + 1, \ldots, \frac{N}{2} \ . \tag{32}$$

Considering, for simplicity, definition (17) we get the expression for the total heat flux (30)

$$J_{\mathrm{H}} = \mathrm{im} \sum_k v_k \omega_k Q_k \dot{Q}_k^* \ , \tag{33}$$

where $v_k = \omega_k'$ is the group velocity of phonons and the mode frequencies are given by

$$\omega_k = 2\sqrt{\frac{g_2}{m}} \left| \sin\left(\frac{\pi k}{N}\right) \right| \ . \tag{34}$$

It is furthermore convenient to introduce the complex amplitudes a_k through the standard transformations

$$Q_k = \frac{1}{2}\left(a_k \mathrm{e}^{\mathrm{i}\omega_k t} + a_{-k}^* \mathrm{e}^{-\mathrm{i}\omega_k t}\right), \quad \dot{Q}_k = \frac{\mathrm{i}\omega_k}{2}\left(a_k \mathrm{e}^{\mathrm{i}\omega_k t} - a_{-k}^* \mathrm{e}^{-\mathrm{i}\omega_k t}.\right) \ . \tag{35}$$

A straightforward calculation shows that the heat flux can be expressed as

$$J_{\mathrm{H}} = \sum_k v_k E_k \ , \tag{36}$$

where $E_k = \frac{1}{2} m\omega_k^2 |a_k|^2$ is interpreted as the energy in the kth normal mode. This expression, originally proposed by Peierls [2], has a simple intuitive interpretation and shows that the heat flux is a constant of motion for the harmonic chain at equilibrium. Notice also that its equilibrium average $\langle J_{\mathrm{H}} \rangle = 0$ as it should: this stems from equipartition of energy $\langle E_k \rangle = k_{\mathrm{B}} T$ and from the fact that $v_k = -v_{-k}$.

3. Heat baths

Theoretical and numerical investigations of statistical mechanical systems invariably rely upon a suitable modeling of the interaction with thermal reservoirs. At equilibrium, this is usually accomplished by well known methods like micro-canonical molecular dynamics and Monte Carlo simulations. Out of equilibrium, the lack of a general theoretical framework forces to define meaningful interactions with external thermal baths. The importance of such approach to simulations of transport processes in crystalline solids has been already recognized since decades [26].

Conceptually, the correct way to proceed requires considering non-equilibrium states of infinite systems. In the context of this review, one could imagine, for example, an infinite chain with an initial condition such that all atoms to the left and to the right of some prescribed subset (defining the system of interest) are in equilibrium at different temperatures. However, the only specific case in which such an approach can be effectively implemented is that of harmonic systems [27–30]. In fact, the degrees of freedom corresponding to the dynamics of the reservoirs can be traced out and, as a result, one can prove the existence of stationary non-equilibrium states and thereby determine the relevant thermodynamic properties. As soon as non-linear effects are included, it is no

longer possible to reduce the evolution of the heat baths to a tractable model. One can, nevertheless, study non-linear chains by assuming that non-linearity is restricted to the system of interest, while still considering linear interactions for the semi-infinite chains that correspond to the two reservoirs. By following this approach, several results have been obtained (see Ref. [3] and references therein). In particular, it has been recently proved the existence of a unique invariant non-equilibrium measure in chains of highly non-linear coupled oscillators subject to arbitrary large temperature gradients [31].

If the baths are modeled with linear wave equations (the continuum limit of the harmonic lattice), the Hamiltonian dynamics of the full system reduces to the stochastic Markovian evolution of a few variables. In the simplest coupling scheme, one can write [3]

$$\begin{aligned} m_n\ddot{q}_n &= -F(q_{n+1}-q_n)+F(q_n-q_{n-1})+r_+\delta_{n1}+r_-\delta_{nN}\ , \\ \dot{r}_+ &= -\gamma_+(r_+-\lambda_+q_1)+\xi_+\ , \\ \dot{r}_- &= -\gamma_-(r_--\lambda_-q_N)+\xi_-\ , \end{aligned} \tag{37}$$

where the $\xi_\pm$'s are independent Wiener processes with zero mean and variance $2\gamma_\pm\lambda_\pm T_\pm$. Moreover, $\lambda_\pm$ is the coupling strength between the chain and the corresponding bath, while $1/\gamma_\pm$ is the relaxation time. This approach is rather recent and we are not aware of any numerical study where it is implemented and compared with other methods.

3.1. Stochastic baths

A traditional way to implement the interaction with reservoirs amounts to introducing simultaneously random forces and dissipation according to the general prescription of fluctuation-dissipation theorem. This could be regarded as the limit case of the previous model when $\gamma_\pm$ becomes very large. Consequently, the reservoirs are not affected by the system dynamics. In the simple case of an equal-mass chain, this results in the following set of Langevin equations:

$$m\ddot{q}_n = F(q_n-q_{n-1})-F(q_{n+1}-q_n)+(\xi_+-\lambda_+\dot{q}_n)\delta_{n1}+(\xi_--\lambda_-\dot{q}_n)\delta_{nN}\ , \tag{38}$$

where $\xi_\pm$'s are again independent Wiener processes with zero mean and variance $2\lambda_\pm k_B T_\pm$. In practice, this model too is amenable only to numerical investigation for non-linear forces.

Once the non-equilibrium stationary state is attained, one evaluates the average flux j defined in (29) and estimates the thermal conductivity as $\kappa = |j|L/\Delta T$ where $\Delta T = T_+ - T_-$. The average flux can be obtained also directly from the temperature profile. In fact, direct stochastic calculus shows that the average amount of energy exchanged between the first particle and the hot reservoir is

$$j(\lambda,N) = \frac{\lambda_+}{m_1}(T_+ - T_1) \tag{39}$$

and an equivalent expression holds on the opposite boundary. This formula states that the heat flux is proportional to the difference between the kinetic temperature of the particle in contact with the heat bath and the temperature of the reservoir itself.

A "microscopic" implementation that has been widely used amounts to imagining each reservoir as a one-dimensional ideal gas of particles of mass $M_\pm$ interacting with the chain through elastic collisions [32]. A simple strategy consists in selecting a random sequence of times t_i when each

thermostated atom collides with a particle of the corresponding reservoir. A natural choice for the distribution $W(\tau)$ of the intervals τ between consecutive collisions would be the Poissonian

$$W(\tau) = \frac{1}{\bar{\tau}} \exp\left(-\frac{\tau}{\bar{\tau}}\right) \ , \tag{40}$$

where $\bar{\tau}$ is the average collision time. The kinematics of the collision implies that

$$\dot{q}_1 \to \dot{q}_1 + \frac{2M_+}{m + M_+}(v - \dot{q}_1) \tag{41}$$

for the left reservoir (an analogous expression holds for the right one). The velocity v of the gas particle is a random variable distributed according to the Maxwellian distribution [4]

$$P_+(v) = \sqrt{\frac{M_+}{2\pi k_B T_+}} \exp\left(-\frac{M_+ v^2}{2k_B T_+}\right) \ . \tag{42}$$

In the case $M_\pm = m$, the procedure reduces to assigning the velocity after the collision equal to random variable v (the particles exchange their velocities). On the other hand, in the limit $M_\pm \ll m$, the interaction with the heat baths becomes Langevin-type as in Eq. (38) with $\lambda_\pm = 2M_\pm/\bar{\tau}$.

This method is computationally very simple, as it avoids the problem of dealing with stochastic differential equations: the integration can, in fact, be performed by means of conventional algorithms. In particular, the explicit absence of dissipation allows using symplectic integration schemes [33,34] between collisions. Furthermore, a physically appealing feature of this approach is that damping is not included a priori in the model, but is self-consistently generated by the dynamics.

A related but different scheme consists in determining the collision times from the interaction with "thermal walls" suitably placed at the boundaries of the chain. This method has the advantage of allowing for the inclusion of pressure effects in the molecular dynamics simulation. In this case, the velocity of the thermostated particle is randomized whenever it reaches the wall. While the sign of the velocity component normal to the wall has to be chosen in order to ensure that it is reflected, its modulus has to be distributed according to a Maxwellian distribution at the wall temperature (see Ref. [35] for a discussion of possible pitfalls of different choices).

3.2. Deterministic baths

In the attempt of providing a self-consistent description of out-of-equilibrium processes, various types of deterministic heat baths have been introduced [36]. This was also motivated by the need to overcome the difficulties of dealing with stochastic processes. The scheme that has received the largest support within molecular-dynamics community is perhaps the so-called Nosé-Hoover thermostat [37,38]. More precisely, the evolution of the particles in thermal contact with the bath α is ruled by the equation

$$m\ddot{q}_n = F(q_n - q_{n-1}) - F(q_{n+1} - q_n) - \begin{cases} \zeta_+ \dot{q}_n & \text{if } n \in S_+ \ , \\ \zeta_- \dot{q}_n & \text{if } n \in S_- \ , \end{cases} \tag{43}$$

[4] In one-dimension, it coincides with the Gaussian distribution.

where $\zeta_\pm$ are two auxiliary variables modeling the microscopic action of the thermostat, and $S_\pm$ denote two sets of $N_\pm$ particles (at the beginning and the end of the chain, respectively) in contact with the reservoirs.

The dynamics of $\zeta_\pm$ is governed by the equation

$$\dot{\zeta}_\pm = \frac{1}{\Theta_\pm^2}\left(\frac{1}{k_B T_\pm N_\pm}\sum_{n\in S_\pm} m\dot{q}_n^2 - 1\right) , \tag{44}$$

where $\Theta_\pm$ are the thermostat response times. The action of the thermostat can be understood in the following terms. Whenever the (kinetic) temperature of the particles in $S_\pm$ is, say, larger than $T_\pm$, $\zeta_\pm$ increases becoming eventually positive. Accordingly, the auxiliary variable acts as a dissipation in Eq. (43). Since the opposite occurs whenever the temperature falls below $T_\pm$, this represents altogether a stabilizing feedback around the prescribed temperature. Actually, the justification of this scheme rests on a more solid basis. In fact, in Refs. [37,38], it has been shown to reproduce the canonical equilibrium distribution.

In the limit case $\Theta \to 0$, the model reduces to the so-called isokinetic (or Gaussian) thermostat: the kinetic energy is exactly conserved and the action of the thermal bath is properly described without the need to introduce a further dynamical variable, since $\zeta_\pm$ becomes an explicit function of the $\dot{q}$'s [36]:

$$\zeta_\pm = \frac{\sum_{n\in S_\pm} \dot{q}_n[F(q_n - q_{n-1}) - F(q_{n+1} - q_n)]}{\sum_{n\in S_\pm} \dot{q}_n^2} . \tag{45}$$

This latter thermostat scheme can be derived by variational methods after including the non-holonomic constraint due to the imposed kinetic energy conservations [36].

More generally, it has been shown in Refs. [37,38] that the dynamical equations of this entire class of deterministic thermostats possess a Hamiltonian structure in a suitably enlarged phase-space. An interesting property that is preserved by the projection onto the usual phase space is time-reversibility. In fact, a simple inspection of the equations reveals that they are invariant under time reversal composed with the involution I

$$\dot{q}_n \to -\dot{q}_n \quad n = 1,\ldots,N, \quad \zeta_\pm \to -\zeta_\pm . \tag{46}$$

This property represents the main reason for the success of this class of thermostats, since dissipation is not included a priori, but it rather follows self-consistently from the dynamical evolution. In particular, at equilibrium $\langle\zeta_\pm\rangle = 0$, indicating that the action of the bath does not break microscopic reversibility, while out of equilibrium $\langle\zeta_+\rangle + \langle\zeta_-\rangle > 0$ and this value has been connected with entropy production [39].

Another procedure can be defined by combining the idea of a thermostat acting through collisions at the boundaries with that of a deterministic and reversible rule for the collisions themselves. The first context where a scheme of this type has been successfully introduced is that of sheared fluids [40]; more recently, van Beijeren [41] has proposed an implementation that is suitable for one dimensional systems. The idea is very similar to that of the above discussed thermal wall with the crucial difference that the velocity v' after the collision is a deterministic and reversible function

$v' = \Phi(v)$ of the initial velocity v. A class of reversible transformations is that defined as $\Phi = GRG^{-1}$, with $R = R^{-1}$. A further constraint is that the equilibrium distribution be left invariant under the transformation Φ. The choice adopted in Ref. [90] consists in fixing $G(v) = \exp(-mv^2/k_B T)$ and $R(x) = 1 - x$. According to this choice, G transforms the Maxwellian distribution into a uniform one on the unit interval, which, in turn, is left invariant by R. Although this and the previous choices of reversible thermostats do not correspond to any physical mechanism, they offer a convenient framework for the application of dynamical-system concepts [39].

In the above methods, the system is driven out of equilibrium by a suitable forcing at the boundaries: an approach that is aimed at closely reproducing experimental conditions. A different philosophy [36] consists in introducing an external field acting in the bulk of the system to keep it steadily out of equilibrium. The main advantage of this approach is the possibility to work with homogeneous systems with, e.g. a uniform temperature along the whole sample. In particular, periodic boundary conditions can be enforced thus further reducing finite-size effects. This is sometimes referred to as the Evans heat-flow algorithm and has been applied to heat conduction in one-dimensional lattices [42–44].

More precisely, a fictitious heat field $F_e D_n$ is added to the equation of motion for the nth particle. The coupling D_n must satisfy two conditions: (i) the energy dissipation is proportional to jF_e, i.e., $\dot{H} = NjF_e$; (ii) phase-space flux remains divergence-free (this is referred to as the adiabatic incompressibility of phase space [36]). Finally, in order to stabilize the dynamics at a prescribed temperature, a thermostat rule has to be applied. The resulting equation of motion reads as

$$m\ddot{q}_n = F(q_n - q_{n-1}) - F(q_{n+1} - q_n) + F_e D_n - \zeta \dot{q}_n \ . \tag{47}$$

A definition of D_n satisfying the above requirements is [44]

$$D_n = \frac{1}{2}[F(q_{n+1} - q_n) + F(q_n - q_{n-1})] - \frac{1}{N}\sum_{j=1}^{N} F(q_{j+1} - q_j) \ , \tag{48}$$

Moreover, we can consider a Gaussian thermostat:

$$\zeta = \frac{1}{2K_0}\sum_{j=1}^{N} \dot{q}_j [F(q_n - q_{n-1}) - F(q_{n+1} - q_n) + F_e D_j] \ ,$$

$$K_0 = \frac{m}{2}\sum_{j=1}^{N} \dot{q}_j^2 \ . \tag{49}$$

Notice that at variance with the previous schemes, the thermostat acts on all particles (this is possible since we recall that the temperature is uniform).

The thermal conductivity can then be determined from the ratio of the heat flux to the applied heat field

$$\kappa = \lim_{F_e \to 0} \frac{\langle j \rangle}{T F_e} \ , \tag{50}$$

where $\langle j \rangle$ can be equivalently interpreted as a time average or a suitable ensemble average. Furthermore, the limit $F_e \to 0$ is dictated by the need to ensure the validity of the linear

response theory that is implicitly contained in the initial assumptions. This requirement is all the way more substantial in view of the difficulties encountered while working with too large heat fields [44] (to some extent this is also true for the Nosè-Hoover method described above [45]).

3.3. Comparison of different methods

In all schemes of heat baths there is at least one parameter controlling the coupling strength: let us generically call it g. It can either be the inverse of the average time between subsequent collisions, or the dissipation rate λ in the Langevin equation, or the inverse of the time-constant Θ in the Nosé-Hoover scheme. Fixing g is a practical question which is usually solved empirically by insuring that different choices do not appreciably affect the outcomes of a simulation. On general grounds, one should start by choosing g to be of the order of some typical frequency of the system [46]. In the present context, an interesting question immediately arises about the dependence of heat transport on g in the various schemes.

In the case of stochastic reservoirs, the heat flux vanishes both in the weak-($\lambda \to 0$) and strong-coupling ($\lambda \to \infty$) limit. The first implication follows quite easily from the relation (39) and from the observation that $(T_+ - T_1)$, cannot increase above $(T_+ - T_-)$ (more precisely, one expects that $T_1 \to (T_+ + T_-)/2$ for $\lambda \to 0$, since the profile should become increasingly flat). The opposite regime is less trivial: here below, we explain why the same qualitative behavior can be found in two different heat-bath schemes. Let us first consider a reservoir acting through collisions separated by random intervals τ. In this case the coupling constant g is given by the inverse of the average collision time $\bar{\tau}$. For small $\bar{\tau}$, one can rely on a perturbative approach and write the kinetic energy K_1 a time $\bar{\tau}$ after the collision as (it is sufficient to consider the first particle)

$$K_1 = (v + F\bar{\tau})^2 \tag{51}$$

where v is the random, "initial" velocity. As a result, K_1, on the average, changes by an amount that is proportional to $\bar{\tau}^2$, since v has zero average. This means that the deviation of the (kinetic) temperature from the equilibrium value is also proportional to $\bar{\tau}^2$. In order to have the energy flux one should multiply this contribution by the number $1/\bar{\tau}$ of collisions per unit time. Accordingly, we find that the flux goes to zero as $1/g$ in the strong coupling limit. It is interesting to notice that the quadratic dependence of the energy could also be inferred from the invariance under time reversal of the microscopic equations: after a collision there should be no difference between choosing the forward or backward direction for the time axis: as a result we have to expect a quadratic behavior!

Rather similar is the analysis for thermal baths *à la* Langevin. In that case, for large λ, $\dot{q}_1$ can be adiabatically eliminated, giving rise to

$$\dot{q}_1 = \frac{\xi}{\lambda} + \frac{F}{\lambda} \ . \tag{52}$$

Again, one can see that the average value of the kinetic temperature deviates $\mathcal{O}(1/\lambda^2)$ from the equilibrium one.

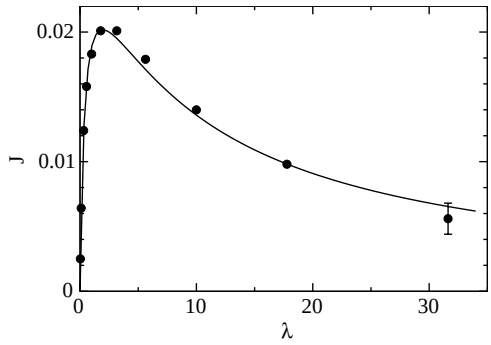

Fig. 3. Heat flux dependence on the coupling constant λ for an FPU chain in contact with two Langevin stochastic reservoirs at temperature $T_+ = 1.1$ and $T_- = 0.9$. The chain length is $N = 128$ and fixed b.c. have been imposed.

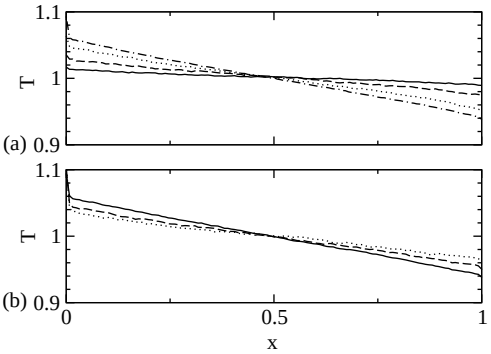

Fig. 4. Temperature profile in the same set up of the previous figure. In panel (a), the profiles correspond to (from bottom to top in the left part) $\lambda = 10^{-3/2}, 10^{-1}, 10^{-1/2}, 10^{0}$; panel (b) refers to the strong coupling case. Again from bottom to top in the left part, the curves correspond to $\lambda = 10^{1/4}, 10^{3/4}, 10$.

The simplest way to combine the behavior of the average flux in the strong and weak coupling limit is through the following heuristic formula

$$j(\lambda) = \frac{a\lambda}{1 + b_1\lambda + b_2\lambda^2} \tag{53}$$

that exhibits the expected λ dependence in both limits $\lambda \to 0$ and $\lambda \to \infty$. In Fig. 3 we have plotted the flux for an FPU chain in contact with stochastic Langevin heat baths. Circles correspond to direct numerical results, while the solid curve is a fit with formula (53). The parameter values turn out to be $a = 0.07$, $b_1 = 2.45$, and $b_2 = 0.26$. The good agreement is to be considered as rather incidental, given the heuristic nature of the fitting formula.

For what concerns the temperature profile, one can see from panel (a) of Fig. 4 that it is increasingly flat for $\lambda \to 0$. Less obvious is the tendency of the profile to become flat also in the strong coupling-limit. In fact, there is a small but crucial difference for the temperature of the first and last particle. For $\lambda \to 0$ the temperature of the extremal particles obviously tends to be equal to that in

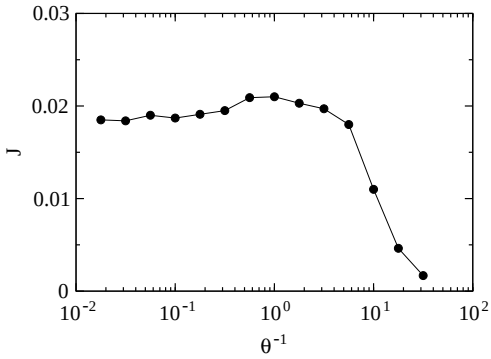

Fig. 5. Heat flux dependence on the coupling constant $1/\Theta$ for an FPU chain in contact with two Nosé-Hoover reservoirs at temperature $T_+ = 1.1$ and $T_- = 0.9$. The chain length is $N = 128$ and fixed b.c. have been imposed. The line is just a guide for the eyes.

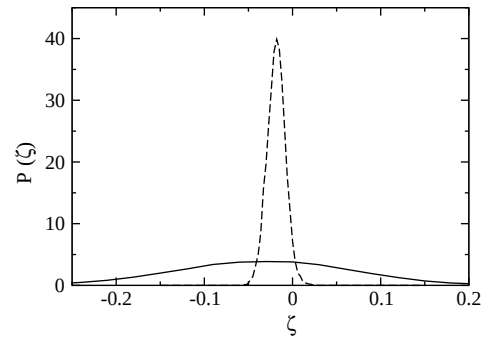

Fig. 6. Histogram $P(\zeta)$ of the left-heat variable in an FPU chain in the same condition as in the previous figure and two different values of Θ: 10 (solid line), 100 (dashed line).

the bulk; on the contrary for $\lambda \to \infty$, such temperatures converge to the temperature of the reservoir. In other words the temperature-drop is observed between the boundary particle and its neighbor.

If we repeat the same analysis by using Nosé-Hoover thermostats, we find a similar behavior in the strong coupling limit. Indeed, in Fig. 5 we see that the heat flux vanishes when the response time Θ goes to 0. This is the limit of a strictly isokinetic bath and, one is, therefore, bound to conclude that such a type of heat baths are unable to sustain heat transport (as long as one single particle is thermalized at each extremum). Perhaps more surprising is the opposite limit $\Theta \to \infty$, since we can see that the heat flux does not go to zero even though the action of the heat baths becomes increasingly slow.

A partial understanding of this unexpected behavior comes from the observation that the variable ζ, though slowly, reaches the same asymptotic values for arbitrarily large time constants Θ. This is illustrated in Fig. 6 where we have plotted the histogram of ζ values for $\Theta = 10$ (solid line) and 100 (dashed line). Both curves are clean Gaussians centered around the same value -0.018 but with standard deviations differing by a factor 10 (the same factor existing between the time constants).

In practice, we are led to conclude that, in the limit of $\Theta \to \infty$ the distribution of ζ values becomes a δ-function centered at a fixed dissipation value that depends only on the chain length, the energy and the temperature drop. This result seems to be at odds with the fluctuation–dissipation theorem as it seems to suggest that for $\Theta \to 0$ fluctuations disappear while the dissipation remains finite. However, one should notice that a correct measure of the amount of fluctuations is obtained by integrating over a sufficiently long time to let correlations decay: the divergence of the time-constant still ensures the validity of the fluctuation–dissipation theorem.

As a result of this analysis we can conclude that values of Θ of order 1 (in the chosen dimensionless units) are the optimal choices for numerical simulations, since smaller values imply smaller heat fluxes, while larger ones would require longer simulation times (in order to ensure the decay of correlations).

3.4. Boundary resistances

Temperature discontinuities usually appear when heat flux is maintained across an interface among two substances. This discontinuity is the result of a boundary resistance, generally denoted as Kapitza resistance. Its origin is traced back to the "phonon mismatch" between two adjacent substances [47]. Such a phenomenon is invariably present in simulations (see e.g. Fig. 4 and Fig. 21 below) and may actually reduce the accuracy of the measurements. The conductivity evaluated as $\kappa_{\mathrm{eff}} = jL/\Delta T$ represents an effective transport coefficient that includes both boundary and bulk resistances. In practice, one may circumvent the problem by referring to a subchain far enough from the ends and compute a bulk conductivity as the ratio between J and the actual temperature gradient in the subchain. Notice, however, that the advantage of reducing boundary effects may be partly reduced by the increased difficulty of dealing with very small temperature differences.

By denoting with $\delta T_{\pm}$ the temperature jumps at the edges $x=0$ and $x=L$, the imposed temperature difference, $\Delta T = T_+ - T_-$, can be written as

$$\Delta T = \delta T_+ + \delta T_- + \int_0^L \mathrm{d}x\, \nabla T$$

Let us now express the jumps $\delta T_{\pm}$ as [48]

$$\delta T_{\pm} = \epsilon \ell_{\pm} \nabla T|_{\pm} \tag{54}$$

where $\nabla T|_{\pm}$ is the value of the temperature gradient extrapolated at the boundary ($x = 0, L$), $\ell_{\pm}$ is the mean free path at the corresponding temperature; the phenomenological and dimensionless constant ϵ measures the coupling strength between the thermostats and the system.

This equation has been numerically tested by plotting $\delta T/\ell$ versus ∇T for different thermostats [49,50]. From the slope of the various curves it has been found that in the FPU-β model the coupling parameter may vary from $\epsilon = 0.8$ for the thermostats adopted in Ref. [50], to $\epsilon = 2.$ for Nosé-Hoover thermostats, to $\epsilon = 400$ for stochastic reservoirs as evidenced in the large boundary jumps seen, e.g., in Fig. 4. This reflects the empirical fact that the shape of the temperature profile for given $T_{\pm}$ may depend on the choice of thermostats. Nevertheless, the scaling is independent of this choice.

In the near-equilibrium regime, we can assume $\delta T_+ \simeq \delta T_-$, $\ell_+ \simeq \ell_- = \ell$ and the gradient to be constant, $\nabla T|_{\pm} = \nabla T$ obtaining

$$(2\epsilon\ell + L)\nabla T = \Delta T \ . \tag{55}$$

If we further denote by $\kappa = j/\nabla T$ the bulk conductivity we obtain

$$\kappa_{\rm eff} = \frac{j}{\Delta T/L} = \frac{\kappa}{1 + 2\epsilon\ell/L} \ . \tag{56}$$

When the mean free path is much larger than the system size $\ell \gg L$ (the so-called Casimir limit [48]) energy flows almost freely through the system, boundary scattering takes over, the system is almost harmonic with $\kappa_{\rm eff} \propto L$ and a flat temperature profile occurs. In the opposite case $\ell \ll L$, $\kappa_{\rm eff} \simeq \kappa$ and one is indeed probing the bulk interaction.

4. Harmonic systems

The simplest and almost unique class of systems for which one can perform analytic calculations is represented by harmonic chains. Even though they are characterized by a peculiar dynamics, basically because of the integrability of the motion, their behavior can help shedding some light on various aspects of heat conductivity. One of the properties of harmonic chains is the possibility to decompose the heat flux into the sum of independent contributions associated to the various eigenmodes. This analysis is particularly useful to obtain a deeper insight about the role of boundary conditions.

We first discuss the dynamics of homogeneous chains, since it is possible to obtain an analytic expression for the invariant measure in the general case of arbitrary coupling strength. The effect of disorder is discussed in the subsequent section, where perturbative calculations of the relevant quantities are illustrated. For completeness, we also recall the localization properties of the eigenfunctions and self-averaging properties of several observables such as the temperature profile and the heat flux. The approach that we have followed is mainly based on the Fokker-Planck equation and simple stochastic calculus. An important alternative approach based on transmission coefficients can be found in Ref. [28].

4.1. Homogeneous chains

We consider a homogeneous harmonic chain with fixed boundary conditions in contact with stochastic Langevin heat baths. Eq. (38) reduces to

$$\ddot{q}_n = \omega^2(q_{n+1} - 2q_n + q_{n-1}) + \delta_{n1}(\xi_+ - \lambda\dot{q}_1) + \delta_{nN}(\xi_- - \lambda\dot{q}_N) \ , \tag{57}$$

where we have set $\lambda_+ = \lambda_- = \lambda$ to lighten the notations and assumed unitary masses. This set of stochastic equations can be solved [51] by passing to a phase-space description, i.e. by writing down the Liouville equation that, in this case, corresponds to the following Fokker–Planck equation

$$\frac{\partial P}{\partial t} = A_{ij}\frac{\partial}{\partial x_i}(x_j P) + \frac{D_{ij}}{2}\frac{\partial^2 P}{\partial x_i \partial x_j} \ , \tag{58}$$

where here and in the following we adopt the summation convention (i.e., sums over repeated indices are understood without explicitly writing down the summation sign); $x_i = q_i$ for $1 \leqslant i \leqslant N$, $x_i = \dot{q}_i$ for $N < i \leqslant 2N$. A_{ij} and D_{ij} are elements of the $2N \times 2N$ matrices $\mathbf{A}$ and $\mathbf{D}$ that we write in terms

of $N \times N$ blocks

$$\mathbf{A} = \begin{pmatrix} \mathbf{0} & -\mathbf{I} \\ \omega^2 \mathbf{G} & \lambda \mathbf{R} \end{pmatrix}, \quad \mathbf{D} = \begin{pmatrix} \mathbf{0} & \mathbf{0} \\ \mathbf{0} & 2\lambda k_B T(\mathbf{R} + \eta \mathbf{S}) \end{pmatrix} , \tag{59}$$

where we have introduced the average temperature $T = (T_+ + T_-)/2$ and the rescaled temperature difference $\eta = (T_+ - T_-)/T$. Moreover, $\mathbf{0}$ and $\mathbf{I}$ are the null and identity matrices, $\mathbf{G}$ is a tridiagonal matrix defined as

$$G_{ij} = 2\delta_{ij} - \delta_{i+1,j} - \delta_{i,j+1} ,$$

while $\mathbf{R}$ and $\mathbf{S}$ are defined as

$$R_{ij} = \delta_{ij}(\delta_{i1} + \delta_{iN}) ,$$
$$S_{ij} = \delta_{ij}(\delta_{i1} - \delta_{iN}) . \tag{60}$$

The general solution of this equation can be sought of the form

$$P(x) = \frac{\mathrm{Det}\{\mathbf{C}^{-1/2}\}}{(2\pi)^N} \exp\left[-\frac{1}{2} C_{ij}^{-1} x_i x_j\right] , \tag{61}$$

where $\mathbf{C}$ is the symmetric covariance matrix

$$C_{ij} \equiv \langle x_i x_j \rangle \equiv \int \mathrm{d}x\, P(x) x_i x_j \tag{62}$$

By replacing the definition of $\mathbf{C}$ into Eq. (58), one finds that

$$\dot{\mathbf{C}} = \mathbf{D} - \mathbf{A}\mathbf{C} - \mathbf{C}\mathbf{A}^\dagger , \tag{63}$$

where $\mathbf{A}^\dagger$ denotes the transpose of $\mathbf{A}$. Accordingly, the asymptotic stationary solutions can be determined from the following equation [52]:

$$\mathbf{D} = \mathbf{A}\mathbf{C} + \mathbf{C}\mathbf{A}^\dagger \tag{64}$$

In order to solve the problem, let us write $\mathbf{C}$ in terms of $N \times N$ blocks,

$$\mathbf{C} = \begin{pmatrix} \bar{\mathbf{U}} & \bar{\mathbf{Z}} \\ \bar{\mathbf{Z}}^\dagger & \bar{\mathbf{V}} \end{pmatrix} , \tag{65}$$

where the matrices $\bar{\mathbf{U}}$, $\bar{\mathbf{V}}$, and $\bar{\mathbf{Z}}$ express the correlations among positions and velocities,

$$\bar{U}_{ij} = \langle q_i q_j \rangle, \quad \bar{V}_{ij} = \langle \dot{q}_i \dot{q}_j \rangle, \quad \bar{Z}_{ij} = \langle q_i \dot{q}_j \rangle , \tag{66}$$

If the temperatures of the two heat baths coincide (i.e. $\eta = 0$), it can be easily seen that

$$\mathbf{U}_e = \frac{k_B T}{\omega^2} \mathbf{G}^{-1}, \quad \mathbf{V}_e = k_B T\ \mathbf{I}, \quad \mathbf{Z}_e = 0 \tag{67}$$

represent a meaningful solution, since it coincides with the equilibrium Boltzmann distribution $P(x) \approx \exp(-H/k_B T)$.

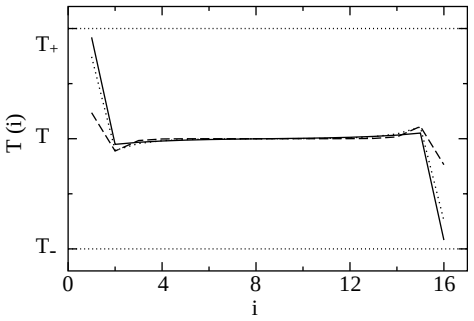

Fig. 7. The temperature profile for the harmonic chain, formula (68), for coupling parameter $v = 0.05$, 0.2, 1.0 (solid, dotted and dashed lines, respectively).

The derivation of the stationary solution in the out-of-equilibrium case is reported in Appendix B. All relevant correlations can be expressed in terms of the function $\phi(j)$ (see Eq. (B.13)) that decays exponentially with the rate α defined in Eq. (B.12). As it can be seen by direct inspection of correlations, α measures the length over which the boundary reservoirs significantly affect the chain dynamics. As expected, α diverges in the weak coupling limit ($v = \omega^2/\lambda^2 \to \infty$).

From Eqs. (B.8) and (B.10), it follows that position–position and velocity–velocity correlations are equal for all pairs of particles (i, j) such that $i+j$ is constant. The qualitative explanation of this property relies on the exponential decay of the boundary effects. In fact, the amplitude of, e.g., $\langle q_i q_j \rangle$ decreasing exponentially with both i and j has to depend on $i + j$. Less obvious is the left-right antisymmetry ($V_{ij} = V_{N-i+1,N-j+1}$), which implies that the boundary effects are exactly the same for the two thermostats, whatever is their temperature. This is nicely reproduced by the temperature profile

$$T(i) = T(1 + \eta V_{ii}) = \begin{cases} T_+ - v\eta T\phi(1), & i = 1 \ , \\ T[1 - \eta v\phi(2i - 1)], & 1 < i \leqslant N/2 \ , \\ T[1 + \eta v\phi(2(N - \mathrm{i}) - 1)], & N/2 < i < N \ , \\ T_- + v\eta T\phi(1), & i = N \ , \end{cases} \tag{68}$$

which exhibits a further unexpected property (see Fig. 7): the temperature is higher in the vicinity of the coldest reservoir (the only exception being represented by the first and last particles)!. Because of the exponential decay of $\phi(i)$, in the bulk, the temperature profile is constant as if the system were at equilibrium at temperature T. However, this is only superficially true, as position-velocity correlations significantly differ from the equilibrium ones.

Also the average stationary local flux can be computed explicitly:

$$j_i = \omega^2 \bar{Z}_{i-1,i} = \frac{\omega^2 k_B T \eta}{\lambda} \phi(1) \ , \tag{69}$$

Eq. (B.5) implies that the value of $Z_{i,k}$ depends only on $i-k$ rather than on $i+k$, as before. Physically, this symmetry reflects the fact that $j_i = j$ independent of the lattice position i in the stationary state.

In the limit of large N, Eqs. (B.12), (B.13) imply

$$j = \frac{\omega^2 k_B T}{2\lambda}\left[1 + \frac{\omega^2}{2\lambda^2} - \frac{\omega}{\lambda}\sqrt{\frac{\omega^2}{4\lambda^2}+1}\right](T_+ - T_-)\ . \tag{70}$$

Accordingly, the heat flux is proportional to the temperature difference rather than to the gradient as it should be, were the Fourier law to be satisfied. This proves that, as expected, homogeneous harmonic chains do not exhibit normal transport properties since the effective conductivity $\kappa = jN/(T_+ - T_-) \propto N$, while the bulk conductivity diverges exponentially, since the temperature gradient away from the baths is exponentially small.

For what concerns the dependence of the flux on λ, we see that J vanishes both in the limit of large and small couplings. The asymptotic expressions

$$j = \begin{cases} \dfrac{\omega^2}{2\lambda} k_B (T_+ - T_-), & \lambda \gg \omega, \\ \dfrac{\lambda}{2} k_B (T_+ - T_-), & \lambda \ll \omega \end{cases} \tag{71}$$

are thus consistent with the heuristic formula (53) derived in the general case. The maximum flux is attained for $\lambda/\omega = \sqrt{3}/2$, a value that is close to the one observed numerically in the non-linear case (see again Fig. 5).

Let us conclude this section by recalling that a similar procedure can be adopted to solve the problem for heat baths characterized by stochastic elastic collisions. In Ref. [51], it is shown that very similar expressions are found also in this case, with only minor quantitative differences in the numerical factors. Furthermore, it is worth mentioning the model of self-consistent reservoirs introduced in Ref. [53], that can be solved exactly.

4.2. Disordered chains

While remaining in the realm of harmonic systems, we now consider the role of disorder on transport properties. More specifically, we shall consider random-mass (or isotopically disordered) chains

$$m_n \ddot{q}_n = q_{n+1} - 2q_n + q_{n-1}\ . \tag{72}$$

As we shall see, boundary conditions play a crucial role, but, for the moment, we leave them unspecified. Before entering in a more detailed discussion it is worth mentioning the general results by Lebowitz and collaborators [27,29]: they showed rigorously that the system approaches a unique stationary non-equilibrium state for a large class of heat baths.

As it is known, the presence of disorder generally induces localization of the normal modes of the chain and one may thus expect the latter to behave as a perfect thermal insulator. Nonetheless, the actual situation turns out to be much more complicated, depending on boundary conditions and on the properties of the thermostats.

Localization of the eigenmodes. To understand the transport properties it is first useful to recall some basic facts about localization. For illustration, let us consider the example of a disordered

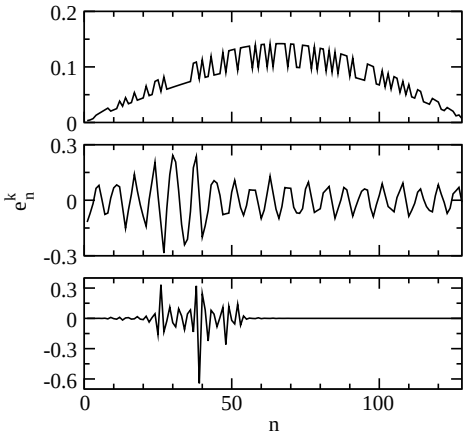

Fig. 8. The first, 41st and 100th eigenvector (from top to bottom) in a chain of 130 particles with random masses with an even distribution of 1 and 1/2 values. The increasing localization with increasing eigenvalue is transparent.

chain with two evenly distributed types of particles. Some of the numerically computed eigenvectors are shown in Fig. 8. Upon ordering them with increasing eigenfrequencies, a distinct difference in their localization properties can be recognized. Indeed, for small frequencies (upper panel of Fig. 8), randomness induces only a relatively weak modulation of the amplitude; a partial localization can be recognized in the intermediate panel, while a clear evidence of localization is visible only for the high-frequency eigenvector reported in the bottom panel.

A rigorous investigation can be performed by applying the transfer matrix approach to the eigenvalue equation. After inserting the expression $q_n = v_n e^{i\omega t}$ in Eq. (72), we obtain

$$-m_n\omega^2 v_n = v_{n-1} - 2v_n + v_{n+1} \ . \tag{73}$$

It is well known that the spectral properties of linear operators involving the discrete Laplacian can be determined from a recursive equation for the new variable $R_n = v_n/v_{n-1}$. The most known example where this approach has been successfully employed is that of Anderson quantum localization in the tight-binding approximation (see, e.g. [54]). In the present context, Eq. (73) yields

$$R_{n+1} = 2 - m_n\omega^2 - \frac{1}{R_n} \ , \tag{74}$$

an equation that can be interpreted as a "discrete time" stochastic equation. The mass m_n plays the role of a noise source (with bias), whose strength is gauged by the frequency ω. In particular, the inverse localization length γ is given by

$$\gamma = \langle \ln R_n \rangle \ , \tag{75}$$

while the integrated density of states $I(\omega)$ follows from node counting arguments, i.e. $I(\omega) = f$, where f is the fraction of negative R_n values. In Fig. 9 it is shown that I increases linearly for small ω and exhibits some irregular fluctuations at larger frequencies. The upper band edge (at $\omega \simeq 2.8$) is easily identifiable as the point above which $I(\omega)$ remains constant and equal to 1. At variance with the standard Anderson problem, where all eigenmodes are exponentially localized, here γ tends to zero for $\omega \to 0$. This can be easily understood from Eq. (74): Since ω^2 multiplies the stochastic

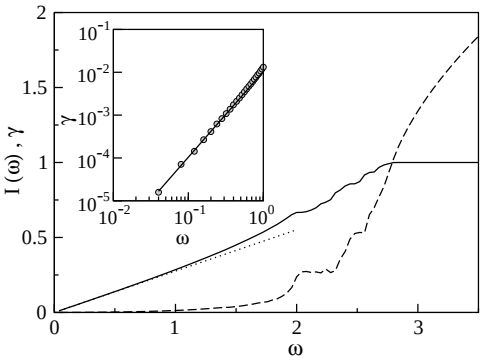

Fig. 9. Integrated density of states, $I(\omega)$ (solid line), and inverse localization length, γ (dashed line), as a function of the frequency ω for a chain with mass disorder: the particles have either mass 1 or 1/2 with equal probability. The dotted line corresponds to the analytic expression (80). In the inset the inverse localization length is plotted in doubly logarithmic scales (circles) and compared with the theoretical formula (83)—solid line.

term, disorder becomes less and less relevant in the small frequency limit. In this limit, one can thus resort to a perturbative approach. Let us start noticing that for $\omega = 0$, $R = 1$ is a marginally stable fixed point of the recursive equation (74). For small ω, an intermittent process sets in: after a slow drift driving R_n below one, a re-injection to values larger than one occurs and non-linearity becomes suddenly relevant. The process repeats again and again. By writing $R_n = 1 + r_n$ and expanding in powers of r_n, we find that the dynamics in the vicinity of $R_n = 1$ is described by

$$r_{n+1} = r_n - r_n^2 - \omega^2\langle m\rangle + \omega^2\delta m \ , \tag{76}$$

where we have included only the first non-linear correction and written separately the average value of the noise term. In the limit of small ω, this equation can be approximated by the Langevin equation

$$\dot{r} = -r^2 - \omega^2\langle m\rangle + \omega^2\delta m \ , \tag{77}$$

where, for the sake of simplicity, we have kept the same notations. The corresponding Fokker–Planck equation writes

$$\frac{\partial P}{\partial t} = \frac{\partial(r^2 + \omega^2\langle m\rangle)P}{\partial r} + \frac{\sigma_m^2}{2}\frac{\partial^2 P}{\partial r^2} \ , \tag{78}$$

where $\sigma_m^2 = \langle m^2\rangle - \langle m\rangle^2$ stands for the variance of the mass distribution. Given the steady incoming and outcoming flow, the stationary solution can be obtained by imposing

$$(r^2 + \omega^2\langle m\rangle)P + \frac{\sigma_m^2}{2}\frac{\mathrm{d}P}{\mathrm{d}r} = C \ , \tag{79}$$

where C represents the probability flux to be determined by imposing the normalization of the probability density P. Notice also that C can be identified with the integrated density of states $I(\omega)$, since it corresponds to the probability that, at each iterate, R_n is re-injected to the right,

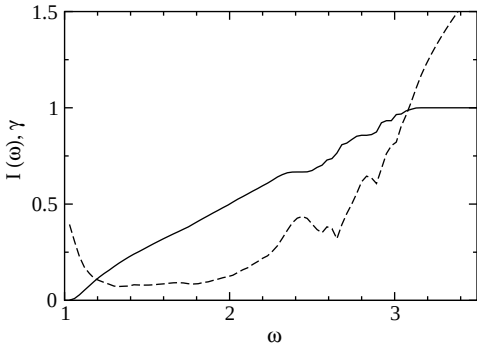

Fig. 10. Integrated density of states, $I(\omega)$ (solid line), and inverse localization length, γ (dashed line) for a random-mass chain as in Fig. 9 with the addition of a unit frequency on-site potential.

i.e. the probability of having a node in the eigenvector. In the absence of disorder ($\sigma_m = 0$),

$$I(\omega) = C = \frac{\sqrt{\langle m \rangle}}{\pi}\,\omega \tag{80}$$

and, correspondingly,

$$P_0(r) = \frac{1}{\pi}\,\frac{\omega\sqrt{\langle m \rangle}}{r^2 + \omega^2\langle m \rangle}\ . \tag{81}$$

This approximation is already sufficient to reproduce the behavior of $I(\omega)$ at small frequencies, as in the limit $\omega \to 0$ the variance of the disorder goes to zero faster than the average value. This is confirmed by comparing the dotted line in Fig. 9 (corresponding to the analytic expression (80)) with the numerically determined integrated density.

On the other hand, the above approximation is not accurate enough to determine the localization length, as disorder is totally disregarded. Indeed, the symmetry of P_0 implies that $\gamma \approx \langle r \rangle = 0$. By going one step further, we can write $P(r)$ as P_0 plus a small perturbation. A simple calculation shows that

$$P(r) = P_0(r) + \frac{\omega^5\sigma_m^2 r\sqrt{\langle m \rangle}}{\pi(r^2 + \omega^2\langle m \rangle)^3} \tag{82}$$

From expression (75) for the inverse localization length γ, we find that

$$\gamma = \langle r \rangle = \frac{\omega^2\sigma_m^2}{8\langle m \rangle} \quad \text{for } \omega \to 0 \tag{83}$$

an equation derived in Ref. [55] (see Fig. 9).

If we add a harmonic on-site potential to Eqs. (72), the corresponding scenario becomes analogous to that of the 1d Anderson problem, with all eigen-functions being exponentially localized. This is illustrated in Fig. 10, where we have added harmonic springs with unit constant (i.e. a force term $-q_n$

acting on the nth particle) to the chain with random masses considered above. The lower band-edge is now strictly bounded away from zero and the inverse localization length does not vanish.

The temperature profile. In order to study the non-equilibrium properties, we need to include the coupling with the thermal reservoirs. Here below, we consider Langevin-type heat baths, as they allow an analytic treatment, though limited to the weak-coupling regime. The starting equation writes

$$m_n\ddot{q}_n = q_{n+1} - 2q_n + q_{n-1} + \delta_{n1}(\xi_+ - \lambda\dot{q}_1) + \delta_{nN}(\xi_- - \lambda\dot{q}_N) \ , \tag{84}$$

where for simplicity we have assumed $\lambda_+ = \lambda_- = \lambda$. Although the equations are still linear, there is no general method to derive an analytic solution for generic values of the coupling constant λ. Accordingly, we restrict ourselves to considering the perturbative regime $\lambda \ll 1$. It is convenient to introduce the new variable

$$u_n = \sqrt{m_n}q_n \ , \tag{85}$$

which allows rewriting Eq. (84) as

$$\ddot{u}_n = \frac{u_{n+1}}{\sqrt{m_n m_{n+1}}} - 2\,\frac{u_n}{m_n} + \frac{u_{n-1}}{\sqrt{m_n m_{n-1}}} + \frac{\delta_{n1}}{m_1}\,(\sqrt{m_1}\xi_+ - \lambda\dot{u}_1) + \frac{\delta_{nN}}{m_N}\,(\sqrt{m_N}\xi_- - \lambda\dot{u}_N) \ . \tag{86}$$

The advantage of this representation is that the operator describing the bulk evolution is symmetric and, accordingly, is diagonalized by an orthogonal transformation. In other words, upon denoting with e_n^k the nth component of the kth eigenvector, it turns out that $\sum_n e_n^k e_n^h = \delta_{kh}$ and $\sum_k e_n^k e_j^k = \delta_{nj}$.

With reference to the new variables $U_k = \sum_n u_n e_n^k$, the equations of motion write as

$$\ddot{U}_k = -\omega_k^2 U_k - \lambda \sum_j C_{kj}\dot{U}_j + \frac{e_1^k}{\sqrt{m_1}}\,\xi_+ + \frac{e_N^k}{\sqrt{m_N}}\,\xi_- \ , \tag{87}$$

where $-\omega_k^2$ is the real, negative kth eigenvalue of the unperturbed evolution operator and

$$C_{kj} = \frac{e_1^k e_1^j}{m_1} + \frac{e_N^k e_N^j}{m_N} \ . \tag{88}$$

Eq. (87) shows that the normal modes are coupled among themselves through the interaction with the reservoirs. Standard stochastic calculus applied to the modal energy $E_k = (\dot{U}_k^2 + \omega_k^2 U_k^2)/2$ shows that the stationarity condition for the time average $\langle \dot{E}_k \rangle = 0$ implies

$$C_{kk}\langle \dot{U}_k^2 \rangle + \sum_{j\neq k} C_{kj}\langle \dot{U}_k \dot{U}_j \rangle = T_+\,\frac{(e_1^k)^2}{m_1} + T_-\,\frac{(e_N^k)^2}{m_N} \ . \tag{89}$$

Let us now show that, in the small-coupling limit, this sum is negligible. In fact, from the equality

$$\frac{\mathrm{d}\langle \dot{U}_k U_h \rangle}{\mathrm{d}t} = 0 \ , \tag{90}$$

we find that

$$\langle \dot{U}_k \dot{U}_h \rangle - \omega_k^2 \langle U_k U_h \rangle - \lambda \sum_j C_{jh} \langle \dot{U}_j U_h \rangle = 0 \ . \tag{91}$$

By solving this equation together with the symmetric expression obtained by exchanging k and h, it is transparent that $\langle \dot{U}_k \dot{U}_h \rangle$ is proportional to λ for $k \neq h$. Accordingly, up to first order in λ, one has

$$\langle \dot{U}_k^2 \rangle = \frac{1}{C_{kk}} \left(T_+ \frac{(e_1^k)^2}{m_1} + T_- \frac{(e_N^k)^2}{m_N} \right) \ . \tag{92}$$

As a consequence, by neglecting first order corrections, the local temperature T_n reads

$$T_n = \left\langle \left(\sum_k \dot{U}_k e_n^k \right)^2 \right\rangle \approx \sum_{k=1}^{N} \frac{(e_n^k)^2}{C_{kk}} \left(T_+ \frac{(e_1^k)^2}{m_1} + T_- \frac{(e_N^k)^2}{m_N} \right) \ . \tag{93}$$

This is basically the expression derived by Matsuda and Ishii [55]. As a consistency check, one can easily verify that if $T_+ = T_- = T$, the local temperature T_n is equal to T for all values of n (this follows from the normalization condition on the eigenvectors). Furthermore, the profile is flat also when $T_+ > T_-$ and the amplitude of all eigenvectors is the same at the two chain-ends: in this case, $T_n = (T_+ + T_-)/2$. An obvious limiting case is the homogeneous chain. Generally speaking, even though the dynamics of a generic disordered chain is statistically invariant under left-right symmetry, the same does not hold true for each individual eigenvector. This induces some spatial dependence that we shall investigate in the following.

Visscher [56] challenged Eq. (93) by arguing that quasi-resonances could be generic enough to affect typical realizations of the disorder. In fact, a crucial assumption in the derivation of the expression for the temperature profile is that cross-correlations in Eq. (93) are negligible. This is basically correct unless pairs of frequencies are sufficiently close to each other, in which case the resonance phenomena should be properly taken into account. Visscher indeed discussed particular examples of mass distributions, where a more refined theory is needed. However, as long as one is interested in generic realizations, the problem is whether quasi-degeneracies in the spectrum are sufficiently frequent to significantly affect the overall validity of formula (93). In all the cases we have considered this issue turned out to be practically irrelevant.

Formula (93) does not allow to obtain an analytic form of the profile since it requires the knowledge of the eigenvectors and, on the other hand, the localization length alone does not suffice to predict their amplitude at the boundaries. Therefore numerical diagonalization of the Hamiltonian for each different realization of the disorder is required. In Fig. 11, we have plotted the stationary temperature profile for a single realization of the disorder versus the rescaled lattice position $x = n/N$. Strong fluctuations accompany an average decrease of the temperature from T_+ to T_-.

This suggests averaging over independent realizations of the disorder in order to better investigate the convergence properties with the system size. In Fig. 12a we have plotted the profile averaged over 1000 realizations. Upon increasing the chain length, the profile seems to slowly attain a linear shape, but sizeable deviations are still present for chains as long as $N = 512$. Such a slow convergence is

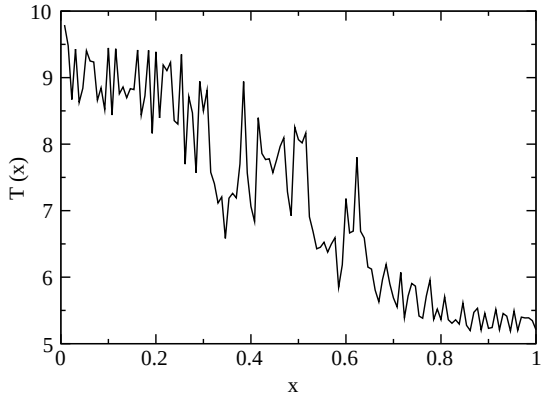

Fig. 11. Temperature profile as predicted from Eq. (93) for a given realization of disorder in a chain of length $N = 128$, with $T_+ = 10$ and $T_- = 5$.

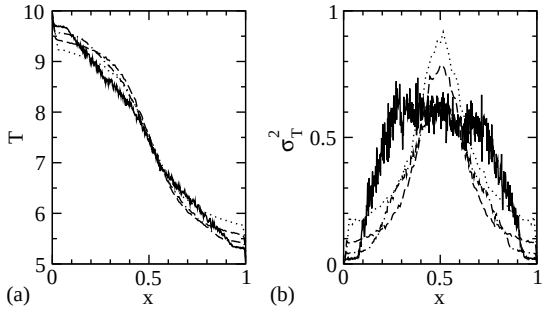

Fig. 12. (a) The disorder-averaged temperature profile as predicted from the formula (93) for different chain lengths (dotted, dashed, dot–dashed and solid curves refer to $N = 64$, 128, 256, and 512, respectively). (b) The variance of the temperature in the same notations as in panel (a).

confirmed in Fig. 12b, where we plotted the sample-to-sample variance σ_T^2 of the temperature field. Although its asymptotic behavior is even less clear, it is at least evident that fluctuations do not vanish in the thermodynamic limit. This is tantamount to saying that the temperature profile is not a self-averaging quantity.

Such difficulties dramatically emerge when performing direct simulations of a disordered chain. This issue is of great practical importance also in view of more complex models where analytical results are not available. The major problem is represented by the extremely slow convergence towards the asymptotic regime that can be explained as follows. Eq. (87) shows that the effective coupling of each eigen-mode with the reservoirs is proportional to its square amplitude at the extrema. Therefore, all eigenmodes that are localized away from the boundaries can thermalize only in astronomically long times. To be more specific, the coupling strength of an eigen-mode characterized by an inverse localization length γ is of order $\exp(-\gamma N)$, since it is localized at a distance equal, on the average, to the half of the chain length. This implies that the asymptotic profile is attained over times that grow exponentially with N. In other words, the stationary state is never

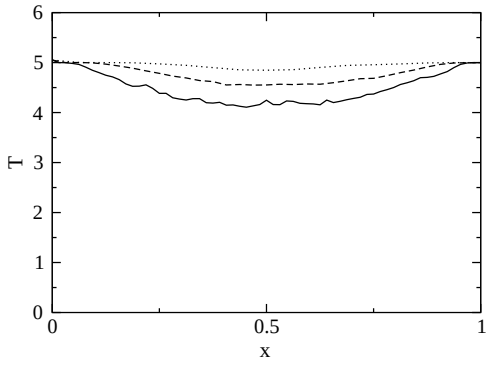

Fig. 13. Average temperature profile of random-mass chains for $N = 16$, 32 and 64 (dotted, dashed and solid curve, respectively). The coupling constant is $\lambda = 1$. The average is performed over 1000 realizations of the disorder each of 5×10^5 time units.

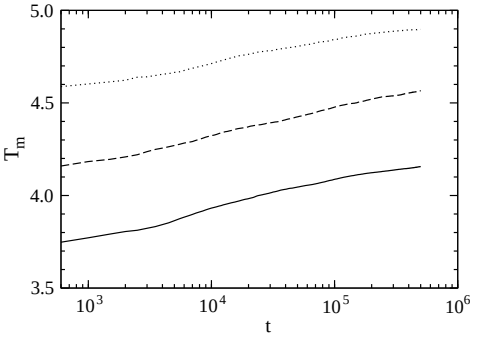

Fig. 14. Behavior of the time average of the temperature in the 5 central sites for $N = 16$, 32 and 64 (dotted, dashed and solid curve, respectively).

reached in the thermodynamic limit. To practically illustrate the issue, we have simulated a chain in contact with two stochastic heat baths operating at the same temperature $T = 5$ (see Fig. 13). To further emphasize the slow convergence, all atoms have been initially set at rest in their equilibrium positions. Even for relatively short chains ($N \sim \mathcal{O}(10^2)$) almost 10^6 time units do not suffice to fully thermalize the bulk. A more direct way of looking at the convergence to the flat temperature profile is by monitoring the cumulative time average T_m, performed on the 5 central sites (and averaged also over different realizations of the disorder). The data reported in Fig. 14, with the choice of a logarithmic scale for the time axis, give an idea of the time needed to reach the equilibrium value $T_m = 5$.

Heat flux. In the case of stochastic heat baths, like those considered in the previous section, one can determine the total heat flux by using Eq. (39). By making use of Eq. (93) we obtain [55,56]

$$j(\lambda, N) = \lambda(T_+ - T_-) \sum_k \frac{(e_1^k)^2 (e_N^k)^2}{m_N (e_1^k)^2 + m_1 (e_N^k)^2} \equiv \sum_k J_k \ , \tag{94}$$

where the kth addendum J_k is naturally interpreted as the contribution of the kth mode. As intuitively expected, the latter is larger for modes that have larger amplitudes at the boundaries and couple thus more strongly with the reservoirs. This interpretation can be justified from Eqs. (87). Indeed, in so far as cross-coupling can be neglected, the dynamics of the kth eigenmode is approximately described by the equation

$$\ddot{U}_k = -\omega_k^2 U_k - \lambda C_{kk}\dot{U}_k + \frac{e_1^k}{\sqrt{m_1}}\xi_+ + \frac{e_N^k}{\sqrt{m_N}}\xi_- \ . \tag{95}$$

Standard stochastic calculus shows that, in the stationary regime, the energy exchanged per unit time with the two thermal baths is equal to J_k, where J_k coincides with the expression implicitly defined by Eq. (94).

However, heat transport is characterized by more subtle mechanisms than one could infer from this simple picture of independent modes. This is immediately understood if we look at the general expression for the local heat flux, Eq. (27), that, in the case of harmonic chains, reduces to

$$j = \langle j_n \rangle = -\langle q_n \dot{q}_{n+1} \rangle \ . \tag{96}$$

By expanding q_n and $\dot{q}_{n+1}$ in eigenmodes, this equation can be rewritten as

$$\langle j_n \rangle = -\sum_{k,h=1}^{N} \frac{e_{n+1}^k e_n^h}{\sqrt{m_n m_{n+1}}} \langle U_k \dot{U}_h \rangle \ , \tag{97}$$

an expression that, in spite of the explicit presence of the subscript n, is independent of n. The interesting point that is made transparent by this formula is that a non-vanishing heat flux is necessarily associated with the existence of *correlations among different modes*. This is all the way more relevant, once we realize that diagonal terms with $k = h$ vanish, being $\langle U_k \dot{U}_k \rangle$ the average of the derivative of a bounded function. This observation seems to be in contrast with the derivation of Matsuda-Ishii formula itself, that is basically obtained by treating all modes as evolving independently of each other. Anyway, we should notice that the heat flux is proportional to λ and this is compatible with the existence of weak modal correlations. In fact, "velocity–velocity" or "position–velocity" correlations may arise from the fact that all eigenmodes are subject to the same noise source (except for a multiplicative factor) and this may well induce a sort of synchronization among them.

The existence of this type of coherence has been numerically investigated and confirmed in Ref. [57], where the behavior of a homogeneous harmonic chain has been thoroughly studied. Here below, we proceed with our perturbative analysis by deriving an analytic expression. Let us start by noticing that the equality $\mathrm{d}\langle U_k U_h \rangle / \mathrm{d}t = 0$ implies that

$$\langle \dot{U}_k U_h \rangle = -\langle \dot{U}_h U_k \rangle \ . \tag{98}$$

This antisymmetry property together with the further equality $\mathrm{d}\langle \dot{U}_k \dot{U}_h \rangle / \mathrm{d}t = 0$ imply that

$$\lambda C_{kh}(\langle \dot{U}_k^2 \rangle + \langle \dot{U}_h^2 \rangle) - (\omega_k^2 - \omega_h^2)\langle \dot{U}_k U_h \rangle = 2\lambda \left(T_+ \frac{e_1^k e_1^h}{m_1} + T_- \frac{e_N^k e_N^h}{m_N} \right) \ . \tag{99}$$

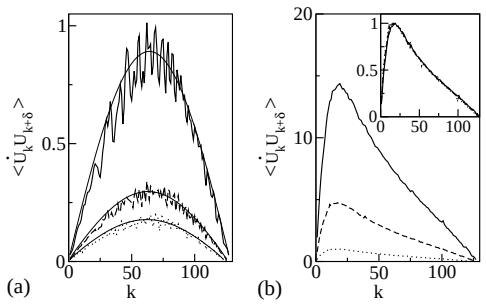

Fig. 15. Modal correlations for a harmonic chain of length $N = 128$ with fixed boundary conditions. Averaging has been performed on a time $t = 10^8$ units. Solid, dashed and dotted curves correspond to $\delta = 1$, 3, and 5, respectively, while the thin lines correspond to the analytic expressions (100). (a) refers to a weak-coupling case: the times between consecutive collisions are uniformly distributed in the interval [19–21]. (b) corresponds to a strong coupling: collision times distributed in [0.9–1.1]. The inset contains the same curves, after rescaling to the maximum values.

After replacing the expression of $\langle \dot{U}_k^2 \rangle$ (see Eq. (92)) in the above equation, the latter can be solved for $\langle \dot{U}_k U_h \rangle$.

Instead of discussing the general case, we prefer to illustrate the presence of these correlations coming back to the simpler case of a homogeneous harmonic chain (see also Ref. [57]). In his context, one can, in principle, obtain a general expression for the correlations by transforming Eq. (B.5) (derived for an arbitrary λ value) in k space. However, the calculations, though straightforward, are rather tedious. Therefore, we limit ourselves to considering the weak-coupling limit. The symmetry of the eigenmodes imply that if $\delta = h - k$ is an even number correlations vanish, while for an odd δ we have

$$\langle \dot{U}_k U_{k+\delta} \rangle = 2 \frac{\lambda (T_+ - T_-)}{m} \frac{e_1^k e_1^{k+\delta}}{\omega_{k+\delta}^2 - \omega_k^2} \ . \tag{100}$$

In Fig. 15a we report the numerical results for a chain of length $N = 128$ with fixed boundary conditions and interacting with two thermal baths at temperatures $T_+ = 75$ and $T_- = 25$. Apart from the residual statistical fluctuations, a reasonable agreement with expression (100) is found upon letting $\lambda = 0.056$ (approximately equal to the inverse of the average separation between consecutive collisions). Fig. 15b shows the results for the same length but a stronger coupling strength. The different shape of the curves is a clear indication that higher order terms must be taken into account, since the perturbative approach implies that the coupling constant acts just as a multiplicative factor. It is anyhow interesting that shape itself is invariant under change of δ as it can be seen in the inset where the three curves are rescaled to their maximum value.

The thermal conductivity. If obtaining an accurate analytic estimate of the heat flux is as difficult as determining the temperature profile, we can at least make use of Eq. (94) to determine its scaling properties. In fact, since high-frequency eigenmodes are strongly localized, it is clear that only the first part of the spectrum contributes significantly to the heat flux. Let thus N_e be the number of modes whose localization length is larger than the sample size N. From Eqs. (80) and (83), it follows that $\gamma \simeq \sigma_m^2 I(\omega)^2 / \langle m \rangle$. Upon writing $I = N_e/N$ and imposing $\gamma = 1/N$,

we find that

$$N_e = \frac{\langle m \rangle}{\sigma_m}\sqrt{N} \ . \tag{101}$$

At this point, it becomes crucial to specify the boundary conditions. Let us first consider the case of free ones: the square amplitude of an extended eigenmode in a lattice of size N is of the order $1/N$. This implies that the contribution to the heat flux of one of such modes is $\lambda(T_+ - T_-)/N$ and the heat flux in Eq. (94) can be estimated as

$$j_{\rm free}(\lambda, N) \propto \lambda(T_+ - T_-)\frac{\langle m \rangle}{\sigma_m}\frac{1}{\sqrt{N}} \ . \tag{102}$$

As a result, the conductivity diverges as

$$\kappa_{\rm free} \propto \lambda \frac{\langle m \rangle}{\sigma_m}\sqrt{N} \ . \tag{103}$$

This scaling was first derived in Ref. [55] and later confirmed in Ref. [58] by means of a different approach. On the other hand, for fixed boundary conditions the result is completely different. In this case all eigenmodes must vanish for $n = 0$ and $n = N + 1$. By approximating the site-to-site variation of e_n^k with the wavenumber k/N, we find that the square amplitude of e_1^k and e_N^k is of order k^2/N^3. As a consequence, summing all such addenda up to $k = N_e$ in Eq. (94) yields

$$j_{\rm fix}(\lambda, N) \propto \lambda(T_+ - T_-)\left(\frac{\langle m \rangle}{\sigma_m}\right)^3 \frac{1}{N^{3/2}} \tag{104}$$

and, accordingly, the thermal conductivity vanishes as

$$\kappa_{\rm fix} \propto \lambda \left(\frac{\langle m \rangle}{\sigma_m}\right)^3 \frac{1}{\sqrt{N}} \ . \tag{105}$$

The above estimates give only the leading orders in N. In view of the previously encountered strong finite-size effects, it is crucial to check directly the convergence to the asymptotic results. To this aim it is convenient to compute the effective exponent

$$\alpha_{\rm eff}(N) = \frac{{\rm d}\ln\kappa}{{\rm d}\ln N} \ . \tag{106}$$

The results are shown in Fig. 16 for the case of fixed boundaries. For weak coupling, the conductivity has been evaluated by numerically computing the eigenvectors and averaging the Matsuda-Ishii formula (94) over 1000 realizations of the disorder. The asymptotic regime $\alpha = -1/2$ is approached very slowly (see the circles): one should consider N values much greater than 10^3. Similar results are found at stronger coupling by directly simulating chains that interact with stochastic baths. The data (diamonds in Fig. 16) suggest that a relatively strong coupling reduces the amplitude of finite-size corrections. Finally, it is important to realize that the small coupling of the exponentially localized modes with the thermal baths does not cause any problem to the temporal convergence of $j(\lambda, N)$, since independently of whether such modes have reached their stationary state, their contribution to the total heat flux is anyhow negligible.

In summary, not only boundary conditions affect the scaling behavior of κ, but they give rise to qualitatively different scenarios: for free boundaries, disordered harmonic chains exhibit an anomalous

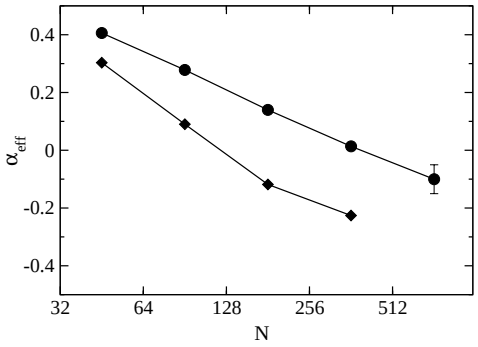

Fig. 16. The effective exponent defined in (106) versus the chain length. The logarithmic derivative has been evaluated with finite differences, subsequent points correspond to chain of double length. Circles are obtained from the Matsuda-Ishii formula, while diamonds correspond to a direct simulation of a chain interacting with stochastic baths operating at $T_+ = 10$ and $T_- = 5$, respectively. The collision times were uniformly distributed in the range [1–2].

conductivity as it diverges in the thermodynamic limit. On the contrary, a disordered chain with fixed boundaries behaves as good insulator! This latter scenario is brought to an extremum if we add an on-site potential. In fact, we have already mentioned that all eigen-functions become exponentially localized and this implies that conductivity is exponentially small in N. This is again very much reminiscent of the electrical conductivity of the Anderson problem.

Dhar [60] went even further and showed how the scaling behavior of the conductivity with the system size depends also *on the spectral properties of the heat baths*. More precisely, if $\kappa \propto N^{\alpha}$ then the exponent α is determined by the low-frequency behavior of the noise spectrum. This implies that a suitable choice of the latter can even lead to a finite conductivity! Such a scenario is less unphysical than it may appear at a first glance. Integrability of the motion implies that the only scattering mechanism that determines the heat resistance is the interaction with the baths. It is therefore reasonable that the actual way in which the latter transfer energy among the modes plays a crucial role.

Modal fluxes. We conclude this section with a discussion of the modal heat fluxes J_k as defined from Matsuda-Ishii formula (94). Besides providing a finer verification of the latter, the analysis is useful in understanding the individual contributions of each "channel" to the heat transport. The spectra J_k obtained for different chain lengths are reported in Fig. 17. They have been scaled each to the maximum J_M, while k has been scaled to the wavenumber k_M of the maximum itself. In practice, this is asymptotically equivalent to scaling the vertical axis by a factor N^2 and the horizontal axis by $1/\sqrt{N}$. We have preferred to adopt this strategy in order to possibly get rid of the strong finite-size corrections revealed by the previous analysis. Indeed, the good data collapse (except for the right tail) noticeable in Fig. 17 is very suggestive of the existence of an asymptotic spectrum. Additionally, the quadratic growth predicted for fixed b.c. is much more clear (see the inset) than one could have expected from the scaling behavior of the total heat flux for the same chain lengths.

Besides looking at the average heat fluxes J_k, we have studied their sample-to-sample fluctuations, by computing the variance σ_J^2. The relative variance plotted versus the scaled (as in the previous figure) wavenumber indicates that fluctuations are independent of the chain length (see the almost overlapping curves in Fig. 18): this means that J_k is not a self-averaging quantity in the

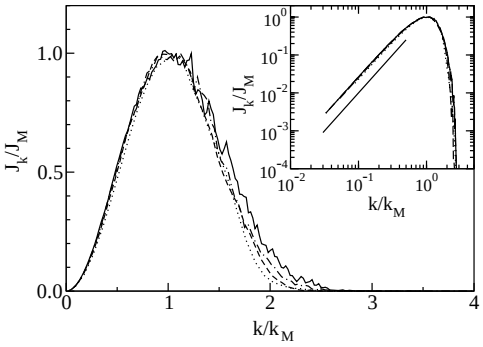

Fig. 17. The heat flux (scaled to the maximum value) versus the wavenumber k (scaled to the position of the maximum) for different chain-lengths (dotted, dashed, dot–dashed and solid curves refer to $N = 32$, 64, 128 and 256, respectively. The same quantities are reported in doubly logarithmic scales in the inset, to show the quadratic growth for small k.

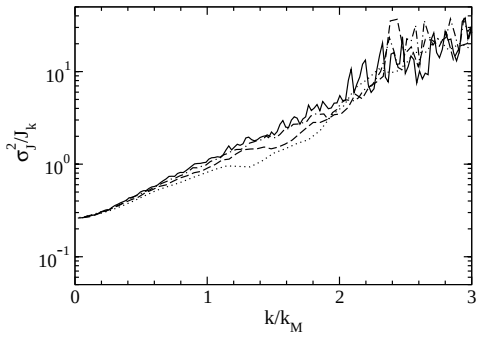

Fig. 18. The relative standard deviation versus the rescaled wavenumber k reveals a clear exponential growth.

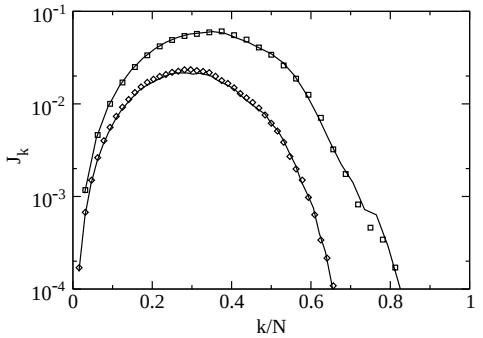

Fig. 19. Comparison between numerical results and the theoretical formula for the heat flux (solid curve) (see Eq. (94)). The agreement is fairly good for both $N = 32$ (squares) and $N = 64$ (diamonds).

thermodynamic limit and this holds true even for low k-wavenumbers, whose behavior results, in principle, from a spatial averaging over increasingly long spatial scales. More precisely, we observe that the variance increases exponentially with k, starting approximately from 0.26 for the longest

wavelength. Moreover, we have compared the theoretical results with non-equilibrium simulations with stochastic heat baths and collision times distributed uniformly in the interval [30–60]. The data plotted in Fig. 19 reveal a very good agreement over various orders of magnitude if the coupling constant is set equal to 1/54.

5. Linear response theory

5.1. The Boltzmann–Peierls equation

In this section, we briefly review the "traditional" approaches to the determination of thermal conductivity. Although they have a major importance in solid state applications, here, we limit ourselves to a very sketchy discussion, since it is sufficient to point out only those general issues that are of interest for our purposes. In this respect, our presentation is inspired by the review article of Jackson [61].

The most elementary picture of heat conductivity is based on the analogy with kinetic theory of gases where $\kappa = Cv_s\ell/3$, C being the heat capacity, v_s the sound velocity and ℓ the mean free path. In a lattice, one can imagine to replace particles with normal modes, but it is, of course, necessary to take into account that the latter have different group velocities, $v_{\mathbf{k}} = \partial\omega/\partial\mathbf{k}$, depending on their wavenumber. Accordingly, the above expression for κ generalizes to

$$\kappa = \frac{1}{3}\int \mathrm{d}\mathbf{k}\, C_{\mathbf{k}} v_{\mathbf{k}}^2 \tau_{\mathbf{k}} \ , \tag{107}$$

where we have introduced the relaxation time $\tau_{\mathbf{k}} = \ell_{\mathbf{k}}/v_{\mathbf{k}}$ that can be determined by phenomenologically including all possible scattering mechanisms (anharmonicity, impurities, boundary effects, electrons, etc.) that must be computed in some independent way.

A less heuristic derivation of the above formula is obtained by solving the Boltzmann equation in the relaxation time approximation [62]. In 1929 R. Peierls proposed his celebrated theoretical approach based on the Boltzmann equation. The main idea is again taken from kinetic theory: lattice vibrations responsible for heat transport can be described as an interacting gas of phonons [2]. Accordingly, one can introduce the time-dependent distribution function $N_k(x,t)$ of phonons with wavenumber k in a macroscopically small volume around x.[5] If we further limit ourselves to considering only the cubic term in the interaction potential (three-phonon processes), the kinetic equations are of the form

$$\frac{\partial N_k}{\partial t} + v_k \frac{\partial N_k}{\partial x} = \iint \mathrm{d}k'\,\mathrm{d}k''\{[N_k N_{k'} N_{k''} - (N_k+1)(N_{k'}+1)N_{k''}]W_{kk'k''} + \frac{1}{2}[N_k(N_{k'}+1)(N_{k''}+1) - (N_k+1)N_{k'}N_{k''}]W_{kk'k''}\} \ , \tag{108}$$

where the transition probability $W_{kk'k''}$ is basically obtained from the Fermi's golden rule. The r.h.s. is the collision integral, i.e. the difference between the number of processes (per unit time) that either

[5] Here, for simplicity, we are referring to a one-dimensional ordered crystal.

increase or decrease the number of phonons in the state k. These non-linear integro-differential equations are clearly impossible to solve in general. An approximate solution is obtained in the limit of small applied gradients, i.e. by looking for small perturbations of the equilibrium distribution $N_k = N_k^{\rm eq} + \delta N_k$, where $N_k^{\rm eq} = (\exp(\hbar\omega_k/k_{\rm B}T) - 1)^{-1}$. This allows to write a linearized kinetic equation [2,48] that, in the stationary case, is of the form

$$v_k \frac{\partial N_k^{\rm eq}}{\partial T} \frac{\partial T}{\partial x} = \mathscr{I}(\delta N) \ , \tag{109}$$

where $\mathscr{I}$ is the linearized collision integral, which is a linear functional of the δN_ks. The τ_k are thus determined as the eigenvalues of the problem.

Anyway, some useful information about thermal conductivity can be obtained by looking directly at the dynamics in Fourier space. Whenever third and fourth order terms are present in the equations of motion (as in the FPU model (4)), one can write

$$\ddot{Q}_k = -\omega_k^2 Q_k - \sum_{k_1,k_2} V^{(3)}_{kk_1k_2} Q_{k_1} Q_{k_2} - \sum_{k_1,k_2,k_3} V^{(4)}_{kk_1k_2k_3} Q_{k_1} Q_{k_2} Q_{k_3} \ . \tag{110}$$

Accordingly, the harmonic part of the flux given by Eq. (33) satisfies the dynamical equation

$$\begin{aligned} \dot{J}_{\rm H} = {} & \frac{\rm im}{3} \sum_{kk_1k_2} [\, - v_k\omega_k + v_{k_1}\omega_{k_1} + v_{k_2}\omega_{k_2}] V^{(3)}_{-kk_1k_2} Q_k Q_{k_1} Q_{k_2} \\ & + \frac{\rm im}{4} \sum_{-kk_1k_2k_3} [\, - v_k\omega_k + v_{k_1}\omega_{k_1} + v_{k_2}\omega_{k_2} + v_{k_3}\omega_{k_3}] V^{(4)}_{-kk_1k_2k_3} Q_k Q_{k_1} Q_{k_2} Q_{k_3} \ . \end{aligned} \tag{111}$$

As expected, this implies that $J_{\rm H}$ is a constant of motion in the harmonic case. In a perfect lattice, one has the selection rules (remember that the mode indices range between $-N/2+1$ and $N/2$)

$$\begin{aligned} & V^{(3)}_{-kk_1k_2} \neq 0 \quad \text{for} \quad -k + k_1 + k_2 = 0, \pm N \ , \\ & V^{(4)}_{-kk_1k_2k_3} \neq 0 \quad \text{for} \quad -k + k_1 + k_2 + k_3 = 0, \pm N \ . \end{aligned} \tag{112}$$

Peierls observed that if there is no dispersion, i.e. $\omega_k = v_{\rm s}|k|$, both three- and four-phonon contributions to (111) vanish when the sums in (112) are equal to zero. Therefore, the only finite contributions to $\dot{J}_{\rm H}$ are those arising from the so-called *Umklapp* processes corresponding to the above sums being equal to $\pm N$.

Besides the above general considerations, there are some specific comments regarding the role of dimensionality that can be drawn in the framework of perturbative theories. Indeed, by evaluating the r.h.s of (111) to lowest order (i.e. by replacing Q_k with the harmonic solution (35)) and averaging out the fast oscillations, one is left with the leading resonant terms that satisfy additional conditions like

$$-\omega_k + \omega_{k_1} + \omega_{k_2} = 0, \quad -\omega_k + \omega_{k_1} + \omega_{k_2} + \omega_{k_3} = 0 \ , \tag{113}$$

etc. Thus there is a big difference between three and four phonon processes in 1-dimension, as in the former case the first of conditions (112) and (113) cannot be simultaneously satisfied (see Ref. [63]

for some numerical results). The net result of this argument due to Peierls is that the lowest-order contributions to thermal resistance in one-dimension arises from four phonon *Umklapp* processes. Of course, in higher dimensions, the situation is different, because the energy and momentum constraints can be satisfied also by three-phonon processes due to the existence of different (longitudinal and transverse) branches of the frequency spectrum. Let us finally notice that, although—in the spirit of a perturbative calculation—only the harmonic component of the flux J_{H} has been considered, no basic difference arises upon including also the non-linear component [61].

Similar conclusions can be drawn from the analysis of the high-temperature limit of the Boltzmann equation, following a standard argument originally due to Pomeranchuk (see for example Chapter VII in Ref. [48]). In this limit, with reference to processes involving three long-wavelength phonons of wavenumber k, k', k'', the transition probability $W_{kk'k''} \sim kk'k'' \sim k^3$, whereby $N_k^{\mathrm{eq}} \approx k_{\mathrm{B}}T/\hbar\omega_k \sim 1/k$. From this consideration and from Eq. (108), one can estimate the linearized collision integral appearing in Eq. (109) as $\mathscr{I} \sim \delta N_k/\tau_k \sim k^{d+1}\delta N_k$, in dimension d. Accordingly, the solution of Eq. (109) diverges as $\delta N_k \sim k^{-(2+d)}$. Finally, using the expression for the heat flux (33) with $\langle E_k \rangle = \hbar\omega_k N_k$ yields

$$\langle J_{\mathrm{H}} \rangle = \sum_{\mathbf{k}} \hbar\omega_{\mathbf{k}} v_{\mathbf{k}} \delta N_k \propto \int \frac{\mathrm{d}k}{k^2} \ . \tag{114}$$

This means that the contribution of such processes would lead to a thermal conductivity diverging like $1/k$ in any dimension. In order to avoid this divergence it is therefore necessary that long wavelength phonons are scattered by short-wavelength ones. Following Ref. [48], let us consider the process in which a short-wavelength phonon of index k annihilates into two phonons of index k' and $k - k' - N$ with $k \ll N$ and $k \ll k'$. Condition (113) requires $\omega_k = \omega_{k-k'} + \omega_{k'}$ that, in turn can be satisfied only for $v_k \simeq v_{\mathrm{s}}$. More generally, one can show that, in the absence of degeneration points in the spectrum, the condition to be fulfilled is that the group velocity of short wavelength phonons is *larger* than the sound velocity i.e. $|v_{\mathbf{k}}| > v_{\mathrm{s}}$. Once again this constraint cannot be satisfied in one-dimensional homogeneous chains and one would conclude that a finite conductivity can be possibly established only by means of higher-order processes.

The Boltzmann–Peierls approach is certainly one of the milestones of the theory of thermal transport in solids. Nonetheless, it is important to recall that its derivation is essentially based on second-order perturbation theory (through the collision kernel $W_{kk'k''}$, which is evaluated by means of Fermi's golden rule) and involves the use of random phase approximation among the phonon modes, which is certainly less appealing than the *Stosszahlansatz* originally introduced by Boltzmann for molecular collisions. It is however remarkable to notice how classical perturbative approaches are able to predict some peculiarities in low-dimensional anharmonic lattices.

5.2. The Green–Kubo formula

The other major tool, commonly used when dealing with transport processes, is linear response theory. At variance with the response to mechanical perturbations (e.g. an external electric field), heat conduction is a process driven by boundary forces. Therefore, a conceptual difficulty arises, since there is no explicit small term in the Hamiltonian to be used as an expansion parameter. This difficulty can be overcome at the price of a stronger assumption, namely that *local equilibrium holds*. The hypothesis looks physically reasonable, but it is far from being rigorously based even in simple

mathematical models and it has been often devised as one of the weak points in the foundation of the whole theory. If local equilibrium holds, a temperature field $T(\mathbf{x})$ can be defined accordingly, thus allowing to introduce a non-equilibrium distribution function

$$\rho = Z^{-1} \exp\left(- \int \mathrm{d}\mathbf{x} \beta(\mathbf{x}) h(\mathbf{x}) \right) , \tag{115}$$

where $h(\mathbf{x})$ is the Hamiltonian density, while Z is the partition function. By now assuming that the deviations from global equilibrium are small, we can write $\beta(\mathbf{x}) = \beta(1 - \Delta T(\mathbf{x})/T)$ and thus

$$\rho = Z^{-1} \exp[- \beta(\mathscr{H} + \mathscr{H}')] , \tag{116}$$

where $\mathscr{H}'$ is the perturbative Hamiltonian

$$\mathscr{H}' = -\frac{1}{T} \int \mathrm{d}\mathbf{x} \Delta T(\mathbf{x}) h(\mathbf{x}) . \tag{117}$$

It is therefore possible to proceed with a perturbative expansion, obtaining the well known Green–Kubo formula that in the classical case reads [25]

$$\kappa_{\mathrm{GK}} = \frac{1}{k_{\mathrm{B}} T^2} \lim_{t\to\infty} \int_0^t \mathrm{d}\tau \lim_{V\to\infty} V^{-1} \langle \mathbf{J}(\tau)\mathbf{J}(0) \rangle , \tag{118}$$

where $\mathbf{J}$ is the total heat flux defined by Eq. (31) and κ_{GK} should, more properly, be a tensor. However, in the simple case of isotropic homogeneous solids made of atoms placed on a regular hyper-cubic lattice, the thermal conductivity tensor has a diagonal representation, with equal non-zero components: upon these assumptions, in dimension d, κ_{GK} reduces to the scalar quantity

$$\kappa_{\mathrm{GK}} = \frac{1}{k_{\mathrm{B}} T^2 d} \lim_{t\to\infty} \int_0^t \mathrm{d}\tau \lim_{V\to\infty} V^{-1} \langle \mathbf{J}(\tau) \cdot \mathbf{J}(0) \rangle . \tag{119}$$

As often stated, Eq. (118) relates the non-equilibrium transport coefficient to the fluctuations of a system at equilibrium. It has to be reminded that its rigorous mathematical foundation is still lacking [3]. Besides this, there are several subtleties connected with a correct implementation of this formula. First of all, one should notice that the infinite-volume limit should be taken before the long-time limit, in order to avoid the problem of Poincaré recurrences. This is a particularly delicate matter whenever a slow decay of correlations is present.

The next issue concerns the meaning of the ensemble average $\langle \cdot \rangle$. In the derivation *á la* Kubo, it denotes a canonical average, while the formally identical expression obtained by Green refers to the micro-canonical ensemble. In this latter case, if the total momentum P is conserved, it has to be set equal to zero, otherwise $\langle \mathbf{J} \rangle \neq 0$ and the integral in Eq. (118) would trivially diverge. Alternatively, as observed in [3], one may compute the truncated correlation functions $\langle \mathbf{J}(t)\mathbf{J}(0) \rangle_T = \langle \mathbf{J}(t)\mathbf{J}(0) \rangle - \langle \mathbf{J} \rangle^2$ for any $P \neq 0$.[6]

[6] Overlooking this point may lead to some confusion as in Ref. [64].

Another way to see the problem was pointed out by Green himself [65]. He noticed that the microscopic expression of the heat flux to be employed in Eq. (118), *depends on the chosen ensemble*. Indeed, he showed that while Eq. (31) is the correct expression in the micro-canonical case, a "counter-term" must be subtracted in the grand-canonical case. This is readily seen by letting $\dot{\mathbf{x}}_i \to \dot{\mathbf{x}}_i - \mathbf{v}$ where $\mathbf{v}$ is the velocity of the center of mass. Up to terms of order less than $\sqrt{N}$, one has

$$\mathbf{J}_{\rm gc} = \mathbf{J}_{\rm mic} - (E + pV)\mathbf{v} = \mathbf{J}_{\rm mic} - H\mathbf{v} \ , \tag{120}$$

where E is the average energy, p the pressure and H the total enthalpy of the system. The micro-canonical and grand-canonical ensembles give the same results provided that the micro-canonical energy density is chosen to correspond to the canonical temperature T. The reason for the different expressions to be used is that the same observable has different time-correlations in the different ensembles.

5.3. Mode-coupling theory

Despite the conceptual difficulties lying behind the derivation of Eq. (118), this formula provides a well defined prescription for determining the thermal conductivity $\kappa_{\rm GK}$ from the current-current correlation function at equilibrium. An effective method for estimating this correlation function is provided by the well known mode-coupling theory (MCT), introduced some decades ago to approach the problem of long-time tails in fluids [5]. Since a rigorous proof of this statement is still lacking, we prefer to illustrate first some simple arguments to support the claim. Afterwards, we introduce MCT in the simple context of the FPU model with cubic non-linearity. Finally we briefly recall the major quantitative results in various dimensions.

According to the classical perturbative approach outlined in the first section of this chapter, the time scale for the relaxation process towards the stationary state can be determined by linearizing the collision operator in Eq. (108). However, this may be insufficient, because of the possible existence of subtle dynamical correlations that escape the predicting ability of a perturbative approach: see, for instance, the necessity to invoke higher order processes at high temperatures, or the well known existence of slow relaxation processes at low temperatures when the dynamics is almost integrable.

A more powerful approach can be built starting from the observation that in solids, like in fluids, the slowest processes arise from the "diffusion" of conserved quantities (such as energy and momentum). Actually, macroscopic conservation laws necessarily imply the existence of a hydrodynamic behavior, dominated by the time scales $1/\gamma_k$ associated with the dynamics of long-wavelength, i.e. low-$\mathbf{k}$, modes. It is then crucial to observe that the damping factor γ_k is expected to vanish in the limit $k \to 0$ both in crystals characterized by the existence of an acoustic band, as well as in fluids (e.g., hard spheres interacting via short-range potentials). In fact, as $\mathbf{k} = 0$ modes correspond to exactly conserved quantities, long-wavelength ones must, by continuity reasons, be characterized by a slow dynamics. It is then of primary interest to notice that this is true independently of the strength of the perturbative terms. Accordingly, γ_k may be very small also for strong non-linearities, when no standard perturbative approach can be meaningfully implemented. As a matter of fact, numerical studies of several models of anharmonic crystals with confining nearest-neighbor interactions

(like the FPU model) nicely confirm this scenario [66] also at high temperatures, when high-k modes behave like "thermal" variables, rapidly relaxing to equilibrium.[7]

According to the previous discussion, the long-time behavior of any current–current correlation function depends on how $\gamma_k \to 0$ in the limit $k \to 0$. In particular, if the damping factor γ_k vanishes too rapidly with $k \to 0$, the temporal decay of the heat-flux correlation function may be so slow that the integral in Eq. (118) diverges. In general this effect ought to depend also on the space dimension. Indeed, almost conserved modes propagating with the sound velocity through the lattice are expected to propagate more efficiently in low than in high dimensions, where the presence of transverse modes favors collision mechanisms. Actually, a well defined, i.e. finite, transport coefficient in anharmonic solids should emerge from an efficient dissipation of the energy of sound waves. In this sense, it is worth recalling that Fourier law follows from the assumption that the temperature field obeys a diffusive equation.

As already anticipated, we illustrate an application of MCT to the FPU model with cubic non-linearities. The procedure is an extension of linear response theory and represents a first step towards the construction of a formal approach for the description of transport properties in models of 1d solids. Moreover, it provides the theoretical background for arguing that the same features should be observed in all models where non-linear effects can be ascribed to the two leading algebraic terms.

In the framework of linear response theory, the dynamics of slow modes is described by generalized Langevin equations. These are linear stochastic equations with memory terms and are usually derived with the projection method introduced independently by Mori and Zwanzig [25]. To illustrate this in the present context, let us consider a one-dimensional chain like (2) with periodic boundary conditions. The equations of motion for the normal coordinates (32) can be written as (see also Eq. (110))

$$\ddot{Q}_k = -\omega_k^2 Q_k + \mathscr{F}_k \ , \tag{121}$$

where $\mathscr{F}_k$ accounts for mutual interactions among the modes while ω_k denotes the normal-mode frequency. One can then define a projection operator $\mathscr{P}$, acting on the generic scalar observable O as

$$\mathscr{P}O = \sum_k \left[\frac{\langle O Q_k^* \rangle}{\langle |Q_k|^2 \rangle} Q_k + \frac{\langle O \dot{Q}_k^* \rangle}{\langle |\dot{Q}_k|^2 \rangle} \dot{Q}_k \right] \ . \tag{122}$$

Due to the conservation law of total momentum, we expect that the slow dynamics should be associated with the long-wavelength Fourier modes Q_k with $|k| \ll N/2$. Moreover, translational invariance implies that each mode is uncorrelated from the others, so that we can consider each mode separately. The corresponding projected equations of motion (that are still exact) read as [68]

$$\ddot{Q}_k + \int_0^t \Gamma_k(t-s)\dot{Q}_k(s)\,\mathrm{d}s + \tilde{\omega}_k^2 Q_k = R_k \ , \tag{123}$$

[7] In the high-energy regime, the same models are known to exhibit a strongly chaotic and convincingly ergodic behavior. The time-scale separation between low-k and high-k modes seems to contradict this statement. This is not the case, since it has to be noticed that low-k modes, although playing a major role in transport phenomena, are a negligible fraction of the spectrum in the thermodynamic limit. Accordingly, equilibrium properties are dominated by thermal modes and "hydrodynamic" deviations from ergodicity can be detected only as higher order corrections.

where the random force $R_k(t) = (1 - \mathscr{P})\ddot{Q}_k$ is related to the memory kernel Γ_k by the fluctuation-dissipation theorem

$$\Gamma_k(t) = \beta\langle R_k(t)R_k^*(0)\rangle \ . \tag{124}$$

The first effect of non-linearities is to induce a temperature-dependent renormalization of the dispersion relation

$$\tilde{\omega}_k^2 = (\beta\langle|Q_k|^2\rangle)^{-1} = (1+\alpha)\omega_k^2, \quad \alpha(\beta) = \frac{1}{\beta}\frac{\int \exp -\beta V(x)\,\mathrm{d}x}{\int x^2 \exp -\beta V(x)\,\mathrm{d}x} - 1 \ . \tag{125}$$

This amounts to renormalizing the sound velocity from the "bare" value v_s to $\tilde{v}_s = v_s\sqrt{1+\alpha}$.[8] A straightforward consequence of Eq. (123) is that the normalized correlation function $\mathscr{G}_k(t) = \beta\tilde{\omega}_k^2\langle Q_k(t)Q_k^*(0)\rangle$ $(\mathscr{G}_k(0) = 1)$ obeys the equation of motion

$$\ddot{\mathscr{G}}_k(t) + \int_0^t \Gamma_k(t-s)\dot{\mathscr{G}}_k(s)\,\mathrm{d}s + \tilde{\omega}_k^2\mathscr{G}_k(t) = 0 \ . \tag{126}$$

Up to here we performed an exact but formal manipulation of the equations of motion. The crucial point is the explicit computation of the memory kernel $\Gamma_k(t)$. MCT is an approximate, self-consistent method for obtaining such an expression in terms of $\mathscr{G}_k(t)$. A first conceptual difficulty of the projection approach is that R_k does not evolve with the full Liouvillean operator. One can bypass the problem with the replacement [5]

$$\langle R_k(t)R_k^*(0)\rangle \to \langle \mathscr{F}_k(t)\mathscr{F}_k^*(0)\rangle \ , \tag{127}$$

whose validity is based on the implicit hypothesis that the slow terms possibly contained in $\mathscr{F}_k(t)$ can be neglected in the thermodynamic limit. A second simplification amounts to factorizing multiple correlations. For example, in the case of a quadratic force, one obtains [68]

$$\Gamma_k(t) \propto \frac{\tilde{\omega}_k^2}{N}\sum_{k'} \mathscr{G}_{k'}(t)\,\mathscr{G}_{k-k'}(t) \ . \tag{128}$$

This approximate expression of the memory kernel constitutes, together with Eq. (126), a closed system of equations for $\mathscr{G}_k$ that has to be solved self-consistently by introducing the Laplace transform of Γ_k,

$$\Gamma_k(z) = \int_0^\infty \mathrm{e}^{-\mathrm{i}zt}\Gamma_k(t)\,\mathrm{d}t \ , \tag{129}$$

and, analogously, $\mathscr{G}_k(z)$. One finds that (with $\dot{\mathscr{G}}_k(0) = 0$)

$$\mathscr{G}_k(z) = \frac{\mathrm{i}z + \Gamma_k(z)}{z^2 - \tilde{\omega}_k^2 - \mathrm{i}z\Gamma_k(z)} \ . \tag{130}$$

As long as dissipation is small enough, $\mathscr{G}_k$ has the form

$$\mathscr{G}_k(t) \sim \exp(\mathrm{i}\lambda_k t) \ , \tag{131}$$

[8] Notice that for $T \to 0$ $(\beta \to \infty)$, $\alpha(\beta) \to 0$ as the integrals in Eq. (125) reduce to Gaussian integrals.

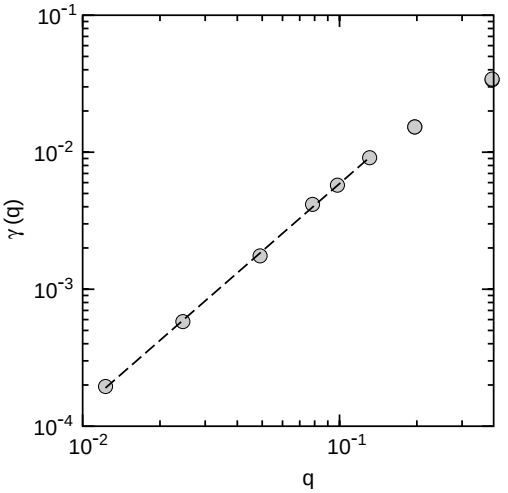

Fig. 20. The wavenumber dependence of the relaxation rates $\gamma(q)$ for the quartic FPU potential (4) $g_4\epsilon = 8.8$. All the points were obtained from the initial decay of the envelope of $\mathscr{G}_1$ for increasing values of N up to $N = 2048$. The dashed line is a power-law fit $q^{1.64}$.

where the pole λ_k of the above transform is approximately given by

$$\lambda_k = \pm\tilde{\omega}_k + \mathrm{i}\frac{\Gamma_k(|\tilde{\omega}_k|)}{2} \ , \tag{132}$$

which can be regarded as a generalized dispersion relation. The imaginary part γ_k of λ_k represents the effective relaxation rate of each Fourier mode as a consequence of its interaction with all the other modes.

As discussed in Ref. [5], in one dimension, the self-consistent calculation predicts a singularity of the memory function at $z = 0$: $\Gamma(z,q) \sim z^{-1/3}q^2$. Substituting this result into the approximate dispersion relation (132) yields the non-analytic dependence of the relaxation rate in the limit of small wavenumbers [67]

$$\gamma(q) \propto q^{5/3} \ . \tag{133}$$

The scaling behavior (133) has been confirmed in molecular-dynamics simulations performed at equilibrium for the FPU model [68] in a significative range of chain sizes (see Fig. 20). The above discussion can be generalized to the case in which a cubic force is present [68]. Although the dependence of the relaxation rate on the temperature depends on the specific form of the anharmonic potential, the rate q is expected to be the same for all one-dimensional models, where the theory applies. Application to 2d lattices has been also discussed [69].

More in general (see again [67]), the following dependences are found for $d = 1$–3,

$$\begin{aligned}
&\lambda(q) \simeq cq - \mathrm{i}c'q^{5/3} + \cdots \quad (d = 1) \ , \\
&\lambda(q) \simeq cq - \mathrm{i}c'q^2 \ln q + \cdots \quad (d = 2) \ , \\
&\lambda(q) \simeq cq - \mathrm{i}c'q^2 + \cdots \quad (d = 3) \ ,
\end{aligned} \tag{134}$$

where c' is a suitable multiplicative factor. Direct numerical evidence of the peculiar behavior of one-dimensional systems has been found also in fluids [70,71].

In order to understand the consequences of the above reasoning for transport phenomena, it is convenient to look at the dynamics of Fourier modes. If we assume that memory effects are all contained in a mode-dependent relaxation-time, Eq. (123) effectively reduces to its Markovian limit,

$$\ddot{Q}_k + \gamma_k \dot{Q}_k + \tilde{\omega}_k^2 Q_k = R_k \tag{135}$$

(referred to the finite-length case), where the random force is well approximated by a Gaussian white process

$$\langle R_k(t) R_k^*(t') \rangle = \frac{\gamma_k}{\beta}\, \delta(t - t') \ , \tag{136}$$

and, for the sake of simplicity, we have neglected the small frequency shift possibly arising from the solution of (132). At this level of approximation, the physical implications of the mode-mode interactions are contained in the dispersion relation γ_k. Eq. (135) provides a convincing description of the numerical results reported in Refs. [66,68], where the Fourier-mode dynamics was studied for the FPU-β model.

Let us now split V into its harmonic and anharmonic parts and consequently write the flux (30) as $J = J_{\mathrm{H}} + J_{\mathrm{A}}$. For a strongly anharmonic system, like the one we consider here, we do not expect J_{A} to be negligible. Nevertheless, in the spirit of Section 5.1, one can argue that the two terms exhibit the same leading asymptotic behavior, so that we can restrict ourselves to considering the autocorrelation of J_{H} alone. This hypothesis has been also successfully tested in simulations [72].

It is convenient to rewrite expression (36) as

$$J_{\mathrm{H}} = \sum_k v_k (E_k - \langle E_k \rangle) = \sum_k v_k \delta E_k \tag{137}$$

(compare also with Eq. (114) where δE_k are the energy fluctuations of each mode). Notice also that, in view of the renormalization of the frequencies, E_k should now be defined on the basis of the transformations (35) with ω_k replaced by $\tilde{\omega}_k$. From Eq. (135), one expects that, for small γ_k, energy fluctuations satisfy the Langevin equation

$$\delta \dot{E}_k = -\gamma_k\, \delta E_k + R'_k \ , \tag{138}$$

with no oscillation for δE_k. In such a limit, R'_k is well approximated by a Gaussian and delta-correlated random process and $\langle (\delta E_k)^2 \rangle = k_{\mathrm{B}}^2 T^2$. For large N, we obtain [72]

$$\langle J_{\mathrm{H}}(t) J_{\mathrm{H}}(0) \rangle \propto \sum_k v_k^2 \langle (\delta E_k)^2 \rangle \mathrm{e}^{-\gamma_k t} = \frac{Na}{2\pi}\, k_{\mathrm{B}}^2 T^2 \int_{-\pi/a}^{\pi/a} \mathrm{d}q\, v^2(q)\, \mathrm{e}^{-\gamma(q) t} \ . \tag{139}$$

Since the integral is dominated by the low-q contribution at large times, we can estimate the long-time behavior of Eq. (139) by letting $c(q) \simeq v_{\mathrm{s}}$ and extending the integration to infinity. Furthermore, in accordance with Eq. (133), we let $\gamma(q) = c' q^{\delta}$, obtaining

$$\langle J_{\mathrm{H}}(t) J_{\mathrm{H}}(0) \rangle \propto \frac{v_{\mathrm{s}}^2 k_{\mathrm{B}}^2 T^2 Na}{(c' t)^{1/\delta}} [1 + \mathcal{O}(t^{-2/\delta})] \ . \tag{140}$$

This result can be generalized to derive the following long-time behavior for the heat-flux correlation function:

$$\langle \mathbf{J}(t)\mathbf{J}(0)\rangle \sim t^{-3/5} \quad (d=1)\ ,$$
$$\langle \mathbf{J}(t)\mathbf{J}(0)\rangle \sim t^{-1} \quad (d=2)\ ,$$
$$\langle \mathbf{J}(t)\mathbf{J}(0)\rangle \sim t^{-3/2} \quad (d=3)\ . \tag{141}$$

The knowledge of the asymptotic behavior of $\langle \mathbf{J}(t)\mathbf{J}(0)\rangle$ now allows determining the dependence of κ on N. In fact, upon restricting the integral in Eq. (118) to times smaller than the typical transit time Na/v_s, one obtains,

$$\kappa \sim N^{2/5} \quad (d=1)\ ,$$
$$\kappa \sim \ln N \quad (d=2)\ ,$$
$$\kappa \sim \text{finite} \ (d=3)\ . \tag{142}$$

It is worth stressing again that these results can be derived without making any explicit reference to the details of the interactions among atoms in the lattice. In practice, this is tantamount to stating that all models characterized by short range interactions and momentum conservation should exhibit the same kind of anomalous behavior (for $d<3$). In the next section we shall see that this is not completely correct, as for non confining potentials, a normal conductivity is found already in one dimension. In all other cases, in spite of the intrinsic approximations contained in the MCT, the predicted scaling behavior of κ agrees with the numerical estimates obtained from both equilibrium and non-equilibrium simulations. This is not surprising if one considers that, at relatively high energies, the time scale associated with high-k modes is well separated from the hydrodynamic ones, so that the leading term predicted by MCT is likely to contain all the relevant information already in relatively small systems.

6. Anharmonic chains with momentum-conserving potentials

6.1. Early results

This section is devoted to a historical review of molecular-dynamics studies of thermal conduction in the class of models (2). The first simulations date back to the pioneering work of Payton, Rich and Visscher [32] and to the contribution of Jackson, Pasta and Waters [73]. In both cases, the Authors performed non-equilibrium studies of the FPU model (4) with coupling constants g_2, g_3, and g_4 chosen in such a way to represent the leading terms of the expansion of the Lennard–Jones potential (3). In order to study the effect of impurities in the crystal, either a disordered binary mixture of masses [32] or random non-linear coupling constants [73] were considered. Ironically enough, those very first computer studies attacked the problem from the most difficult side. In fact, even before the effect of disorder was fully understood in harmonic chains, they studied systems where anharmonicity and disorder are simultaneously present. Nevertheless, those early works have

at least the merit to have showed how the interplay of the two ingredients can lead to unexpected results that, in our opinion, are still far from being fully understood. Indeed, Ref. [32] revealed that the simple perturbative picture in which anharmonicity and impurities provide two independent (and thus additive) scattering mechanisms does not hold. More precisely, the Authors found even cases in which anharmonicity *enhances* thermal conductivity. A qualitative explanation was put forward by claiming that anharmonic coupling induces an energy exchange between the localized modes, thus leading to an increase of the heat flux.

The limited computer resources available at that time prevented, however, addressing the issue whether the combined effect of anharmonicity and disorder can lead to a finite conductivity. On the other hand, it was payed attention at the temperature profile $T(x)$, noticing irregularities that depended on the realization of the disorder. While we know that $T(x)$ is not a self-averaging observable of disordered harmonic chains, it has not yet been clarified whether the dependence on the realization of the disorder persists over long enough time scales in anharmonic chains as well.

Additional questions that have been investigated concern the concentration of impurities. Besides the obvious finding that disorder reduces the value of heat conductivity (for fixed finite-chain length), it was noticed an asymmetric behavior between the case of a few heavy atoms randomly added to an otherwise homogeneous light-atom chain and its converse. The smaller values of the conductivity observed in the former cases were traced back to the larger number of localized modes [32].

Having recognized the difficulty of simultaneously coping with the effects of non-linearity and disorder, we now turn to the simpler case of anharmonic homogeneous chains. Some early work in this direction was performed by Nakazawa [74] who considered equal-masses FPU and Lennard–Jones chains composed of 30 particles and coupled with Langevin baths at their boundaries. This setup required the integration of a set of stochastic differential equations, a task that was admittedly unfeasible with the computer resources available at that time. As a consequence, several attempts of designing artificial but easy-to-simulate models followed these first studies. Some examples are reviewed in Ref. [75].[9] Let us mention among them the case of the harmonic hard-rod potential, i.e. a harmonic well delimited by an infinite barrier located at a given distance from the equilibrium position. A diverging conductivity was observed with a method akin to Green–Kubo one [75].

The long period of time (almost a decade) during which the problem was practically forgotten signals perhaps the frustration encountered in the search for the minimal and general requirements for building simple 1d models with good transport properties. In the mid eighties several authors got again interested in the problem, being able to perform non-equilibrium simulations of chains with smooth inter-particle potentials and a few hundreds of particles. In particular, a good deal of work was devoted to reconsidering the FPU model [76,77] and to studying the diatomic Toda chain [78–81] whose Hamiltonian is of the type (2), with

$$V(x) = \frac{a}{b}\left[\exp(-bx) + ax\right] , \tag{143}$$

and m_l being a sequence of alternating light and heavy masses with given ratio r. At variance with the homogeneous case $r = 1$, this model is no longer integrable at equilibrium and can be thus considered as a meaningful candidate for testing the validity of the Fourier law. Notice that at variance with homogeneous models, (143) admits also an optical branch in the harmonic limit.

[9] Those attempts eventually led to the invention of the so-called ding-a-ling model described in the following Section as it belongs to the different class of chains with external substrates.

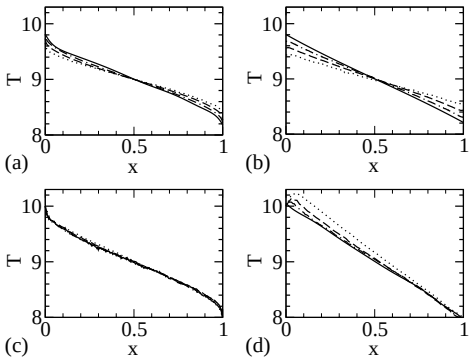

Fig. 21. Temperature profiles for the FPUβ model for $T_+ = 10$ and $T_- = 8$. Panels (a) and (b) refer to stochastic reservoirs (acting through the randomization of the velocity at random times uniformly distributed in the interval $[1,2]$). Dotted, dashed, dot–dashed, and solid lines correspond to $N = 128$, 256, 512, and 1024, respectively. Panels (c) and (d) refer to Nosé-Hoover thermostats with $\Theta = 1$. In this case, dotted, dashed, dot–dashed, and solid lines correspond to $N = 32$, 64, 128, and 256. In (a) and (c), fixed b.c. are imposed, while free b.c. are imposed in (b) and (d).

Out of the many conflicting results, Mareschal and Amellal [82] recognized that fluctuations of the heat current display peculiar features that are normally absent in higher dimensions. More precisely, they computed the equilibrium autocorrelation function of the heat flux (the Green–Kubo integrand) for a Lennard–Jones chain of 200 particles. On a qualitative level, they noticed that the initial fast decay was followed by a very slow convergence to zero. This is consistent with the possibility that such a long-time tail be responsible for a diverging transport coefficient, in close analogy with what happens in low-dimensional fluids [5]. Additionally, in Ref. [82] it was checked the robustness of this feature against the introduction of further, extrinsic, scattering mechanisms. Indeed, the time tails survive the addition of a moderate fraction of impurities, introduced as either mass defects or variable interaction potentials. For instance, it was considered the case where every fourth particle has a purely repulsive interaction with its neighbors, of the type

$$V_{\mathrm{im}}(x) = \varepsilon \left(\frac{\sigma}{x}\right)^{12} . \tag{144}$$

A slow decay was finally observed also in the presence of an external sinusoidal field (akin to the Frenkel–Kontorova substrate potential considered in the following). It has, however, to be recognized that this last observation contrasts the recent results obtained for several models with on-site forces (see Section 7).

6.2. Divergence of heat conductivity

It took almost another decade for the first systematic studies on the size dependence of the conductivity to appear. An extensive series of non-equilibrium simulations were performed for the FPU chain with quadratic and quartic [83,84,72] or cubic [63] interaction potential as well as for the diatomic Toda one [85,86].

Some evidence of anomalous transport properties is already given by the temperature profiles. While a fairly linear shape is obtained for free boundary conditions (see Fig. 21b,d), as predicted from the Fourier law, strong deviations are observed for fixed boundary conditions (see Fig. 21a,c).

Table 1
The estimated exponent α of divergence of the conductivity with size N, as obtained from both non-equilibrium molecular dynamics (NEMD) simulations and through Green–Kubo (GK) equilibrium studies. Only the significative digits are reported as given in the quoted references

Model	Reference	α (NEMD)	α (GK)
FPU-β	[84,72]	0.37	0.37
FPU-α	[63]	$\lesssim 0.44$	—
Diatomic FPU $r=2$	[86]	0.43	Compatible
Diatomic Toda $r=2$	[85]	0.35–0.37	0.35
	[86]	0.39	Compatible
Diatomic Toda $r=8$	[86]	0.44	Compatible
Diatomic hard points	[85]	0.35	—

More important, such deviations persist upon increasing the chain length: the nice overlap observed in panel (c) indicates that the asymptotic temperature gradient is definitely non-uniform. Altogether, this scenario is suggestive of the existence of long-range effects.

Before discussing the divergence of κ, let us remark that, as anticipated in Section 3, a much smaller boundary-resistance and thus smaller finite-size corrections are found in Nosé-Hoover thermostats than in stochastic ones (see Fig. 21).

As a result of the recent numerical studies, one can now safely claim that the conductivity of long but finite chains diverges as

$$\kappa(N) \propto N^{\alpha} \ . \tag{145}$$

In Table 1 we compare the available estimates of the exponent α determined by different authors in various models. The numerical values range between 0.35 and 0.44, suggesting a non-trivial universal behavior. It is also remarkable to notice the overall consistency among the results obtained with different thermostat schemes (ranging from deterministic to stochastic ones).

In order to better appreciate the quality of the divergence rate that can be numerically obtained, in Fig. 22 we have plotted the finite-length conductivity $\kappa(N) = JN/(T_+ - T_-)$ versus the number of particles in the FPU-β model for fixed and free boundary conditions. In the inset, one can see that the effective growth rate α_{eff} defined in (106) is basically the same in both cases, despite the clear differences in the actual values of the flux itself. Additionally, α_{eff} does not deviate significantly from the MCT prediction ($\alpha = 0.4$).

It is instructive to notice also that the now widely confirmed divergence of the thermal conductivity with the chain length was already observed in previous simulations in spite of opposite claims made by the authors themselves. We refer to a paper by Kaburaki and Machida, where it was conjectured a slow convergence [76] of $\kappa(N)$ towards a finite value in the FPU-β model. By re-plotting their data in doubly logarithmic scales, a convincing power-law behavior is clearly seen instead, with even a quantitative agreement for the divergence exponent (see Fig. 23).

Once the divergence is clearly established, the next question concerns the universality of the divergence rate. The discussion of this point involves considering a possible dependence on the temperature as well as on the leading non-linearities [63]. Both questions are addressed in Fig. 24, where $\kappa(N)$ is computed in the FPU-α model at a relatively low temperature. The convergence

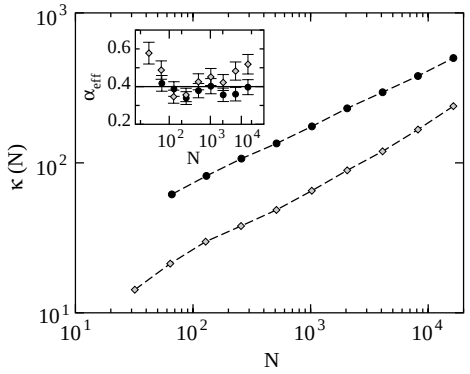

Fig. 22. Thermal conductivity of the FPU-β model versus lattice length N for $T_+ = 0.11$, $T_- = 0.09$, and $\Theta = 1$. The inset shows the effective growth rate α_{eff} versus N. Circles and diamonds correspond to free and fixed b.c., respectively.

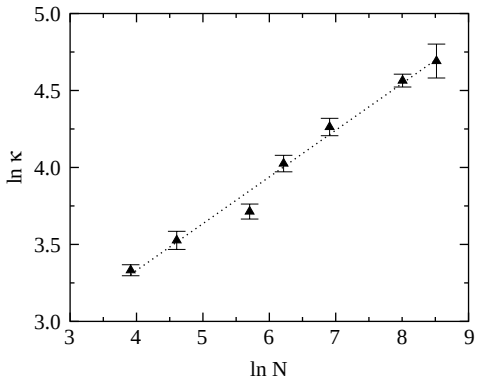

Fig. 23. Thermal conductivity of the FPU-β model, $T_+ = 150$, $T_- = 15$, fixed boundary condition. The data are taken from Ref. [76].

of the effective exponent towards 0.4 (see the inset in Fig. 24) suggests that the presence of a quadratic non-linearity in the force field does not modify the overall scenario observed in the FPU-β model. Additionally, notice that changes in the temperature gradient, without modifying the average $T = (T_+ + T_-)/2$, modify the effective conductivity only at relatively small sizes. In fact, we see in Fig. 24 that the two sets of measures corresponding to $\Delta T = 0.1$ and 0.02 (triangles and circles, respectively) approach each other for N larger than 10^3. In both cases $\kappa(N)$ increases linearly with N for $N < 10^3$ and no sizeable temperature gradient forms along the chain. Both facts hint at a weakness of anharmonic effects up to this time/length scales. This is confirmed by the comparison with the results for a pure harmonic chain (with the same setup and same parameters) that exhibit a clean linear growth of κ with N (see the solid line in Fig. 24) and a few-percent differences in the initial size range. The fact that κ is smaller for larger ΔT can be thus attributed to a stronger boundary scattering that reduces the conductivity.

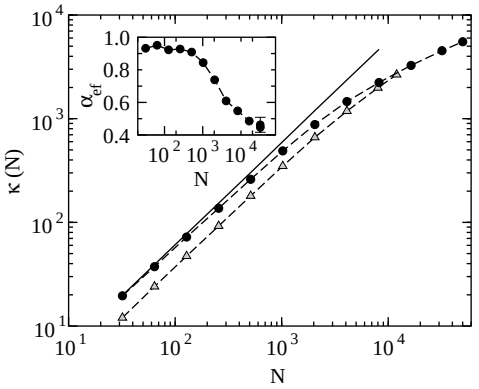

Fig. 24. Thermal conductivity of the FPU-α model versus lattice length N for $g_3 = 0.25$, $T = 0.1$, and $\Theta = 1$. Triangles and circles refer to $\Delta T = 0.1$ and $\Delta T = 0.02$, respectively. The solid line corresponds to the linear divergence observed in a harmonic chain with the same temperatures. The inset shows the effective divergence rate $\alpha_{\rm eff}$ versus N for the data corresponding to full circles.

The overall scenario is confirmed by the computation of κ through the Green–Kubo formula. The very existence of an anomalous transport coefficient can be inferred from the slow decay of the corresponding autocorrelation function. In particular, if $\langle J(t)J(0)\rangle$ decays as $t^{-\beta}$ with $\beta < 1$, the integral in Eq. (118) diverges, thus signalling an infinite conductivity. Obviously, in finite chains one expects that an exponential decay eventually sets in, so that simulations should be performed for different chain lengths in order to be sure to pick up the truly asymptotic scaling behavior. From a numerical point of view, a simpler way to proceed consists in looking at the low-frequency divergence of the power spectrum $S(\omega)$ of the total heat flux: by the Wiener–Khinchin theorem, a power-law decay of the autocorrelations with exponent β translates into an $\omega^{\beta-1}$ behavior of $S(\omega)$ at small ω.

The spectrum plotted in Fig. 25 is asymptotic in N in the selected frequency range. The low-frequency divergence of $S(\omega)$ implies that the autocorrelation of J decays with a rate $\beta \simeq 0.63$, i.e. that its time integral diverges.

A quantitative comparison with the previous results can be performed by noticing that energy propagates with the constant sound velocity v_s. This can be understood by, e.g., looking at the spatio-temporal correlation function $C(i,t) = \langle j_i(t) j_0(0)\rangle$ of the local heat flux [72] plotted in Fig. 26. Accordingly, one can turn the time divergence of κ as determined from the Green–Kubo formula into a divergence with N by restricting the integral in formula (118) to times smaller than the "transit time" Na/v_s. This amounts to ignoring all the contributions from sites at a distance larger than N. With the above estimate of C_J, one obtains that $\kappa \propto N^{1-\beta}$. The latter exponent is the one reported in the last column of Table 1.

It is instructive to repeat the modal analysis for the contribution to the heat flux also in the non-linear case. In spite of the fact that there are no longer eigenmodes, one can determine the contribution of each mode to the heat flux (the modes to be considered being defined according to the imposed boundary conditions) [87]. The relevant difference with the harmonic case is that, because of the lack of integrability, the kth mode does not only exchange energy with the left and right

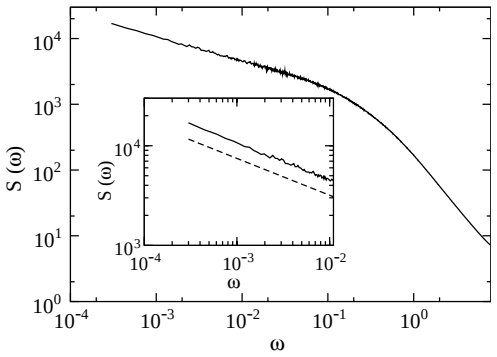

Fig. 25. Power spectrum $S(\omega)$ (in arbitrary units) of the global flux for an FPU-β chain of length $N=1024$ at a temperature $T=11.07$. The curve results from an average over 1400 independent initial conditions. A blow-up of the low-frequency region is reported in the inset: the dashed line is a shifted fit with slope -0.37.

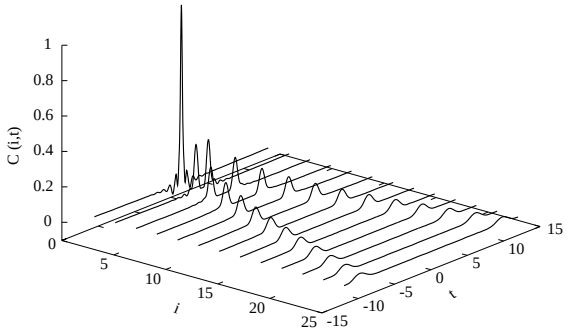

Fig. 26. The spatio-temporal correlation function $C(i,t)=\langle j_i(t)j_0(0)\rangle$ of the local flux for the FPU β model. Micro-canonical simulations, energy density 8.8.

reservoirs, but also with all other modes (this is precisely the mechanism that is eventually responsible —in 3d—for a normal conductivity). Accordingly, one can write an energy balance equation for the kth mode as

$$J_k^+ + J_k^- + J_k^{nl} = 0 \ , \tag{146}$$

where $J_k^{\pm}$ is a self-explanatory notation for the fluxes towards the two heat baths, while J_k^{nl} is the energy exchanged with the other modes as a consequence of the non-integrable dynamics. Obvious global constraints imply that $\sum_k J_k^{nl} = 0$. Direct simulations performed with both free and fixed boundary conditions suggest a much stronger property, namely that each "non-linear" flux vanishes, $J_k^{nl} = 0$. The same simulations indicate that the effect of the boundary conditions on the modal fluxes is qualitatively similar to that in harmonic systems. In fact, from Fig. 27, we can see that for fixed boundary conditions, the contribution of low-k modes is depleted and goes to 0 for $k \to 0$, while a growth, if not a divergence, is observed for free boundary conditions.

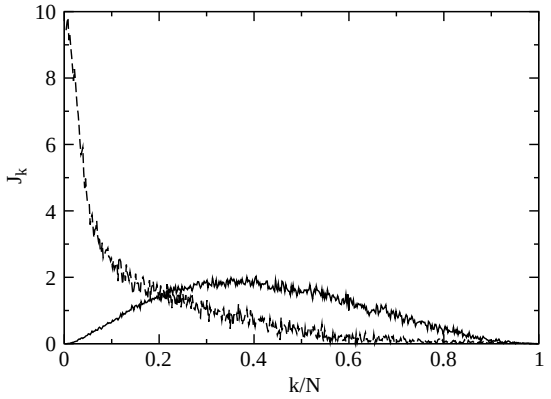

Fig. 27. Modal fluxes in an FPU chain of length 512 for fixed (solid line) and free (dashed line) boundary conditions. Vertical units are fixed in such a way that the total flux is normalized to unity in both cases.

From the hydrodynamic description put forward in the previous chapter, one understands that the contribution to the anomalous behavior of heat conductivity arises from the behavior of long-wavelength modes in a similar way to the anomaly observed in disordered harmonic chains. It is therefore natural to ask why boundary conditions are so important in disordered harmonic chains that they may turn a diverging into a vanishing conductivity, while the same does not occur in non-linear systems. The question becomes even more intriguing after having noticed that non-linear systems are characterized by a similar dependence of the modal fluxes to that found in harmonic chains. A precise answer to this question would require combining in a single model internal relaxations (self-consistently described by mode-coupling theory) and dissipations due to the coupling with the external heat baths. Such a type of description is still lacking.

Finally, we discuss the role of the boundary resistance in connection with the temperature dependence of conductivity. In fact, an interesting application of Eq. (56) has been proposed in Ref. [50] with reference to the FPU-β model. There, it has been empirically found that the bulk conductivity scales with L and T as

$$\kappa \simeq \begin{cases} 1.2L^{\alpha}T^{-1} & (T \lesssim 0.1)\ , \\ 2L^{\alpha}T^{1/4} & (T > 50)\ . \end{cases} \tag{147}$$

According to kinetic theory, the conductivity can also be expressed as $\kappa = \ell v_s C_v$. Since C_v and v_s are almost constant and of order 1 in a wide temperature range, $\ell \sim \kappa$. Hence, at low temperatures the boundary jumps dominate the thermal profile up to the size L_* that can be estimated according to Eq. (56). At low temperatures this effect is very strong since $L_* \sim (2\epsilon/T)^{1/(1-\alpha)}$, while smaller boundary resistances are found at large temperatures, where $L_* \sim (2\epsilon T^{1/4})^{1/(1-\alpha)}$.

6.3. The hard-point gas

Although this review is basically devoted to analysing the behaviour of low-dimensional lattices, it is worth considering also fluid systems in so far as no qualitative differences are expected for the

scaling behaviour of their transport properties. More specifically, in this section we discuss a set of point particles labelled by the index $i = 1,\ldots,N$ moving along a one-dimensional box extending from $x = 0$ to L. The mass, position and velocity of the ith particle are denoted by m_i, x_i, and u_i, respectively. Interaction occurs only through elastic collisions. After a collision between the ith and the $i+1$st particle, the respective velocities acquire the values

$$u_i' = \frac{m_i - m_{i+1}}{m_i + m_{i+1}}\, u_i + \frac{2m_{i+1}}{m_i + m_{i+1}}\, u_{i+1}, \quad u_{i+1}' = \frac{2m_i}{m_i + m_{i+1}}\, u_i - \frac{m_i - m_{i+1}}{m_i + m_{i+1}}\, u_{i+1} \tag{148}$$

as implied by momentum and energy conservation. Between collisions, the particles travel freely with constant velocity. Notice also that they maintain their initial ordering (no crossing is allowed).

The model is particularly suitable for numerical computation as it does not require integration of non-linear differential equations. Indeed, the dynamics amounts simply to evaluating successive collision times and updating the velocities according to Eqs. (148). The only numerical errors are those due to round-off. The coupling with heat baths at the boundaries can be implemented in the usual way, e.g. by using Maxwell thermostats. Thus whenever a particle of mass m collides with a wall at temperature T, it is reflected back with a velocity chosen from the distribution $P(u) = (m|u|/T)\exp[-mu^2/(2T)]$.

In the limit where all the masses are equal, the system becomes integrable and one expects the same behavior observed in harmonic chains (see Section 4.1). In particular, the temperature profile is flat (with $T(x) = \sqrt{T_+ T_-}$), the heat current is independent of the system size and no local equilibrium is attained.[10] However, as soon as the masses are different, the system is non-integrable and (hopefully) ergodic, thus becoming a possible candidate for checking the validity of Fourier's law. Casati [88] considered the case of alternate masses ($m_{2i} = 1$, $m_{2i+1} = (1+\delta)$ in suitable units.[11]) While from his numerical results it was not possible to draw any definite conclusion about the scaling behaviour of the conductivity, more recent simulations by Hatano [85] suggest a divergence rate consistent with what found for FPU (see Table 1). Although we do not see any reason why coupled rotors and FPU should belong to different universality classes, the behaviour of conductivity in the hard-point gas appears to be still quite a controversial issue: simulations performed by Dhar [89] point to a slow divergence ($\kappa \sim L^\alpha$ with $\alpha < 0.2$); equilibrium simulations discussed in Ref. [90] have led the authors even to conjecture a normal behavior; finally, further direct numerical studies confirm instead the existence of a divergence [92]. Accordingly, it seems reasonable to hypothesize that the uncertainty is due to strong finite-size effects that slow down the convergence to the expected asymptotic behaviour.

Besides the dependence of κ on L, in Ref. [89] it has been studied the shape of the temperature profile. The simulations have been performed for different values of δ and for N up to 1281 (adjusting

[10] In this respect, it is worth mentioning that the equal-mass case with dissipation has been studied by Du et al. [91] as a toy model for a granular gas. They obtained a rather surprising stationary state which implied a breakdown of usual hydrodynamics.

[11] From the invariance of the dynamics described by Eq. (148) under mass rescaling ($m_i \to \nu m_i$), it follows indeed that the only independent parameters are the mass ratio $(1+\delta)$ and the ratio of the boundary temperatures T_+/T_-. In fact the temperature profile does not change under $m_i \to \nu m_i$. Also from the boundary conditions, it is easily shown that $T(\nu T_+, \nu T_-, x) = \nu T(T_+, T_-, x)$.

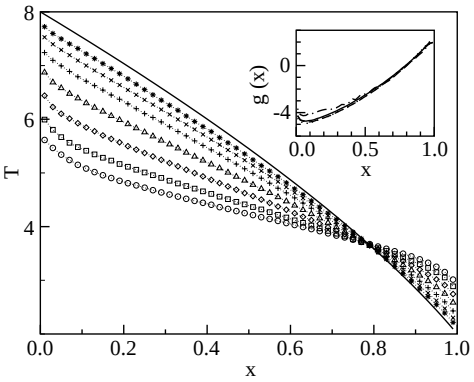

Fig. 28. Temperature profiles of the hard point gas for $\delta = 0.22$, $T_+ = 8$, $T_- = 2$ and sizes $N = 21, 41, 81, 161, 321, 641$ and 1281 (from top to bottom). The solid line corresponds to Eq. (149). In the inset, it is plotted $g(x)$ (see Eq. (150)) with the data for $N = 161, 321, 641$ and 1281.

the system size L so as to keep the average density of particles equal to 2). The number of particles has been chosen to be odd, so that the two particles in contact with the heat baths have always the same mass. Moreover, the averaging of the various observables has been performed over a time span corresponding to 10^9–10^{10} collisions. In Fig. 28, the steady-state temperature profile for different values of N is plotted and the same $\delta = 0.22$. The profile is smooth except at the boundaries, where two temperature drops are observed whose amplitude decreases with the system size.

Upon increasing N, the temperature profile approaches a limiting form. Quite amazingly, this shape is quite close to the one that would be predicted by kinetic theory. In fact, let us recall that kinetic theory applied to a one-dimensional gas predicts the Fourier law with a conductivity $\kappa \sim \sqrt{T}$. By then integrating the equation $\sqrt{T}\,\mathrm{d}T/\mathrm{d}x = c.nt$ with suitable boundary conditions, one obtains

$$T_k(x) = \left[T_+^{3/2}\left(1 - \frac{x}{L}\right) + T_-^{3/2}\frac{x}{L}\right]^{2/3} . \tag{149}$$

This corresponds to the solid curve in Fig. 28. The agreement with the numerical simulations is surprising, since kinetic theory predicts a finite conductivity. We are inclined to interpret this result as a confirmation of the existence of strong finite-size corrections.

The hard-point gas is interesting also for the possibility to investigate the nearly integrable regime when $\delta \ll 1$. The smaller is δ, the larger has to be the system size in order to generate the same temperature profile. In Ref. [89] it has been conjectured that $T(x, N, \delta)$ depends on δ and N only through the scaling combination $\delta^2 N$ and it has been proposed the following scaling form:

$$T(x, N, \delta) = T_k(x) + \frac{1}{(\delta^2 N)^\gamma}\, g(x) . \tag{150}$$

The above relation can be tested with reference to the data reported in Fig. 28. The good data collapse that can be appreciated in the inset of Fig. 28 supports the validity of the scaling relation (150) with $\gamma = 0.67$.

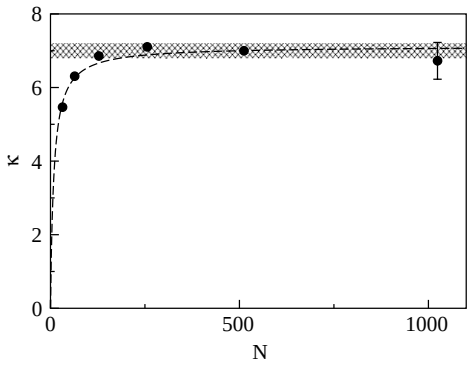

Fig. 29. Conductivity κ versus chain length N as obtained from non-equilibrium molecular dynamics. Circles correspond to the rotator model with temperatures $T_+ = 0.55$ and $T_- = 0.35$. The dashed line represents the best fit with the function $a + b/N$. The shaded region represents the uncertainty about the conductivity on the basis of the Green–Kubo formula.

6.4. The coupled-rotor model

The simplest example of a classical-spin 1d model with nearest-neighbor interactions lies in the class (2) with [93,94]

$$V(x) = 1 - \cos x \ . \tag{151}$$

This model can be read also as a chain of N coupled pendula, where the p_i's and the q_i's represent action-angle variables, respectively. It has been extensively studied [95–97] as an example of a chaotic dynamical system that becomes integrable both in the small and high energy limits, when it reduces to a harmonic chain and free rotors, respectively. In the two integrable limits, the relaxation to equilibrium slows down very rapidly for most of the observables of thermodynamic interest (e.g., the specific heat) [96,97]. As a consequence, the equivalence between ensemble and time averages is established over accessible time scales only inside a limited interval of the energy density e. Here, we focus our attention mainly on heat conduction in the strongly chaotic regime.

In Refs. [93,94], it has been shown that, contrary to the expectations, this model exhibits a finite conductivity in spite of the existence of an acoustic branch in its spectrum in the harmonic limit. In Ref. [93], simulations have been performed for $T_+ = 0.55$, $T_- = 0.35$, and chain lengths ranging from $N = 32$ to 1024 with fixed boundary conditions and Nosé-Hoover thermostats. The equations of motion have been integrated with a 4th order Runge–Kutta algorithm and a time step $\Delta t = 0.01$. The results, reported in Fig. 29 clearly reveal a convergence to a value of κ approximately equal to 7 (see the circles). The dotted line in good agreement with the numerical data is the best fit with the function $a + b/N$ [12]. However, more important than assessing the convergence properties of $\kappa(N)$ is to notice its finiteness for $N \to \infty$.

In fact, this is the first system where normal heat conduction has been convincingly ascertained in the absence of an external field. Precisely because of this atypical behavior, it is important to confirm this result with a computation of thermal conductivity through the Green–Kubo formula.

[12] Notice that this function is asymptotically equivalent to expression (56), derived under the assumption that finite-size corrections are due only to the boundary resistance.

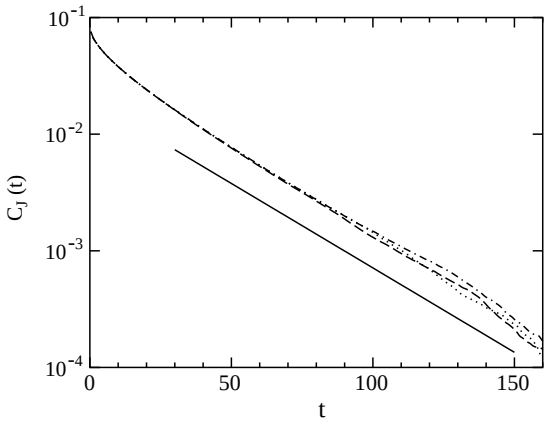

Fig. 30. The autocorrelation function of the total heat flux in a chain of coupled rotors with periodic boundary conditions and energy density $e = 0.5$. Dashed, dot–dashed and dotted lines correspond to $N = 256$, 512, and 1024, respectively. The solid line, corresponding to $C_j = \exp(-t/30)$ has been drawn for reference.

In Ref. [93], micro-canonical simulations have been performed in a chain with periodic boundary conditions. In the absence of thermal baths, the equations of motion are symplectic; accordingly, the Authors have made use of a 6th order McLachlan–Atela integration scheme [33], fixing the energy density equal to $e = 0.5$, a value that corresponds to $T \approx 0.46$, close enough to the average temperature in the non-equilibrium simulations.

The correlation function has been computed by exploiting the Wiener–Khinchin theorem, i.e. by anti-transforming the Fourier power spectrum of the total flux. The curve plotted in Fig. 30 indicate both a clean exponential decay and an independence of the behavior of N for $N \geqslant 256$ (at least in the reported time range). This allows for an accurate determination of the integral of $C_j(t)$. The gray region in Fig. 29 corresponds to the resulting value of κ taking into account statistical fluctuations. The quantitative agreement between the two estimates of the heat conductivity is important in that it confirms also the finiteness of κ in a context where this was not a priori obvious.

In order to emphasize the difference between the dynamics of the present model and that of the previous systems, it is instructive to look at the power spectrum of the low-k Fourier modes. In Fig. 31 it is possible to compare the spectra of some low-k modes in coupled rotors with those in a diatomic FPU-β chain. In the latter case, sharp peaks are clearly visible (notice also that the peaks become increasingly narrow upon decreasing k): this is a signal of an effective propagation of correlations [72]. Conversely, in the rotors, the low-frequency part of the spectrum is described very well by a Lorentzian with half-width $\gamma = Dk^2$ ($D \approx 4.3$). This represents an independent proof that energy diffuses, as one expects whenever the Fourier's law is established.

In the attempt to explain the striking difference in the transport behavior exhibited by this model with respect to that of the previous models in the same class, one cannot avoid noticing that the pair potential $V(q_{i+1} - q_i)$ possesses infinitely many equivalent valleys. As long as $(q_{i+1} - q_i)$ remains confined to the same valley, there is no reason to expect any qualitative difference with, e.g., the FPU-β model. Phase slips (jumps of the energy barrier), however, may very well act as localized random kicks, that contribute to scattering of the low-frequency modes, thus leading to

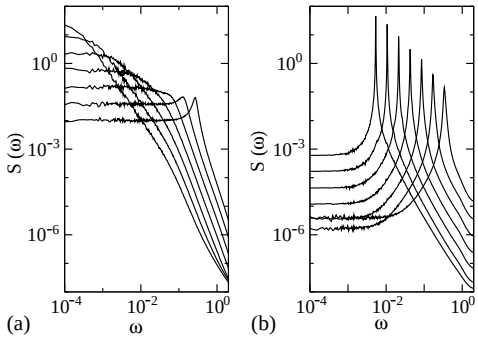

Fig. 31. Power spectra of the 1st, 2nd, 4th, 8th, 16th, 32nd, and 64th Fourier mode in arbitrary units for a chain of $N = 1024$ particles. Panel (a) refers to a chain of rotors with energy density $e = 0.5$ (the wavenumber increases from left to right); panel (b) refers to a diatomic FPU-β chain with masses 1, 2 and energy density $e = 8.8$ (the wavenumber increases from top to bottom in the low-frequency region). In both cases the curves result from an average over 1000 independent simulations.

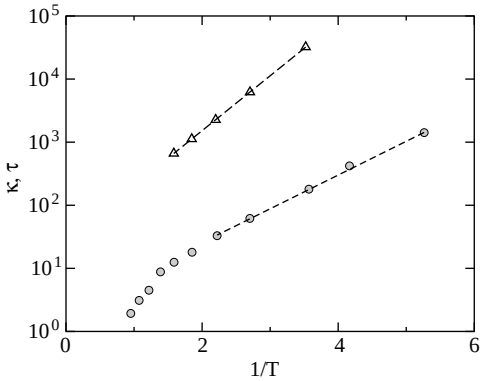

Fig. 32. Thermal conductivity κ versus the inverse temperature $1/T$ in the rotor model (open circles). Triangles correspond to the average time separation between consecutive phase slips in the same system.

a finite conductivity. In order to test the validity of this conjecture, one can study the temperature dependence of κ for low temperatures when jumps across barriers become increasingly rare. The data plotted in Fig. 32 indicate that the thermal conductivity behaves as $\kappa \approx \exp(\eta/T)$ with $\eta \approx 1.2$. The same scaling behavior is exhibited by the average escape time τ (see triangles in Fig. 32) though with a different $\eta \approx 2$. The latter behavior can be explained by assuming that the phase slips are the results of activation processes. Accordingly, the probability of their occurrence is proportional to $\exp(-\Delta V/T)$, where ΔV is the barrier height to be overcome. The behavior of τ is thus understood, once we notice that $\Delta V = 2$. In the absence of phase slips, the dependence of the conductivity on the length should be the same as in FPU-systems, i.e. $\kappa \approx N^{2/5}$. In the presence of phase slips, it is natural to expect that the conductivity is limited by the average distance $\bar{N}$ between consecutive phase slips. Under the further assumption of a uniform distribution of the slips, their spatial and temporal separation has to be of the same order, thus implying that $\kappa(T)$ exhibits the same divergence as

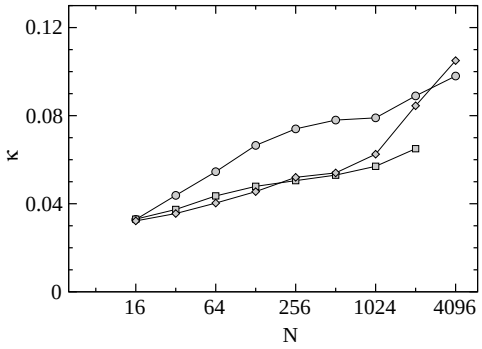

Fig. 33. Thermal conductivity κ versus chain length for the potential (153) and three different average temperatures: 1/16 (circles), 3/32 (squares), and 1/8 (diamonds). In all cases the temperature difference is chosen equal to 1 tenth of the average temperature.

τ for $T \to 0$, though with a different rate $\kappa \approx \exp[2\Delta V/(5T)]$. Therefore, at least on a qualitative level, one can indirectly confirm that phase slips are responsible for the normal heat transport. On a quantitative level, however, there is a discrepancy between the observed and the expected value of the coefficient η (1.2 versus 0.8). Among the possible explanations for the difference, we mention the presence of space–time correlations in the pattern of phase-slips and the existence of ever increasing deviations from the asymptotic law $\kappa \approx N^{2/5}$ for $T \to 0$, due to the vanishing of non-linear terms.

In order to further test the conjecture that jumps between adjacent valleys of the potential are truly responsible for a normal heat transport, some other models have been studied as well.

Let us start by considering an asymmetric version of the rotor model, namely

$$V(x) = A - \cos x + 0.4 \sin 2x \ , \tag{152}$$

where A is fixed in such a way that the minimum of the potential energy is zero. Simulations performed at a temperature corresponding to one quarter of the barrier-height again indicate that the conductivity is finite, confirming the empirical idea that jumps are responsible for breaking the coherence of the energy flux [93].

It is instructive to look more closely at the behavior of this model. In view of the asymmetric potential, one might expect that the average force $\phi = \langle \sum f_i \rangle / N$ is non-zero (like, e.g., in the FPU-α case). Nonetheless, micro-canonical simulations show that although the distribution of forces is definitely asymmetric, their average value is numerically zero. This can be understood by noticing that in view of the boundedness of the potential, the system cannot withstand any compression.

Accordingly, we are led to introduce yet another model where the existence of more than one valley is accompanied by an unbounded potential. The simplest way to achieve this is by considering the double-well potential

$$V(x) = -x^2/2 + x^4/4 \tag{153}$$

(it is the same as in FPU-β with the opposite sign for the harmonic term). The results of direct simulations [98] performed with Nosé-Hoover thermostats are reported in Fig. 33 for three different values of the temperature below the barrier height. One can see that the growth of the conductivity, after an initial slowing down, increases towards, presumably, the same asymptotic behavior observed

in the FPU model. This is at variance with the preliminary simulations reported in Ref. [93], where it was conjectured a normal heat transport. These results thus indicate that jumps alone from one to another valley are not sufficient to destroy the coherence of low-k modes dynamics. It is necessary that subsequent jumps be independent of one another. In the double-well potential (153), $q_{i+1} - q_i$ cannot exhibit two consecutive jumps to the right.

7. Anharmonic chains with external substrate potentials

In this section we consider the class of models described by Hamiltonian (5), with a non-vanishing substrate potential U. This means that translational invariance breaks down and momentum is no longer a constant of the motion. Accordingly, the dispersion relation is such that $\omega(q) \neq 0$ for $q = 0$.

7.1. Ding-a-ling and related models

The so-called ding-a-ling model was first introduced by Dawson [99] as a toy model for a 1d plasma. It can refer to different contexts: (i) a set of identical charge-sheets embedded in a fixed neutralizing background; (ii) a system of harmonic oscillators with the same frequency and equilibrium positions sitting on a periodic lattice and undergoing elastic collisions that exchange their velocities. Notice that in the low-energy limit, it reduces to the 1d Einstein crystal, i.e. set of independent harmonic oscillators all having the same frequency (no dispersion).

Independently of [99], Casati et al. [100] introduced a modified version, where the harmonic oscillators (say the even-numbered particles) alternate with *free* particles of the same (unit) mass. The latter are only constrained to lie between the two adjacent oscillators. The Hamiltonian can be symbolically written as

$$\mathscr{H} = \frac{1}{2}\sum_{l}^{N} [p_l^2 + \omega_l^2 q_l^2] + \text{“hard point core”} , \tag{154}$$

where $\omega_l = \omega$ for even l and zero otherwise. A common feature of this class of models is that within collisions the motion of the particles can be determined analytically so that the basic requirement is the computation of the occurrence times of the collision events. Therefore, the dynamics naturally reduces to a discrete mapping.

For the isolated system (e.g. a chain with periodic boundary conditions) the dynamics depends only on the dimensionless parameter $\epsilon = e/(\omega a)^2$ where e is the energy per particle and a the lattice spacing. The Authors of Ref. [100] studied the dynamical behavior of the model by fixing $e = 1$ and changing ω. They concluded that, for ω and N large enough, the dynamics is strongly chaotic and soliton-like pulses are sufficiently attenuated [88]. This renders the model a good candidate to check the validity of Fourier's law.

Finite thermal conductivity. The validity of the Fourier's law was first established by performing a series of non-equilibrium simulations, where the freely moving end-particles were put in contact with two Maxwellian reservoirs. The average flux J was then computed by summing the amounts of energy δE exchanged with one of the reservoirs in all collisions during the simulation time.

The average temperature gradient was estimated with a linear fit (to get rid of boundary effects). By evaluating the thermal conductivity as a function of the lattice length up to $N = 18$ for $T_+ = 2.5$, $T_- = 1.5$ and $\omega = 1$, it was concluded that $\kappa(N)$ attains a constant limiting value already for $N > 10$.

After having established the existence of a finite value of the transport coefficient, the Authors have compared the value of κ with the result of linear response theory. To this aim, because of the discontinuities due to the collision processes, it was preferred to express the Green–Kubo formula in terms of the integral quantity

$$\Delta Q(t,\tau) = \int_t^{t+\tau} J(t_0)\,\mathrm{d}t_0 \ .$$

From Eq. (118), recalling that the ensemble average is equivalent to a time average (and understanding the limit $N \to \infty$), it is straightforward to show that (for more details see Ref. [103])

$$\kappa_{\mathrm{GK}}(T) = \lim_{\tau\to\infty} \frac{1}{2NT^2\tau}\langle(\Delta Q(t,\tau))^2\rangle_t \ , \tag{155}$$

where the subscript t indicates that the average is performed over the time variable t.

Additionally, it was decided to compute the total heat flux not by summing up the p_l^3 local contributions as, for instance, done in Ref. [90] for the hard point gas,[13] but, more directly, determining $\Delta Q(t,\tau)$ as the amount of energy exchanged in all collisions occurred in the interval $[t, t+\tau]$.

Casati et al. provided a convincing numerical evidence that the limit (155) exists for a closed chain of 48 particles and $\omega = 10$. In this case, the energy transport is diffusive and they showed that the κ_{GK}-value obtained in this way is in good agreement with the one obtained from direct simulations.[14]

The results of Casati et al. have been lately reconsidered by Mimnagh and Ballentine [101] who performed a detailed series of simulations with longer chains and in a wider parameter range. Curiously enough, they found that the value of κ reported in Ref. [100] is not the true asymptotic value (achieved only for $N > 200$) but a minimum of $\kappa(N)$. This can be seen in Fig. 34, where one can also appreciate how the unfortunate choice of working with $N < 20$ may give the false impression of a convergence towards a smaller value. This fact does not affect the correctness of the conclusion reported in Ref. [100] and the importance of the results, but signals again how cautious one should be in drawing conclusions from the study of relatively short systems! Motivated by this observation, Mimnagh and Ballentine carefully studied finite-size corrections in a wide range of ϵ-values, by plotting the resistivity $\rho(N) = 1/\kappa(N)$ versus N. In all cases, the data are well fitted by

$$\rho(N) = \rho_\infty\left(1 + \frac{\mu}{\sqrt{N}}\right) \tag{156}$$

for N large enough. Accordingly, the minimal chain length required to obtain an estimate of ρ_∞ with a fixed relative accuracy is proportional to μ^2, a quantity which is found to increase dramatically

[13] Recall, indeed, that the substrate potential does not contribute to the flux.

[14] As for the similar comparisons discussed in the previous chapter with reference to the coupled rotors, micro-canonical simulations have to be performed for an energy density that corresponds to the average temperature in the non-equilibrium simulations.

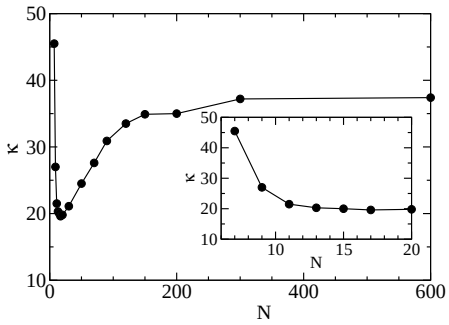

Fig. 34. Thermal conductivity of the ding-a-ling model. Size dependence of κ for $\omega = 1$ and $\epsilon = 1.5$ (from [101]). In the inset, an expanded view is presented in the range of sizes considered in Ref. [100].

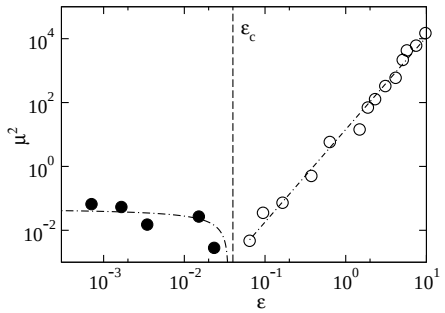

Fig. 35. The coefficient μ^2 as a function of ϵ for the ding-a-ling model (from [101]).

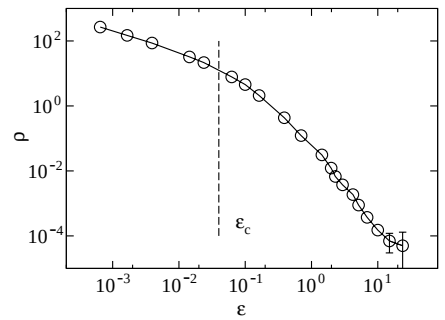

Fig. 36. The asymptotic resistivity ρ_∞ versus ϵ (from [101]).

for $\epsilon > \epsilon_c = 0.04$ (see Fig. 35). This is readily understood as $\epsilon \to \infty$ is an integrable limit that corresponds to a gas of bouncing free particles. The asymptotic resistivity ρ_∞ is a monotonously decreasing function of ϵ, displaying a crossover from a slower to a faster decay at ϵ_c (see Fig. 36). Since a similar crossover is found when looking at both the collision rate and the maximum Lyapunov

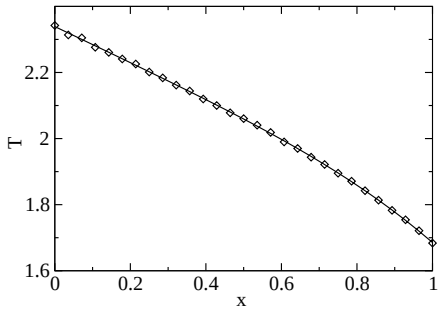

Fig. 37. Temperature profile for the ding-a-ling model, $\omega = 2$ (from [101]).

exponent, it is natural to interpret the phenomenon as a sort of transition from strong to weak chaos, in close analogy with what found, e.g., in the FPU model [102].

Finally, as for the temperature profile, the non-linear shape reported in Fig. 37 reveals a sizeable temperature dependence of the conductivity.

Modified models. Prosen and Robnik [103] considered the original Dawson system where, as already mentioned, the free particles are removed (i.e. they set $\omega_l = 1$ for all particles in (154)). They named it ding-dong model to distinguish it from the one presented above. Their careful numerical study confirmed the validity of Fourier's law in a wide temperature range. Besides direct non-equilibrium simulations with Maxwellian thermostats and the Green–Kubo formula, they also implemented an efficient transient method that allowed them to explore the high temperature regime ($T > 3$), where, because of the nearly integrable dynamics, a slow convergence of the averages with time and/or size is observed. In the opposite, low-temperature, limit ($T < 0.1$), they are able to prove that the conductivity vanishes as $\exp(-1/4T)$ finding a reasonable agreement with numerical results.

Posch and Hoover [104] investigated a modified ding-a-ling model where the harmonic potential is replaced by a gravitational one

$$\mathscr{H} = \sum_{l}^{N} \left[\frac{p_l^2}{2m} + m g_l |q_l| \right] + \text{“hard point core”} \ . \tag{157}$$

where g_l is a constant acceleration for even l and zero otherwise. Their simulations further confirm that thermal conductivity is finite for this class of models. Moreover, they computed the spectrum of Lyapunov exponents in the non-equilibrium steady state, showing that the microscopic dynamics takes place on a strange attractor. Finally they observed that the heat flux is proportional to the difference between the phase-space dimension and that of the strange attractor.

Finally, it is worth mentioning the exactly solvable model studied by Kipnis et al. [105] that could be regarded as the “stochastic version” of the ding-ling model. As in the latter, it consists of a linear array of harmonic oscillators but the interaction occurs via a random redistribution of the energy between nearest neighbors rather than through deterministic collisions. More precisely, upon denoting with $\xi_l = p_l^2 + q_l^2$ the energy of the lth oscillator (in suitable units), the dynamics is given

by the updating rules

$$\xi'_l = P(\xi_l + \xi_{l+1}), \quad \xi'_{l+1} = (1-P)(\xi_l + \xi_{l+1}) \ , \tag{158}$$

where P is a random variable uniformly distributed in the interval $[0,1]$. The total energy is thus kept constant except for the two oscillators at the chain extrema, that are in contact with reservoirs at different temperatures $T_\pm$ according to a Glauber dynamics. The Authors were able to rigorously show that a unique stationary non-equilibrium measure exists and to compute both the temperature profile and the heat flux in the steady state:

$$T(x) = T_- \left(\frac{1-x}{2}\right) + T_+ \left(\frac{1+x}{2}\right), \quad -1 \leqslant x \leqslant 1 \ , \tag{159}$$

$$j = -\frac{k_B}{4}(T_+ - T_-) \ . \tag{160}$$

The last results imply that Fourier's law holds and that the thermal conductivity is equal to $k_B/2$ in the chosen units.

7.2. Klein–Gordon chains

An important subclass of models (5) is the one in which the inter-particle potential is harmonic

$$\mathscr{H} = \sum_{l=1}^{N} \left[\frac{{p_l}^2}{2m} + U(q_l) + \tfrac{1}{2} C(q_{l+1} - q_l)^2 \right] \ ; \tag{161}$$

it is often referred to as the Klein–Gordon lattice. The latter has recently received a great attention as a prototypical system where strong discreteness effects may come into play in the limit of small C.

The first and most complete study of the transport problem in this class of models has been carried on by Gillan and Holloway [42] for the Frenkel–Kontorova potential

$$U(x) = -U_0 \cos\left(\frac{2\pi x}{a}\right) \ . \tag{162}$$

The model can be interpreted as a chain of either coupled particles in an external periodic field or torsion pendula subject to gravity. In the latter case $a = 2\pi$ and q_l represents the angle with respect to the vertical direction: it can be read as the discretized (and non-integrable) version of the well-known sine-Gordon field equation.

Besides energy, the dynamics admits a further conserved quantity, the winding number $\mathscr{P}$, which is an integer defined by the boundary condition $q_{l+N} = q_l + a\mathscr{P}$. In the particle interpretation $\mathscr{P}$ represents the number of potential wells, while for the pendula it can be viewed as the degree of built-in twist in the system. [15] According to the general theory of irreversible processes [1], transport involves thus the flow of both particles and energy caused by gradients of the number density and

[15] In physical terms, one has to apply equal and opposite forces (in the particle version) or torques (pendulum version) to the two end particles, in order to maintain the required value of $\mathscr{P}$ which can be also interpreted as the net number of kink excitations (i.e. the number of kinks minus the number of anti-kinks).

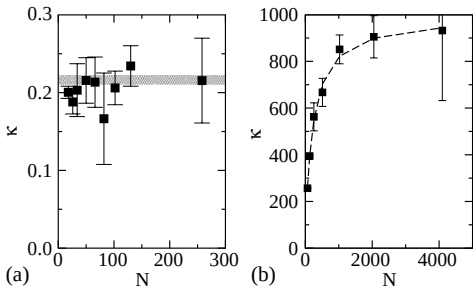

Fig. 38. Thermal conductivity versus chain length in ϕ^4 chains with Nosé-Hoover thermostats ($\Theta = 10$). Panel (a) refers to the single well case ($a = b = 1$ in Eq. (163): the results have been obtained for $C = 1.$, $T_+ = 8$, and $T_- = 6$. The shaded region represents the value obtained from the Green–Kubo formula with its statistical uncertainty. Panel (b) refers to the double-well case ($a = -1$, $b = 1$) for an average temperature $T = 0.37$ and a temperature difference 0.002. The dashed line is just a guide for the eyes.

temperature. Accordingly, a 2×2 matrix of transport coefficients is required, but because of the Onsager relations, there exist only three independent transport coefficients, that are chosen to be the thermal conductivity, the diffusion coefficient and the heat of transport. Gillan and Holloway computed the thermal conductivity numerically in the general case of non-vanishing winding number with three different methods: (i) attaching two heat baths; (ii) through the Green–Kubo formula; (iii) by adding an external field (see Section 3). All the methods give consistent results and clearly indicate that the thermal conductivity is finite.

Their results were later confirmed by a numerical study by Hu et al. [106] who investigated the dependence of the transport coefficient on the lattice length (for $P = 0$). In Ref. [106] it was also shown that the same holds for a more general version of the Frenkel–Kontorova model with an anharmonic inter-site potential.

In order to illustrate the type of behavior that is observed in this class of systems we show in Fig. 38 some data for the ϕ^4 chain

$$U(x) = \frac{a}{2}x^2 + \frac{b}{4}x^4 \ . \tag{163}$$

In panel (a), we present a case of fast convergence to a small κ value for a single-well potential; panel (b) refers instead to a low-temperature regime characterized by large thermal conductivity.

Evidence of a finite conductivity for the case $a = 0$ has been reported in Refs. [49,107]. The conductivity is found to decrease with temperature according to the law [49]

$$\kappa(T) \propto T^{-1.35(2)} \tag{164}$$

that is reminiscent of what often experimentally observed in insulating crystals. Upon increasing ΔT, there exists a "transition" to a non-linear regime characterized by a non-uniform local temperature gradient. By including the empirical law (164) into Fourier's law, it is possible to check the consistency with the measured $T(x)$: a good agreement with the simulations is found, provided boundary jumps are taken into account.

Finally, Tsironis et al. [108] obtained further numerical evidence of the existence of a finite thermal conductivity for systems like (161). Beside reconsidering the Frenkel–Kontorova potential (162), two further examples were analyzed, the sinh-Gordon and bounded single-well potentials,

$$U(x) = \cosh x - 1, \quad U(x) = \tfrac{1}{2}(1 - \operatorname{sech}^2 x) \tag{165}$$

as representatives of the classes of hard and soft anharmonicity, respectively.

8. Integrability and ballistic transport

When the equilibrium dynamics of a lattice can be decomposed into that of independent "modes", the system is expected to behave as an ideal conductor. The simplest such example is obviously the harmonic crystal, that has infinite conductivity and cannot, therefore, support any temperature gradient. However, this applies also to the broader context of integrable non-linear systems. They are mostly one-dimensional models characterized by the presence of "mathematical solitons", whose stability is determined by the interplay of dispersion and non-linearity. This interplay is expressed by the existence of a macroscopic number of *conservation laws* constraining the dynamical evolution. Thereby, the existence of stable non-linear excitations in integrable systems is expected to lead to ballistic rather than to diffusive transport. As pointed out by Toda [109], solitons travel freely, no temperature gradient can be maintained and the conductivity is thus infinite. From the point of view of the Green–Kubo formula, this ideal conducting behavior is reflected by the existence of a non-zero flux autocorrelation at arbitrarily large times. According to the discussion reported in Section 6.2, this, in turn, implies that the finite-size conductivity diverges linearly with the size.

Although integrable models are, in principle, considered to be exactly solvable, the actual computation of dynamic correlations is technically involved. A more straightforward approach is nevertheless available to evaluate the asymptotic value of the current autocorrelation. This is accomplished by means of an inequality due to Mazur [110] that, for a generic observable A, reads as

$$\lim_{\tau\to\infty} \frac{1}{\tau} \int_0^\tau \langle A(t)A(0)\rangle \, \mathrm{d}t \geqslant \sum_n \frac{\langle AQ_n\rangle^2}{\langle Q_n^2\rangle} \ , \tag{166}$$

where $\langle \ldots \rangle$ denotes the (equilibrium) thermodynamic average, the sum is performed over a set of conserved and mutually orthogonal quantities Q_n ($\langle Q_n Q_m\rangle = \langle Q_n^2\rangle \delta_{n,m}$). Furthermore, it is assumed that $\langle A\rangle = 0$.

Zotos [111] applied the above result to the equal-masses Toda chain with periodic boundary conditions, defined, in reduced units, by the Hamiltonian

$$\mathscr{H} = \sum_{l=1}^{N} \left[\frac{p_l^2}{2} + \exp(-r_l) \right] \ , \tag{167}$$

where $r_l = x_{l+1} - x_l$ is the relative position of neighboring particles. As is known [112], the model is completely integrable as admits N independent constants of the motion, the first among

which are

$$Q_1 = \sum_{l=1}^{N} p_l \ , \tag{168}$$

$$Q_2 = \sum_{l=1}^{N} \frac{p_l^2}{2} + \mathrm{e}^{-r_l} \ , \tag{169}$$

$$Q_3 = \sum_{l=1}^{N} \frac{p_l^3}{3} + (p_l + p_{l+1})\mathrm{e}^{-r_l} \ , \tag{170}$$

$$Q_4 = \sum_{l=1}^{N} \frac{p_l^4}{4} + (p_l^2 + p_l p_{l+1} + p_{l+1}^2)\mathrm{e}^{-r_l} + \frac{1}{2}\,\mathrm{e}^{-2r_l} + \mathrm{e}^{-r_l}\mathrm{e}^{-r_{l+1}} \ , \tag{171}$$

$$Q_5 = \sum_{l=1}^{N} \frac{p_l^5}{5} + (p_l^3 + p_l^2 p_{l+1} + p_l p_{l+1}^2 + p_{l+1}^3)\mathrm{e}^{-r_l} \tag{172}$$

$$+ (p_l + p_{l+1})\mathrm{e}^{-2r_l} + (p_l + 2p_{l+1} + p_{l+2})\mathrm{e}^{-r_l}\mathrm{e}^{-r_{l+1}} \ldots \tag{173}$$

The "trivial" conserved quantities Q_1 (the total momentum) and Q_2 (the total energy) are of course present in all translationally invariant systems of the form (2), irrespective of their integrability.

Let us consider the fixed temperature-pressure thermodynamic ensemble,

$$\langle A(t)A(0)\rangle = Z^{-1} \int \prod_{l=1}^{L} \mathrm{d}\,p_l\,\mathrm{d}r_l A(t)A(0)\mathrm{e}^{-\beta(\mathscr{H}+PL)} \ , \tag{174}$$

where $Z = \int \prod_{l=1}^{N} \mathrm{d}\,p_l\,\mathrm{d}r_l \mathrm{e}^{-\beta(\mathscr{H}+PL)}$, $L = \sum_{l=1}^{N} r_l$ is the "volume" of the chain and P is the pressure. In this ensemble, equal-time correlation functions can be calculated analytically. For instance, the average inter-particle distance is

$$\langle r\rangle = \ln\beta - \Psi(\beta P) \tag{175}$$

where $\Psi(z)$ is the digamma function.

The total heat flux is given by (see Eqs. (23) and (30))

$$J = \sum_{l} \left[p_l h_l + \frac{(p_{l+1} + p_l)}{2}\, r_l \mathrm{e}^{-r_l} \right] \ , \tag{176}$$

where $h_l = p_l^2/2 + \frac{1}{2}(\mathrm{e}^{-r_l} + \mathrm{e}^{-r_{l-1}})$. In order to apply the Green–Kubo formula in the chosen ensemble, one has to consider a "shifted" flux (see the discussion at the end of Section 5.2)

$$\tilde{J} = J - \frac{\langle Q_1 J\rangle}{\langle Q_1^2\rangle}\, Q_1 \ . \tag{177}$$

This is equivalent to removing the contribution of Q_1 in the right hand side of the Mazur inequality (166) for $A = J$.

Lower bounds on the long time value of $\langle J(t)J(0)\rangle$ can thus be calculated by the inequality (166), using the first m conservation laws [111]. As Q_3 has a structure very similar to the energy current, a large contribution from this term has to be expected. Moreover, Q_n with even n are uncoupled with $\tilde{J}$, so that it suffices to consider odd values of n.

In order to utilize the inequality (166), it is not necessary to orthogonalize the conserved quantities (168)–(173). One can, indeed, replace the sum of the first m terms in the r.h.s. of Eq. (166) with

$$C^m = \langle \tilde{J}|Q\rangle \langle Q|Q\rangle^{-1} \langle Q|\tilde{J}\rangle \ , \tag{178}$$

where $\langle Q|Q\rangle$ is the $m \times m$ overlap matrix of $Q_{n'n}$ and $\langle Q|\tilde{J}\rangle$ is the overlap vector of $\tilde{J}$ with the $Q'_n s$. The ratio $C^m/\langle \tilde{J}^2\rangle$, representing a lower bound to the conductivity κ, is found to increase monotonously with the temperature. At low T, the growth is linear with a slope comparable to the density of solitons $N_s/N = \ln 2/\pi^2 T$. This trend is interpreted as an evidence for the increasing contribution of thermally excited non-linear modes to ballistic transport.

9. Two-dimensional lattices

It is well known that many properties of statistical systems depend on the dimension d of the space, where they are embedded. In Section 5, we have seen that transport properties are not expected to violate this rule. In this Chapter we discuss some results of molecular-dynamics simulations in two dimensions. In fact, as soon as the dimension of the physical-space is set to a value larger than 1, the direct investigation of sufficiently large systems becomes problematic.

First, we briefly discuss the numerical studies appeared so far in the literature, presenting them in a historical perspective. Then, we more extensively discuss some recent numerical experiments that have allowed verifying the predictions of mode-coupling theory also in two dimensions.

9.1. Early results

To our knowledge, the first attempts of investigating the heat conduction problem in 2d lattices with (at that time) heavy numerical simulations are two papers by Payton et al. [32,113], that appeared more than three decades ago. These Authors investigated the combined effect of non-linearity and disorder on heat conduction in 2d harmonic and anharmonic lattices, with Lennard–Jones pair potentials. Their studies aimed also at analyzing the dependence of heat conductivity κ on the temperature and on the concentration of impurities, as a measure of disorder. They found evidence of an increase of κ in disordered non-linear systems compared to the harmonic case (see also Section 6).

On the other hand, the dependence of κ on the system size was ignored, probably because the Authors did not consider this a problem of major concern. In fact, according to the classical view of Peierls [2], phonon–phonon scattering processes were assumed to be sufficiently efficient to ensure normal transport properties in the presence of strong non-linearity and disorder.

Later, Mountain and MacDonald [114] performed a more careful study on the dependence of κ on the temperature T. They considered a 2d triangular lattice of unit-mass atoms, interacting via a Lennard–Jones 6/12 potential. At variance with the previous investigations, no disorder was included, and their numerical results were consistent with the expected classical law $\kappa \sim T^{-1}$. Again, the dependence of κ on the system size was not investigated.

The first contribution in this direction is the paper by Jackson and Mistriotis [79]. These Authors compared measurements of κ in the 1d and 2d FPU lattices: they concluded that in both cases there was no evidence that the transport coefficient is finite in the thermodynamic limit. It is worth mentioning an interesting remark by these Authors: "the dependence of κ on the system size cannot be adequately described in the high temperature, i.e., classical, limit by Peierls' model of the diluted phonon gas, because the perturbative Umklapp processes cannot account for the genuine non-linear effects that characterize such a dependence".

Conversely, more recent molecular-dynamics simulations of the 2d Toda-lattice [115] have been interpreted in favor of the finiteness of κ in the thermodynamic limit. Further confirmation in this direction can be found in Appendix B of the interesting paper by Michalski [116], where heat conductivity in models of amorphous solids was thoroughly investigated.

The interplay of disorder and anharmonicity, that inspired the first contributions by Payton, Rich and Visscher has been reconsidered by Poetzsch and Böttger [117,118] who investigated percolating and compositionally disordered 2d systems. In particular, they tried to pinpoint the role of third- and fourth-order anharmonicity, concluding that, at equal temperature, the latter yields a larger value of κ than the former one. Moreover, the Authors reported also about the dependence of κ on the system size. They assumed the same point of view of Michalski [116], but a careful inspection of Fig. 5 in [117] shows that their data are also compatible with a systematic increase of κ with the system size.

In a more recent and accurate investigation, Dellago and Posch [119] studied, by molecular-dynamics techniques, heat conduction as well as Lyapunov instability in a generalized version of the XY-model. Besides various interesting results, their paper contains a very clear indication of the finiteness of κ in the thermodynamic limit. In the light of what discussed in Section 6.4, this result is not surprising, since κ is finite already in 1d for models of this type. A further interesting remark contained in Ref. [119] concerns the behavior of κ below the transition temperature of the XY-model when the diffusive behavior of energy transport is lost and anomalous behavior seems to set in.

9.2. Divergence of heat conductivity

Heat conduction in 2d models of oscillators coupled through anharmonic, momentum-conserving interactions is expected to exhibit different properties from those of 1d systems. In fact, MCT predicts a logarithmic divergence of κ with the system size N at variance with the power-law predicted for the 1d case (see Section 5.3).

Following [69], we discuss the results of molecular-dynamics simulations of the FPU-β potential (see Eq. (4), $g_3 = 0$) and the LJ-(6/12) potential (see Eq. (3)). For the sake of simplicity we introduce the shorthand notations $V_1(z)$ and $V_2(z)$ to denote, respectively, the two models. The goal of this twofold choice is to verify that the prediction of MCT is truly independent of the potential, provided it belongs to the class of anharmonic momentum-conserving interactions.

While V_1 does not contain natural scales for both distances and energies, the natural length scale of $V_2(z)$ is the equilibrium distance a, while its energy scale is the well depth ε. Therefore, after having arbitrarily fixed $g_2 = 1$ and $g_4 = 0.1$ in $V_1(z)$, a and ε have been determined ($a = 25$, $\varepsilon = 8.6$) by imposing that the coefficients of the second and fourth order terms of the Taylor expansion of V_2 around its minimum coincide with g_2 and g_4, respectively. Notice, however, that, at variance

with $V_1(z)$, the Taylor expansion of $V_2(z)$ incorporates also a non-vanishing cubic term. Despite both models are characterized by the same shortest harmonic time scale, $\tau_{\min}=\pi/\sqrt{2}$, the L-J model has been integrated with a slightly shorter time step ($\Delta t=5\times 10^{-3}$, compared to 10^{-2} for the FPU model) in order to ensure a sufficient accuracy when the dynamics experiences the strong non-linearities of $V_2(z)$ (nearby the divergence of the Lennard–Jones potential).

In both cases, simulations have been performed with reference to a square lattice containing $N_x\times N_y$ atoms of equal masses m. The equilibrium position of each atom has been chosen to coincide with a lattice site, labelled by a pair of integer indices (i,j). The origin of the Cartesian reference frame is fixed in such a way that $1<i<N_x$ and $1<j<N_y$. Accordingly, the components of the 2d-vector of the equilibrium position, $\mathbf{r}_{ij}^0$, are given by the integer pairs (i,j). Moreover, in analogy to the 1d case, each atom has been assumed to interact with its nearest-neighbors (herein identified with the von Neumann neighborhood).

The model is thus represented by the Hamiltonian

$$\mathscr{H}=\sum_{i=1}^{N_x}\sum_{j=1}^{N_y}\left[\frac{|\mathbf{p}_{ij}|^2}{2m}+V(|\mathbf{q}_{i+1j}-\mathbf{q}_{ij}|)+V(|\mathbf{q}_{ij+1}-\mathbf{q}_{ij}|)\right]\ , \tag{179}$$

where $\mathbf{q}_{ij}(t)=\mathbf{r}_{ij}(t)-\mathbf{r}_{ij}^0$, $\mathbf{r}_{ij}(t)$ is the instantaneous position vector of the (i,j)-atom, and $\mathbf{p}_{ij}(t)$ is the corresponding momentum vector.

For what concerns the definition of local temperature, the following definitions are all equivalent (see also Section 2.2):

$$k_{\mathrm{B}}T_{ij}=\frac{\langle(p_{ij}^{(x)})^2\rangle}{m}=\frac{\langle(p_{ij}^{(y)})^2\rangle}{m}=\frac{\langle(p_{ij}^{(x)})^2+(p_{i,j}^{(y)})^2\rangle}{2m}\ , \tag{180}$$

where $p_{ij}^{(x)}$ and $p_{ij}^{(y)}$ are the x and y components of the momentum vector $\mathbf{p}_{ij}$, respectively.

Moreover, tedious but straightforward calculations, akin to those presented in Section 2.3, allow to express the x and y components of the local heat flux $\mathbf{j}_{ij}$ as

$$\begin{aligned} j_{ij}^{(x)}&=\frac{a}{4m}[f_{ij}^{xx}(p_{ij}^{(x)}+p_{i+1j}^{(x)})+f_{ij}^{yx}(p_{ij}^{(y)}+p_{i+1j}^{(y)})]\ ,\\ j_{ij}^{(y)}&=\frac{a}{4m}[f_{ij}^{xy}(p_{ij}^{(x)}+p_{ij+1}^{(x)})+f_{ij}^{yy}(p_{ij}^{(y)}+p_{ij+1}^{(y)})]\ , \end{aligned} \tag{181}$$

where the components of the local forces are defined as

$$\begin{aligned} f_{ij}^{xx}&=-\frac{\partial V(|\mathbf{q}_{i+1j}-\mathbf{q}_{ij}|)}{\partial q_{ij}^{(x)}} \quad f_{ij}^{yx}=-\frac{\partial V(|\mathbf{q}_{i+1j}-\mathbf{q}_{ij}|)}{\partial q_{ij}^{(y)}}\\ f_{ij}^{xy}&=-\frac{\partial V(|\mathbf{q}_{ij+1}-\mathbf{q}_{ij}|)}{\partial q_{ij}^{(x)}} \quad f_{ij}^{yy}=-\frac{\partial V(|\mathbf{q}_{ij+1}-\mathbf{q}_{ij}|)}{\partial q_{ij}^{(y)}}\ . \end{aligned}$$

Finally, in analogy with Eq. (30), the total heat flux vector is defined as

$$\mathbf{J}=\sum_{i,j}\mathbf{j}_{ij}\ . \tag{182}$$

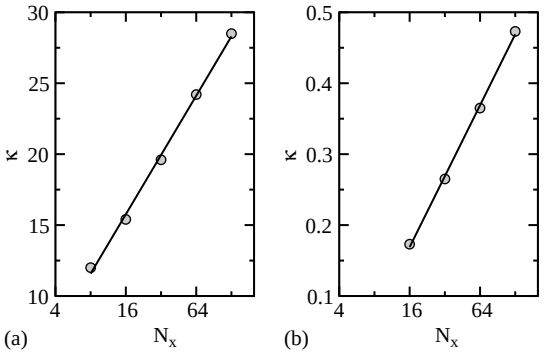

Fig. 39. Heat conductivity κ versus the system size N_x for the 2d FPU β (a) and Lennard–Jones (b) models. In panel (a) $T_+ = 20$ and $T_- = 10$; in panel (b) $T_+ = 1$ and $T_- = 0.5$. In both cases, statistical errors have the size of the symbols.

The non-equilibrium simulations have been performed by coupling all atoms on the left (right) edge of the 2d lattice with the same thermal bath operating at temperature T_+ (T_-). In the numerical studies reported hereafter, thermal baths have been simulated by applying the Nosé-Hoover method. Nonetheless, the Authors of Ref. [69] verified that the same results are obtained upon using stochastic thermal baths, as well. Periodic and fixed boundary conditions have been adopted in the direction perpendicular (y) and parallel (x) to the thermal gradient, respectively. Finally, let us notice that, for the investigation of the thermodynamic limit, the simulations for different lattice sizes should be performed by keeping the ratio $R = N_y/N_x$ constant. From the numerical point of view, it is convenient to choose small R values, since for a given longitudinal length aN_x, the simulations are less time consuming. However, too small ratios would require considering larger system sizes to clearly observe 2d features. In [69] it was checked that $R = 1/2$ is a good compromise for both V_1 and V_2 choices.

With the above physical setup, heat equation (1) implies that a constant thermal gradient should establish through the lattice in the x-direction with $\langle J^{(x)} \rangle > 0$ and $\langle J^{(y)} \rangle = 0$. The time span needed for a good convergence of the time-average $\langle \cdot \rangle$ increases with N_x: for instance, $\mathcal{O}(10^5)$ units proved sufficient for $N_x = 16$, while $\mathcal{O}(10^7)$ units are needed when $N_x = 128$ (for not too small energy densities).

The detailed analysis of temperature profiles performed in Ref. [69] has revealed deviations from the linear shape predicted by Fourier law (this is particularly true in the case of the Lennard–Jones potential V_2), but one cannot exclude that this is to be attributed to the relatively large temperature differences adopted in order to have non-negligible heat fluxes. Anyway, despite such deviations, simulations provide convincing evidence that the temperature gradient scales like N_x^{-1}. Accordingly, the dependence of κ with the system size aN_x can be determined by plotting $\kappa \propto \langle j^{(x)} \rangle N_x$ versus N_x. The data reported in Fig. 39 support the MCT prediction of a logarithmic growth both for the FPU and Lennard–Jones potentials for two rather different choices of heat bath temperatures.

Since also in the 2d case the temperature gradient vanishes in the thermodynamic limit, one is allowed to conjecture that linear response theory should reproduce the behavior of sufficiently large systems.

According to the general discussion carried on in Section 5.2,

$$\kappa = \kappa_{xx} = \frac{1}{k_B T^2} \lim_{t\to\infty} \int_0^t \frac{\langle J^{(x)}(\tau) J^{(x)}(0)\rangle}{V}\, d\tau \ , \tag{183}$$

where $V = Ra^2 N_x^2$ is the system volume and $J^{(x)}$ is the x-component of the total heat flux vector (182). Notice that simulations have to be performed for a sufficiently large size N_x, since the thermodynamic limit has to be taken before the infinite time limit in the above formula.

Numerical simulations at constant energy, with $R = 1/2$ and periodic boundary conditions in both directions [69] convincingly suggest a logarithmic divergence (in time) of the correlation integral appearing in (183). Once more, this scaling behavior is consistent with the outcome of direct non-equilibrium simulations. Indeed, by assuming that Eq. (183) reproduces the correct size dependence if the integral is cut-off at a time $t = aN_x/v_s$ [72], the temporal logarithmic divergence translates into an analogous divergence with the system size (see also Section 6.2).

Let us finally mention that recent results by Shimada et al. [121] confirm the overall scenario and, furthermore, provide the direct confirmation that κ is finite in 3d for this class of models.

10. Conclusions

While this review, hopefully, provides a rather complete account of the existing dynamical approaches to heat conduction in low-dimensional lattices, it certainly does not solve all open questions. Some of the most interesting issues requiring further investigations are briefly summarized in this concluding chapter.

The first problem concerns heat transport at low temperatures. It is well known that many of the Hamiltonian models used for describing anharmonic crystals with nearest-neighbor interactions exhibit very slow relaxation to equilibrium below a typical energy density e_c (or temperature) that depends on the model and on the space dimension. For instance, the 1d FPU β-model shows a crossover between fast and slow relaxation at a value of the energy density $e \approx 1$, with all the parameters of the model set to unity [102]. The same holds for the 1d Lennard–Jones potential at a close value of the energy density for ε and a (see Eq. (3)) chosen in such a way that the coefficients of the second and fourth order terms of the Taylor series expansion around the equilibrium position coincide with those of the FPU β-model. When passing to 2d, for both models, the value of e_c decreases: for instance, in the Lennard–Jones 6/12 potential $e_c \approx 0.3$ [122]. This peculiar behavior in the low-temperature regime can be attributed to long living meta-stable states that slow-down dramatically the relaxation process.[16] A similar scenario can be observed in the 1d rotor model described in Section 6.4. When approaching the two integrable limits of this model (the harmonic and the "free rotors" for small and large temperatures respectively) again slow relaxation mechanisms set in. An even more interesting situation concerns the 2d version of the rotator model, akin to the

[16] It would be interesting to investigate the possibility of experimental tests of such a phenomenon in real solids, where transient effects can be usually resolved by fast spectroscopic techniques. Some authors have also suggested strong analogies with glassy dynamics [123], a subject that has recently become of primary interest for theoretical end experimental investigations in out-of-equilibrium physics.

XY-model (see e.g. [124] and references therein). In fact, it is characterized by the presence of the so-called Kosterlitz–Thouless phase transition at finite temperature between a disordered high temperature phase and a low temperature one, where vortices condensate. From a dynamical point of view, there are analogies with the above mentioned examples, namely also this low temperature phase exhibits slow relaxation dynamics to equilibrium [119]. The possible relation with topological changes of the phase space due to the presence of a phase transition should be investigated.

Upon all what we have discussed in this review, in particular in Section 5, one might expect that the slowing-down of relaxation processes at low temperatures should be even more relevant for transport properties. In fact, recent numerical investigations [69] have shown that in 2d FPU-like models the heat-flux correlation function seemingly exhibits the resurgence of a power-law divergence of the heat conductivity in the thermodynamic limit.[17] Anyway, it is quite difficult to conclude only on the basis of numerical investigations if this has to be attributed to finite size and finite time effects (see the discussion reported in Ref. [69]). The problem could be better tackled in the 1d FPU model, where finite-size effects are expected to be even more relevant below the crossover temperature. This question is closely related to other finite-size effects observed in these models [63].

Another issue that remains partially unexplored concerns the possible role of non-linear excitations in transport. The idea that solitons may play a role in heat conduction dates back to Toda [109]. For instance, it has been invoked to explain the anomalous behavior of the FPU model as a consequence of ballistic transport due to solitons of the modified Korteweg-deVries equation. Actually, such an equation can be obtained as a continuum limit of the FPU lattice model. Numerical experiments indicate that such solutions may persist as long living states of the FPU dynamics. On the other hand, upon what reported in the previous chapters, the leading contribution to the divergence of heat conductivity is given by the slow-relaxation properties of long wavelength modes. We cannot however exclude that also non-linear excitations like solitons or kinks, according to the model at hand, may contribute to the divergence of κ. Recently, it has been proposed that transport properties should be affected also by the presence of periodic, spatially localized lattice waves denoted as *breathers* [108]. Anyway, the effect of any kind of non-linear excitation is quite difficult to be detected. Even if we could assume that the energy flux is the sum of a phononic and a solitonic contribution, $J = J_{\mathrm{ph}} + J_{\mathrm{sol}}$ how can we hope to distinguish the latter if the phononic part already yields anomalous behavior? In general, the chaotic features of the dynamics prevent the possibility of disentangling the contribution of non-linear waves from that of extended modes. In this respect some better insight on the role of non-linear excitations might be obtained from the analysis of integrable systems, as in the problem of ballistic spin transport (see [111] and references therein). Altogether, non-linear excitations are one of the possible ingredients affecting the divergence of heat conductivity. Although it seems rather natural to conjecture that all models characterized by momentum conservation fall in the same universality class (with the only exception of bounded potentials), the numerical discrepancies among the various systems are at least suggestive of relatively strong finite-size corrections. If, on the other hand, we remind that there is no way to control the approximations implicitly contained in the self-consistent mode-coupling theory, we realize that even the problem of determining the asymptotic growth rate of heat conductivity in homogeneous systems may have not yet come to an end.

[17] It is worth recalling that for this class of 2d models, the heat conductivity shows a logarithmic divergence with the system size, see Section 9.

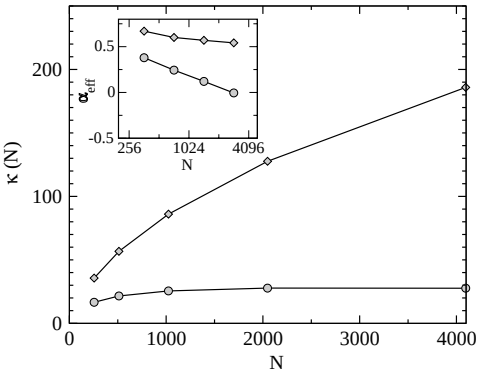

Fig. 40. Finite-length conductivity in disordered FPU chains as from Ref. [125], $T_+ = 1 \times 10^{-3}$, $T_- = 5 \times 10^{-4}$. Diamonds refer to free boundary conditions while full dots refer to fixed b.c.. In the inset we report the effective exponent defined in (106).

A further remark concerns the combination of disorder and non-linearity. This has been considered sporadically in the past [32,113,117,118] in relation with the problem of heat transport (see also Section 9.1). We should say that poor progress has been made in this direction during the last decades. In fact, few results are available and in general no clear conclusion can be drawn about the dependence of the thermal conductivity on the system size. Even the most recent results contained in a contribution by Hu et al. [125] are not convincing in this respect. In Fig. 40 we compare the finite-length heat conductivity $\kappa(N)$ for free and fixed boundary conditions in the same model and for the same parameter values considered in [125]. Upon these results, one can only conclude that the dynamical regime explored in that paper is practically indistinguishable from the disordered harmonic case (see Section 4.2). Despite the already heavy numerical efforts needed to produce the data in Fig. 40, much longer time scales and system sizes have to be explored in order to fully appreciate the role of non-linear terms.

We conclude this section by addressing the reader to a final interesting open question about the study of heat conduction in structurally disordered lattices, as well as in models of amorphous materials [116] or quasicrystals [126]. When the crystal structure of a lattice is destroyed, the phononic contribution to anomalous heat transport is expected to play a much less relevant role. Nonetheless, peculiar transport properties are known to arise in real amorphous materials [127]. The most studied examples are real glasses, where viscosity exhibits a dramatic increase below a transition temperature specific of the material at hand. It is still unclear if phenomena like this should be ascribed to mechanisms other than phononic contributions. The effectiveness of mode-coupling theory in describing thermodynamic-limit divergences in models of solids, as well as glassy dynamics in models of real glasses, indicate the extremely fascinating perspective of a possible unified theory of anomalous transport in condensed matter systems. In this respect, we should also remark that much remains to be done in both cases in order to clarify the reliability of the analytical estimates based on the mode-coupling approach. In particular, the many approximations adopted in the derivation of the scaling laws reported in Section 5.3 are justified by quite rough arguments. A closer inspection of their validity by performing analytical as well as more accurate numerical calculations would be highly desirable. Furthermore, the problem of thermodynamic-limit divergences is not the

only open question in this context. The other crucial facet of the problem is the temperature dependence of heat conductivity in such materials, where various dynamical solutions associated with the non-homogeneous structure of the systems should be considered as responsible of deviations from the expected classical laws.

Acknowledgements

We thank L. Ballentine, A. Dhar, D. Mimnagh, M. Vassalli for providing us numerical data. We acknowledge useful discussions with the members of the research group *Dynamics of Complex Systems* in Florence as well as a partial support by the INFM project *Equilibrium and non-equilibrium dynamics in condensed matter*. This work is also part of the EC network LOCNET, Contract No. HPRN-CT-1999-00163 and of COFIN00 project *Caos e localizzazione in meccanica classica e quantistica*.

Note added in proof

A recent paper by Narayan and Ramaswamy [128] reports a renormalization group calculation of the divergence exponent yielding $\alpha = 1/3$ (see Eq. (145)) for a 1d fluid. Although consistent with the most accurate data for the hard point gas [129], this estimate is still significantly different from data for oscillator chains (see again Table 1). In this respect, the existence of different universality classes and/or crossover scenarios remains still to be settled.

Appendix A. A rigorous definition of temperature

In this appendix we discuss a rigorous dynamical definition of temperature. The starting point is the entropy S since in the μ-canonical ensemble, it plays the role of a generalized thermodynamic potential which allows determining (through the computation of suitable derivatives) any other thermodynamic observable.

In particular, the temperature can be defined from the well known thermodynamic relation,

$$\frac{1}{T} = \left(\frac{\partial S}{\partial E}\right)_V \ , \tag{A.1}$$

where the subscript V indicates partial derivative at constant volume.

Upon assuming that the phase space is equipped with a uniform undecomposable probability measure, S is given by the logarithm of the volume covered by all micro-states with energy $\mathscr{H} \leqslant E$,

$$S(E,N,V) \equiv \ln \Omega(E,N,V) = \ln \int_{\mathscr{H} \leqslant E} \mathrm{d}\Gamma \ , \tag{A.2}$$

where we have neglected an irrelevant multiplicative factor in front of Ω necessary only to make the argument of the logarithm dimensionless.

From Eqs. (A.1), (A.2) one obtains

$$\frac{1}{T} = \frac{1}{\Omega} \int_{\mathscr{H}=E} \frac{\mathrm{d}\sigma}{\|\nabla \mathscr{H}\|} \tag{A.3}$$

where the integral is the "area" of the constant energy hyper-surface $\mathscr{H} = E$. Upon now introducing a vector $\mathbf{u}$ such that $\nabla \cdot \mathbf{u} = 1$ and using the divergence theorem, we obtain

$$\frac{1}{T} = \frac{\int_{\mathscr{H}=E} \mathrm{d}\sigma / \|\nabla \mathscr{H}\|}{\int_{\mathscr{H}<E} \nabla \cdot \mathbf{u}\, \mathrm{d}\Gamma} = \frac{\int_{\mathscr{H}=E} \mathrm{d}\sigma / \|\nabla \mathscr{H}\|}{\int_{\mathscr{H}=E} \nabla \mathscr{H} \cdot \mathbf{u}\, \mathrm{d}\sigma / \|\nabla \mathscr{H}\|} \tag{A.4}$$

It is easy to recognize that the above equation coincides with Eq. (6) which can thus be obtained by following a purely geometrical approach. More details about the derivation of this formula can be found in [20].

Appendix B. Exact solution for the homogeneous harmonic chain

In this appendix we closely follow the procedure adopted in Ref. [51] to solve the Fokker–Planck (58) equation for a homogeneous harmonic chain. Starting from the equilibrium solution (67), let us define

$$\begin{aligned} \bar{\mathbf{U}} &\equiv \mathbf{U}_e + \frac{k_\mathrm{B}(T_+ - T_-)}{2\omega^2}\mathbf{U}\ , \\ \bar{\mathbf{V}} &\equiv \mathbf{V}_e + \frac{k_\mathrm{B}(T_+ - T_-)}{2}\mathbf{V}\ , \\ \bar{\mathbf{Z}} &\equiv \frac{k_\mathrm{B}(T_+ - T_-)}{2\lambda}\mathbf{Z}\ , \end{aligned} \tag{B.1}$$

From Eq. (64), it follows that $\mathbf{U}$, $\mathbf{V}$ and $\mathbf{Z}$ satisfy the equations,

$$\mathbf{Z} = -\mathbf{Z}^\dagger\ , \tag{B.2}$$

$$\mathbf{V} = \mathbf{U}\mathbf{G} + \mathbf{Z}\mathbf{R}\ , \tag{B.3}$$

$$2\mathbf{S} - \mathbf{V}\mathbf{R} - \mathbf{R}\mathbf{V} = v[\mathbf{G}\mathbf{Z} - \mathbf{Z}\mathbf{G}]\ , \tag{B.4}$$

where $v = \omega^2/\lambda^2$ is the only, dimensionless, parameter that matters. In addition, $\mathbf{U}$ and $\mathbf{V}$ are required to be symmetric. From the peculiar structure of the matrices $\mathbf{R}$ and $\mathbf{S}$, it follows that the l.h.s. of Eq. (B.4) is a *bordered* matrix (i.e., its only non-vanishing elements are located on the external columns and rows). Accordingly, the r.h.s. must be bordered as well, i.e. in the bulk, $\mathbf{Z}$ commutes with G. The most general structure of a matrix commuting with $\mathbf{G}$ in the interior is the linear combination of a matrix M^{d}_{ij} with equal elements along the diagonals ($i+j$ constant) and a matrix M^{c}_{ij} with equal elements along the cross-diagonals ($i-j$ constant). The antisymmetry requirement for $\mathbf{Z}$ (see Eq. (B.2)), implies that no contribution of the second type is present and, more precisely, that

$$Z_{ij} = \phi(j-i) \tag{B.5}$$

with the further constraint $\phi(j) = -\phi(-j)$. The quantities $\phi(j)$ are fixed by equating the border elements of the commutator $[G, Z]$ (multiplied by v) with those of the l.h.s. of Eq. (B.4),

$$v\phi(j) = \delta_{j1} - V_{1j} = \delta_{j1} + V_{N,N-j+1}\ , \tag{B.6}$$

where $\phi_N \equiv 0$ by definition. From Eq. (B.3) and its transposed expression it follows that $\mathbf{U}$ satisfies a similar relation to that for Z,

$$\mathbf{GU} - \mathbf{UG} = \mathbf{RZ} + \mathbf{ZR} \ . \tag{B.7}$$

Accordingly, also $\mathbf{U}$ commutes with G in the bulk. The different symmetry property of $\mathbf{U}$ with respect to $\mathbf{Z}$ implies, however, that $\mathbf{U}$ is constant along the cross-diagonals. It is easy to verify that a solution of Eq. (B.7) is given by

$$U_{ij} = \begin{cases} \phi(i+j-1) & \text{if } i+j \leqslant N \ , \\ \phi(2N+1-i-j) & \text{if } i+j \geqslant N \ . \end{cases} \tag{B.8}$$

In principle, this is not the only solution of Eq. (B.7), as one can add any symmetric matrix commuting with G; however, one can check a posteriori that the addition of any such matrix would eventually violate the symmetry properties of $\mathbf{V}$.

As a result of Eq. (B.8), also the matrix $\mathbf{X}$ can be expressed in terms of the auxiliary variables $\phi(j)$. By replacing the $\mathbf{Z}$ and $\mathbf{X}$ solutions in the r.h.s. of Eq. (B.3), we both obtain an equation for the vector $\phi(j)$,

$$\sum_{j=1}^{N-1} K_{ij}\phi(j) = \delta_{1i} \ , \tag{B.9}$$

where $\mathbf{K} = \mathbf{G} + v\mathbf{I}$, and the following expression for $\mathbf{V}$:

$$\mathbf{V} = \mathbf{S} - v\mathbf{U} \ . \tag{B.10}$$

The problem of finding a solution for the heat transport in a homogeneous chain is accordingly reduced to solving Eq. (B.9) that can be written as the recursive relation

$$\phi(j+1) = (v+2)\phi(j) - \phi(j-1) \ , \tag{B.11}$$

which has to be complemented by suitable initial and final conditions. From the above equation, it follows that $\phi(j)$ is the linear combination of two exponentials $\exp(\pm\alpha j)$ with

$$\mathrm{e}^{-\alpha} = 1 + \frac{v}{2} - \sqrt{v + \frac{v^2}{4}} \ . \tag{B.12}$$

Upon imposing the appropriate initial conditions, we finally obtain

$$\phi(j) = \frac{\sinh(N-j)\alpha}{\sinh N\alpha} \tag{B.13}$$

which completes the solution for the stationary probability distribution.

References

[1] S.R. de Groot, P. Mazur, Non-Equilibrium Thermodynamics, Dover, New York, 1984.
[2] R.E. Peierls, Quantum Theory of Solids, Oxford University Press, London, 1955.

[3] F. Bonetto, J. Lebowitz, L. Rey-Bellet, in: A. Fokas, A. Grigoryan, T. Kibble, B. Zegarlinski (Eds.), Mathematical Physics 2000, Imperial College, London, 2000.
[4] J. Maddox, Nature 309 (7) (1984) 511;
F. Mokross, H. Büttner, ibid. 5983 (1984) 217.
[5] Y. Pomeau, R. Résibois, Phys. Rep. 19 (1975) 63.
[6] D.T. Morelli, J. Heremans, M. Sakamoto, C. Uher, Phys. Rev. Lett. 57 (1986) 869.
[7] A. Smontara, J.C. Lasjaunas, R. Maynard, Phys. Rev. Lett. 77 (1996) 5397.
[8] A.V. Sologubenko, et al., Phys. Rev. B 64 (2001) 054412.
[9] H. Forsman, P. Anderson, J. Chem. Phys. 80 (1984) 2804.
[10] T.S. Tighe, J.M, Worlock, M.L. Roukes, Appl. Phys. Lett. 70 (1997) 2687.
[11] M.M. Leivo, J.P. Pekola, Appl. Phys. Lett. 72 (1998) 1305.
[12] W. Holmes, et al., Appl. Phys. Lett. 72 (1998) 2250.
[13] J. Hone, et al., Phys. Rev. B 59 (1999) R2514.
[14] P. Kim, L. Shi, A. Majumdar, P.L. McEuen, Phys. Rev. Lett. 87 (2001) 215 502.
[15] L.G.C. Rego, G. Kirczenow, Phys. Rev. Lett. 81 (1998) 232.
[16] D.M. Leitner, P.G. Wolynes, Phys. Rev. E 61 (2000) 2902.
[17] K. Saito, S. Takesue, S. Miyashita, Phys. Rev. E 61 (2000) 2397, ibid. 54 (1996) 2404, J. Phys. Soc. Japan 65 (1996) 1243.
[18] E. Fermi, J. Pasta, S. Ulam, in: E. Fermi (Ed.), Collected Papers, Vol. 2, University of Chicago Press, Chicago, Vol. 2, 1965, p. 78.
[19] H.H. Rugh, Phys. Rev. Lett. 78 (1997) 772.
[20] C. Giardinà, R. Livi, J. Stat. Phys. 91 (1998) 1027.
[21] J. Lebowitz, J.K. Percus, L. Verlet, Phys. Rev. 153 (1967) 250.
[22] A.I. Khinchin, Mathematical Foundations of Statistical Mechanics, Dover, New York, 1949.
[23] Ph. Choquard, Helv. Phys. Acta 36 (1963) 415.
[24] R.J. Hardy, Phys. Rev. 132 (1963) 168.
[25] R. Kubo, M. Toda, N. Hashitsume, Statistical Physics II, in: Springer Series in Solid State Sciences, Vol. 31, Springer, Berlin, 1991.
[26] R.A. MacDonald, D.H. Tsai, Phys. Rep. 46 (1978) 1.
[27] A. Casher, J.L. Lebowitz, J. Math. Phys. 12 (1971) 1701.
[28] R.J. Rubin, W.L. Greer, J. Math. Phys. 12 (1971) 1686.
[29] A.J. O'Connor, J.L. Lebowitz, J. Math. Phys. 15 (1974) 692.
[30] H. Spohn, J.L. Lebowitz, Commun. Math. Phys. 54 (1977) 97.
[31] J.-P. Eckmann, C.-A. Pillet, L. Rey-Bellet, Commun. Math. Phys. 201 (1999) 657.
[32] D.N. Payton, M. Rich, W.M. Visscher, Phys. Rev. 160 (1967) 706.
[33] R.I. Mclachlan, P. Atela, Nonlinearity 5 (1992) 541.
[34] L. Casetti, Phys. Scr. 51 (1995) 29.
[35] R. Tehver, F. Toigo, J. Koplik, J.R. Banavar, Phys. Rev. E 57 (1998) R17.
[36] D.J. Evans, G.P. Morriss, Statistical Mechanics of Nonequilibrium Liquids, Academic Press, San Diego, 1990.
[37] S. Nosé, J. Chem. Phys. 81 (1984) 511.
[38] W.G. Hoover, Phys. Rev. A 31 (1985) 1695.
[39] Focus issue on "Chaos and irreversibility" CHAOS 8 (2) (1998).
[40] N. Chernov, J.L. Lebowitz, J. Stat. Phys. 86 (1997) 953.
[41] H. van Beijeren, private communication.
[42] M.J. Gillan, R.W. Holloway, J. Phys. C 18 (1985) 5705.
[43] A. Maeda, T. Munakata, Phys. Rev. E 52 (1995) 234.
[44] F. Zhang, D.J. Isbister, D.J. Evans, Phys. Rev. E 61 (2000) 3541.
[45] A. Filippov, B. Hu, B. Li, A. Zelser, J. Phys. A 31 (1998) 7719.
[46] F.D. Di Tolla, M. Ronchetti, Phys. Rev. E 48 (1993) 1726.
[47] M.E. Lumpkin, W.M. Saslow, W.M. Visscher, Phys. Rev. B 17 (1978) 4295.
[48] E.L. Lifshitz, L.P. Pitaevskij, Physical Kinetics, Pergamon Press, New York, 1981.
[49] K. Aoki, D. Kusnezov, Phys. Lett. A 265 (2000) 250.

[50] K. Aoki, D. Kusnezov, Phys. Rev. Lett. 86 (2001) 4029.
[51] Z. Rieder, J.L. Lebowitz, E. Lieb, J. Math. Phys. 8 (1967) 1073.
[52] M.C. Wang, G.E. Uhlenbeck, Rev. Mod. Phys. 17 (1945) 323.
[53] M. Bolsterli, M. Rich, W.M. Visscher, Phys. Rev. A 1 (1970) 1086.
[54] B. Derrida, E. Garner, J. Phys. (Paris) 45 (1984) 1283.
[55] H. Matsuda, K. Ishii, Suppl. Prog. Theor. Phys. 45 (1970) 56.
[56] W.M. Visscher, Prog. Theor. Phys. 46 (1971) 729.
[57] W. Frizzera, A. Monteil, A. Capobianco, Il Nuovo Cimento D 20 (1998) 1715.
[58] J.B. Keller, G.C. Papanicolaou, J. Weilenmann, Comm. Pure App. Math. Vol. XXXII (1978) 583.
[60] A. Dhar, Phys. Rev. Lett. 86 (2001) 5882.
[61] E.A. Jackson, Rocky Mount. J. Math. 8 (1978) 127.
[62] J. Callaway, Quantum Theory of the Solid State, Academic Press, San Diego, 1991.
[63] S. Lepri, Eur. Phys. J. B 18 (2000) 441.
[64] T. Prosen, D.K. Campbell, Phys. Rev. Lett. 84 (2000) 2857.
[65] M.S. Green, Phys. Rev. 119 (1960) 829.
[66] C. Alabiso, M. Casartelli, P. Marenzoni, J. Stat. Phys. 79 (1995) 451.
[67] M.H. Ernst, Physica D 47 (1991) 198.
[68] S. Lepri, Phys. Rev. E 58 (1998) 7165.
[69] A. Lippi, R. Livi, J. Stat. Phys. 100 (2000) 1147.
[70] D. D'Humieres, P. Lallemand, Y. Qian, C. R. Acad. Sci. Paris Ser. II 308 (1989) 585.
[71] T. Naitoh, M.H. Ernst, M.A. van der Hoef, D. Frenkel, Phys. Rev. E 47 (1993) 4098.
[72] S. Lepri, R. Livi, A. Politi, Europhys. Lett. 43 (1998) 271.
[73] E.A. Jackson, J.R. Pasta, J.F. Waters, J. Comput. Phys. 2 (1968) 207.
[74] N. Nakazawa, Progr. Theoret. Phys. 45 (Suppl.) (1970) 231.
[75] W.M. Visscher, in: Methods in Computational Physics, Vol. 15, Academic Press, New York, 1976, p. 371.
[76] H. Kaburaki, M. Machida, Phys. Lett. A 181 (1993) 85.
[77] Y. Ohtsubo, N. Nishiguchi, T. Sakuma, J. Phys.: Condens. Matter 6 (1994) 3013.
[78] F. Mokross, H. Büttner, J. Phys. C 16 (1983) 4539.
[79] E.A. Jackson, A.D. Mistriotis, J. Phys.: Condens. Matter 1 (1989) 1223.
[80] N. Nishiguchi, T. Sakuma, J. Phys.: Condens. Matter 2 (1990) 7575.
[81] O.V. Gendelman, L.I. Manevich, Sov. Phys. JETP 75 (1992) 271.
[82] M. Mareschal, A. Amellal, Phys. Rev. A 37 (1988) 2189.
[83] S. Lepri, R. Livi, A. Politi, Phys. Rev. Lett. 78 (1997) 1896.
[84] S. Lepri, R. Livi, A. Politi, Physica D 119 (1998) 140.
[85] T. Hatano, Phys. Rev. E 59 (1999) R1.
[86] M. Vassalli, Diploma Thesis, University of Florence, 1999.
[87] W. Frizzera, G. Viliani, M. Montagna, A. Monteil, A. Capobianco, J. Phys.: Condens. Matter 9 (1997) 10 867.
[88] G. Casati, Found. Phys. 16 (1986) 51.
[89] A. Dhar, Phys. Rev. Lett. 86 (2001) 3554.
[90] P.L. Garrido, P.I. Hurtado, B. Nadrowski, Phys. Rev. Lett. 86 (2001) 5486.
[91] Y. Du, H. Li, L.P. Kadanoff, Phys. Rev. Lett. 74 (1995) 1268.
[92] G. Casati, T. Prosen, private communication.
[93] C. Giardiná, R. Livi, A. Politi, M. Vassalli, Phys. Rev. Lett. 84 (2000) 2144.
[94] O.V. Gendelman, A.V. Savin, Phys. Rev. Lett. 84 (2000) 2381.
[95] G. Benettin, L. Galgani, A. Giorgilli, Il Nuovo Cimento B 89 (1985) 89.
[96] R. Livi, M. Pettini, S. Ruffo, A. Vulpiani, J. Stat. Phys. 48 (1987) 539.
[97] D. Escande, H. Kantz, R. Livi, S. Ruffo, J. Stat. Phys. 76 (1994) 605.
[98] M. Vassalli, unpublished.
[99] J. Dawson, Phys. Fluids 5 (1962) 445.
[100] G. Casati, J. Ford, F. Vivaldi, W.M. Visscher, Phys. Rev. Lett. 52 (1984) 1861.
[101] D.J.R. Mimnagh, L.E. Ballentine, Phys. Rev. E 56 (1997) 5332.
[102] M. Pettini, M. Cerruti-Sola, Phys. Rev. A 44 (1992) 975.

[103] T. Prosen, M. Robnik, J. Phys. A 25 (1992) 3449.
[104] H.A. Posch, W.G. Hoover, Phys. Rev. E 58 (1998) 4344.
[105] C. Kipnis, C. Marchioro, E. Presutti, J. Stat. Phys. 27 (1982) 65.
[106] B. Hu, B. Li, H. Zhao, Phys. Rev. E 57 (1998) 2992.
[107] B. Hu, B. Li, H. Zhao, Phys. Rev. E 61 (1999) 3828.
[108] G.P. Tsironis, A.R. Bishop, A.V. Savin, A.V. Zolotaryuk, Phys. Rev. E 60 (1999) 6610.
[109] M. Toda, Phys. Scr. 20 (1979) 424.
[110] P. Mazur, Physica 43 (1969) 533.
[111] X. Zotos, J. Low Temp. Phys. 126 (3–4) (2002) 1185.
[112] M. Toda, Theory of Non-linear Lattices, in: Springer Series in Solid-State Sciences, Vol. 20, Springer, Berlin, 1981.
[113] M. Rich, W.M. Visscher, D.N. Payton, Phys. Rev. A 4 (1971) 1682.
[114] R.D. Mountain, R.A. MacDonald, Phys. Rev. B 28 (1983) 3022.
[115] T. Sakuma, Y. Ohtsubo, N. Nishiguchi, J. Phys.: Condens. Matter 4 (1992) 10 227.
[116] J. Michalski, Phys. Rev. B 45 (1992) 7054.
[117] R.H.H. Poetzsch, H. Böttger, Phys. Rev. B 50 (1994) 15 757.
[118] R.H.H. Poetzsch, H. Böttger, J. Phys.: Condens. Matter 10 (1998) 943.
[119] Ch. Dellago, H.A. Posch, Physica A 237 (1997) 95.
[121] T. Shimada, T. Murakami, S. Yukawa, K. Saito, N. Ito, J. Phys. Soc. Japan 10 (2000) 3150.
[122] G. Benettin, A. Tenenbaum, Phys. Rev. A 28 (1983) 3020.
[123] A. Carati, L. Galgani, J. Stat. Phys. 94 (1999) 859.
[124] S. Lepri, S. Ruffo, Europhys. Lett. 55 (2001) 512.
[125] B. Li, H. Zhao, B. Hu, Phys. Rev. Lett. 86 (2001) 63.
[126] E. Maciá, Phys. Rev. B 61 (2000) 6645.
[127] P.B. Allen, J.L. Feldman, Phys. Rev. B 48 (1993) 12 581.
[128] O. Narayan, S. Ramaswamy, Phys. Rev. Lett. 89 (2002) 200601.
[129] P. Grassberger, et al., Phys. Rev. Lett. 89 (2002) 180601.